NUMERICAL INVESTIGATION ON ENERGY EFFICIENT RECEIVER TUBE OF PARABOLIC TROUGH COLLECTOR

Thesis Submitted for the Award of the Degree of

DOCTOR OF PHILOSOPHY

in

Mechanical Engineering

By

Mridul Sharma

Registration Number: 41800758

Supervised By

Dr. Aashish Sharma (16420)

Mechanical Engineering (Associate Professor)

Lovely Professional University

Punjab, India

Co-Supervised By

Dr. Ravindra D. Jilte

Energy Centre (Associate Professor)

Maulana Azad National Institute of Technology

Bhopal, Madhya Pradesh, India

LOVELY PROFESSIONAL UNIVERSITY, PUNJAB

2024

DECLARATION

I, hereby declared that the presented work in the thesis entitled "Numerical Investigation on Energy Efficient Receiver Tube of Parabolic Trough Collector" in fulfillment of degree of **Doctor of Philosophy (Ph.D.)** is outcome of research work carried out by me under the supervision of Dr. Aashish Sharma, working as Associate Professor, in the School of Mechanical Engineering of Lovely Professional University, Punjab, India and co-supervision of Dr. Ravindra D. Jilte, working as Associate Professor, in Energy Centre of Maulana Azad National Institute of Technology, Bhopal, Madhya Pradesh, India. In keeping with general practice of reporting scientific observations, due acknowledgements have been made whenever work described here has been based on findings of other investigator. This work has not been submitted in part or full to any other University or Institute for the award of any degree.

Mridul Sharma

Registration No.: 41800758

School of Mechanical Engineering

Lovely Professional University

Punjab, India

CERTIFICATE

This is to certify that the work reported in the Ph.D. thesis entitled "Numerical Investigation on Energy Efficient Receiver Tube of Parabolic Trough Collector" submitted in fulfillment of the requirement for the reward of degree of **Doctor of Philosophy (Ph.D.)** in the School of Mechanical Engineering, is a research work carried out by Mridul Sharma, 41800758, is bonafide record of his original work carried out under my/our supervision and that no part of thesis has been submitted for any other degree, diploma or equivalent course.

Dr. Aashish Sharma (16420)
Associate Professor
School of Mechanical Engineering
Lovely Professional University,
Punjab, India

Dr. Ravindra D. Jilte
Associate Professor
Energy Centre
Maulana Azad National Institute of Technology, Bhopal, Madhya Pradesh, India

ABSTRACT

Energy use in many forms has become crucial to global economic growth and development. Given the diminishing supplies of fossil fuels, which now serve as the primary energy source, there has been a push to find alternative renewable energy sources. Among the diverse renewable energy sources available, solar energy harnessing has become very common. As a perpetual and direct source of energy, freely accessible sunlight provides a non-polluting fuel reservoir. Various collectors have been developed, built and checked to work in various temperature ranges. The parabolic trough solar collector is found to be the most common among the other collectors in applications such as the distribution of process heat and the production of steam. It is a kind of heat exchanger that transforms solar radiation energy to internal energy of the transport medium. The parabolic trough solar collector (PTSC) is a line-focused concentrating collector. It is capable of operating at temperatures ranging upto 400°C to 500°C.

The economic feasibility of solar thermal systems is heavily reliant on the utilization and conversion of solar heat input. Thermal losses from the PTSC receiver tube considerably affect system performance. Losses reduction considerably affects system effectiveness. The passive approach of thermal augmentation is widely used in PTSC. Since, the bottom portion of the receiver experiences increased temperatures as a result of uneven distribution of solar light. This passive method improves heat transmission by homogenising distribution, increasing heat transfer coefficient, and establishing an appropriate pathway for the heat to be received. Passive approaches include the use of inserts in the flow channel and surface modifications of the receiver pipe. Researchers have suggested many types of inserts and receiver's surface modification methods. The prior literature shows that inserts increase turbulence intensity, which improves heat transmission but increases material consumption. Moreover, inserts have a much higher pressure drop than surface modification methods. As a result, geometric modification of receiver pipe is much more feasible. Moreover, the effect of double corrugated

(symmetrical convex-concave corrugations) receiver has not yet been investigated. Hence, the present work bridges this research gap.

In view of above, the present investigation has been carried out with following objectives:

1. Design and development of modified receiver tube for solar parabolic trough collector.
2. Thermo-hydraulic performance analysis of developed receiver tube for solar parabolic trough collector.
3. To compare the performance of new receiver tube with conventional plain tube of solar parabolic trough collector.

Computational fluid dynamics (CFD) analysis has been used to assess the receiver tube's thermal-hydraulic performance. Corrugation design parameters including pitch (P), height (e), and flow rate are examined to determine performance under non-uniform solar flux. A modified and conventional (smooth) receiver tubes has been compared. The 7.8 m long 316L steel receiver tubes having 70 mm outer diameter and 66 mm inner diameter has been considered. The modified design has corrugation pitches of 4 mm, 6 mm, 8 mm, and 10 mm with heights of 1.5, 2 mm, and 2.5 mm. The receiver wall has symmetrical convex-concave corrugations that extend longitudinally and come into contact with the heat transfer fluid.

Both Nusselt number (Nu) and pressure drop (ΔP) are strongly influenced by flow and geometric characteristics. Corrugation arrangement promotes turbulence, boundary layer dispersion, and flow mixing. Due to the development of axial spinning and vortex formations, significant improvement in heat transmission has been observed. Additionally, flow dissociation, reattachment, and vortex forms boost turbulent kinetic energy near the wall. Thus, double corrugations (convex-concave corrugations) increase turbulence, enhancing heat transmission.

The investigation found that turbulent kinetic energy increases with corrugation pitch from 4 mm to 8 mm and height from 1.5 mm to 2 mm. Increasing both parameters further

reduces turbulent kinetic energy due to decreasing swirl intensity. The receiver tube with 8 mm pitch and 2 mm height corrugations has larger mixing flow areas and recirculation size than other examined cases. Thus, tube with 8 mm corrugation pitch and 2 mm height has the highest Nusselt number. It has been observed that this enhancement lies between 23.16% and 34.98% as compared to a conventional (smooth) pipe. Furthermore, for all examined cases of corrugated tube, the average Nusselt number increases by 6.77% to 28.51%.

Simultaneously, the pressure drop increases as the Reynolds number increases. Pressure penalty rises from 4 mm to 6 mm corrugation pitch. After that, it decreases for the remaining pitch sizes. The pressure penalty is largest at 2.5 mm corrugation height and lowest at 2 mm for all pitch values. For the various examined cases, average friction factor found to be 1.08 to 4.46 times higher than smooth pipe.

The data obtained from CFD investigation has been further used to develop correlations with the use of response surface methodology (RSM) in terms of flow and geometric parameters. The generated correlations are:

$$Nu = (92.89276 + 2.29344 \times \mathrm{A} - 3.22079 \times \mathrm{B} + 46.85805 \times \mathrm{C} + 1.19047 \times \mathrm{AC} - 0.36321 \times \mathrm{BC} - 4.36524 \times \mathrm{A}^2 - 3.72092 \times \mathrm{B}^2 - 2.14202 \times \mathrm{C}^2 - 1.35314 \times \mathrm{A}^2\mathrm{C} - 0.09440 \times \mathrm{AC}^2 - 1.47134 \times \mathrm{B}^2\mathrm{C} + 0.84862 \times \mathrm{BC}^2 - 0.87901 \times \mathrm{A}^3 + 0.46551 \times \mathrm{C}^3)$$

$$\Delta P = (85.93161 - 25.91655 \times \mathrm{A} + 19.92090 \times \mathrm{B} + 98.13314 \times \mathrm{C} - 2.01380 \times \mathrm{AC} + 25.68187 \times \mathrm{BC} - 11.96035 \times \mathrm{A}^2 + 59.39358 \times \mathrm{B}^2 + 34.35148 \times \mathrm{C}^2 - 10.43262 \times \mathrm{A}^2\mathrm{C} + 2.74114 \times \mathrm{AC}^2 + 58.63417 \times \mathrm{B}^2\mathrm{C} + 8.49825 \times \mathrm{BC}^2 + 26.03883 \times \mathrm{A}^3 + 1.01225 \times \mathrm{C}^3)$$

$$f = (0.0466 - 0.0100 \times \mathrm{A} + 0.0092 \times \mathrm{B} + 0.0024 \times \mathrm{C} - 0.0004 \times \mathrm{AC} + 0.0020 \times \mathrm{BC} - 0.0049 \times \mathrm{A}^2 + 0.0226 \times \mathrm{B}^2 + 0.0001 \times \mathrm{C}^2 - 0.0011 \times \mathrm{A}^2\mathrm{C} - 0.0001 \times \mathrm{AC}^2 + 0.0045 \times \mathrm{B}^2\mathrm{C} - 0.0009 \times \mathrm{BC}^2 + 0.0108 \times \mathrm{A}^3 - 0.0005 \times \mathrm{C}^3)$$

$$TEF = (1.16176 + 0.11526 \times \mathrm{A} - 0.08246 \times \mathrm{B} - 0.05550 \times \mathrm{C} + 0.01033 \times \mathrm{AC} + 0.01071 \times \mathrm{BC} - 0.01844 \times \mathrm{A}^2 - 0.19138 \times \mathrm{B}^2 - 0.02708 \times \mathrm{C}^2 + 0.02409 \times \mathrm{A}^2\mathrm{C} - 0.00466 \times \mathrm{AC}^2 - 0.00923 \times \mathrm{B}^2\mathrm{C} + 0.00790 \times \mathrm{BC}^2 - 0.10417 \times \mathrm{A}^3 + 0.01915 \times \mathrm{C}^3)$$

Here, the assigned codes have following meanings: A is Corrugation Pitch (*P*), B is Corrugation Height (*e*) and C is Reynolds number (*Re*).

The RSM analysis identified the most effective design parameters for corrugated receiver. Corrugation pitch equals to 8.145 mm, corrugation height equals to 1.918 mm are found as the optimized design parameters. For these optimized design parameters, CFD test indicates that there is 1.29% deviation between RSM model outcome and simulation result, signifying a remarkable concurrence between them.

Summarizing, it can be stated that the PTSC receiver with double corrugations significantly improves the thermal-hydraulic performance of it as compared to the conventional (smooth) receiver tube. The optimisation study conducted to maximise the thermal enhancement factor (*TEF*) assists designers in predicting the optimal values of geometric parameters. The correlations developed are valuable for designers to analyse the performance of PTSC within the researched parameter range.

ACKNOWLEDGEMENT

"उद्यमेन हि सिध्यन्ति, कार्याणि न मनोरथैः !
न हि सुप्तस्य सिंहस्य प्रविशन्ति मुखे मृगाः !!"

"Similar to how the antelope does not willingly approach the slumbering lion's maw, our success in work can only be achieved by diligent effort rather than mere wants".

I would like to express my deep gratitude and appreciation to all those who have contributed to the completion of this journey. This journey has been challenging and rewarding, and I could not have achieved this milestone without the support and assistance of many individuals and organizations.

With a feeling of bottomless pleasure, I can say that the credit of this work goes to humble personalities, who has brought about "better me" in myself, my supervisor Dr. Aashish Sharma, whose scholarly insight and valuable guidance has molded and enlightened my work into success that in turn is presented here.

Special thanks to Dr. Ravindra D. Jilte (Co-Supervisor), for his untired guidance, great support and kind advice throughout my research studies. It was a real privilege and an honour for me to share his remarkable scientific knowledge but also his extraordinary human qualities.

I also like to express my sincere gratitude towards the DDB and ETP panel's**,** for their constant guidance throughout this journey. Their feedback and endless support helped me to work much better. I would also like to extend the thanks towards the entire team of Lovely Professional University, India for all their support**.**

I express profound gratitude to my parent institution, Jawaharlal Nehru Government Engineering College, Sundernagar, District Mandi (H.P), India, for the consistent support, encouragement, and provision of resources during my Ph.D journey.

How can I forget my students who supported me in setting up resources? Thank you, dear friends. Also, I am thankful to all my friends and well-wishers for supporting and motivated me.

On a personal Note, I would like to express my gratitude towards my loving Parents Mr. Jagdish Chand Sharma and Mrs. Veena Sharma for all their efforts and encouragement they have given throughout my life. I am also thankful to my in-laws, Mr. Dinesh Kumar Bisht and Mrs. Naresh Bisht for encouraging me and providing endless support. Nitasha, my wife, who always tried to come up with the solution to any problem I faced throughout this tenure. A thank you will be the very small word for her. She has been a continuous source of motivation for me. Special love to my beloved daughter Bhaavya, who is one of my most cherished source of inspiration and happiness. Ph.D thesis is an output of extreme hard work and dedication. For me it is also blessing of my almighty that have always kept helping hands to pull me up whenever I have fallen down.

(Mridul Sharma)

TABLE OF CONTENTS

LIST OF FIGURES

LIST OF TABLES

NOMENCLATURE

A_{ap}	aperture area (m^2)
ANOVA	analysis of variance
CFD	computational fluid dynamics
c_p	specific heat at constant pressure (J/Kg-K)
CR	concentration ratio
CSP	concentrated solar power
DCRP	double corrugated receiver pipe
D_{ri}	inner diameter of receiver pipe (hydraulic diameter) (m)
D_{ro}	outer diameter of receiver pipe (m)
DNI	direct normal irradiance (W/m^2)
e	corrugation height (mm)
f	friction factor
f_s	friction factor of smooth receiver pipe
FVM	finite volume method
GA	genetic algorithm
GW	gigawatt
h	heat transfer coefficient (W/m^2-K)
HTF	heat transfer fluid
I	turbulent intensity
I_b	solar irradiance (W/m^2)
K	thermal conductivity (W/m-K)

L	length of receiver pipe (m)
$\dot{m}$	mass flow rate (kg/s)
Nu	Nusselt number
Nu_s	Nusselt number of smooth receiver pipe
P	corrugation pitch (mm)
Δp	pressure drop (Pa)
Pr	Prandtl number
q	heat flux (W/m^2)
Re	Reynolds number
RSM	response surface methodology
TEF	thermal enhancement factor
T_{in}	inlet temperature (K or °C)
TKE	turbulent kinetic energy (J/kg)
T_{out}	outlet temperature (K or °C)
T_{wall}	inner wall temperature (K or °C)
V	velocity of fluid (m/s)
ρ	density (kg/m^3)

CHAPTER 1

INTRODUCTION

1.1 General

Energy use in many forms has become crucial to global economic growth and development. Given the diminishing supplies of fossil fuels, which now serve as the primary energy source, there has been a push to find alternative sources of renewable energy. Solar energy is the most promising long-term solution among several options to address the ever-growing energy demand [1]. As a perpetual and direct source of energy, freely accessible sunlight provides a non-polluting fuel reservoir. Solar energy as intercepted by the earth is much many times than the current rate of energy consumption from all commercial energy sources combined. India's annual solar energy intake exceeds 5000 trillion kWh; with around 5 kWh/m^2 as an average daily global radiation [2]. The primary limitation of this resource is its modest magnitude and sporadic occurrence. Even in the most scorching area on the planet, the amount of solar radiation energy available rarely surpasses 1 kWh/m^2. Despite these constraints, solar energy emerges as the most auspicious of all the renewable energy sources [3]. Efforts have therefore been undertaken to build and construct systems that can efficiently gather and use it [4]. Table 1.1 depicts the renewable energy status of India [5].

Table 1.1: Renewable Energy Status in India (as per annual report 2022-23) [5]

S.No.	Energy Source	Commissioned Capacity (GW)	Under Commissioning (GW)	Bids Floated (GW)
1.	Solar	63.30	51.13	20.34
2.	Wind	41.93	12.93	1.20
3.	Bio	10.73	-----	-----
4.	Hydro (Small)	4.94	0.54	0.00

Sources of renewable energies are mainly listed as:

(i) Solar Energy

(ii) Wind Energy

(iii) Hydro Energy

(iv) Bio Energy

(v) Oceanic Energy

(vi) Geothermal Energy

1.2 Solar Energy

Solar energy is basically generated by capturing energy from the sunlight and converting this energy into any other form like heat, electricity etc. Sun is a gaseous pressure sphere having 1.39×10^9 m diameter and averagely at a distance of 1.5×10^{11} m from our planet. 5777 K is an effective temperature of sun with 8×10^6 to 40×10^6 K as a central interior region temperature [6]. The thermo-nuclear fusion reaction converts hydrogen atoms into helium atoms, due to which sun generates heat continuously [7]. The solar radiation after passing through the earth's atmosphere experienced various attenuations such as scattering and absorption [8]. The three elements of the solar radiation shown in Fig. 1.1 that enters the earth's surface are:

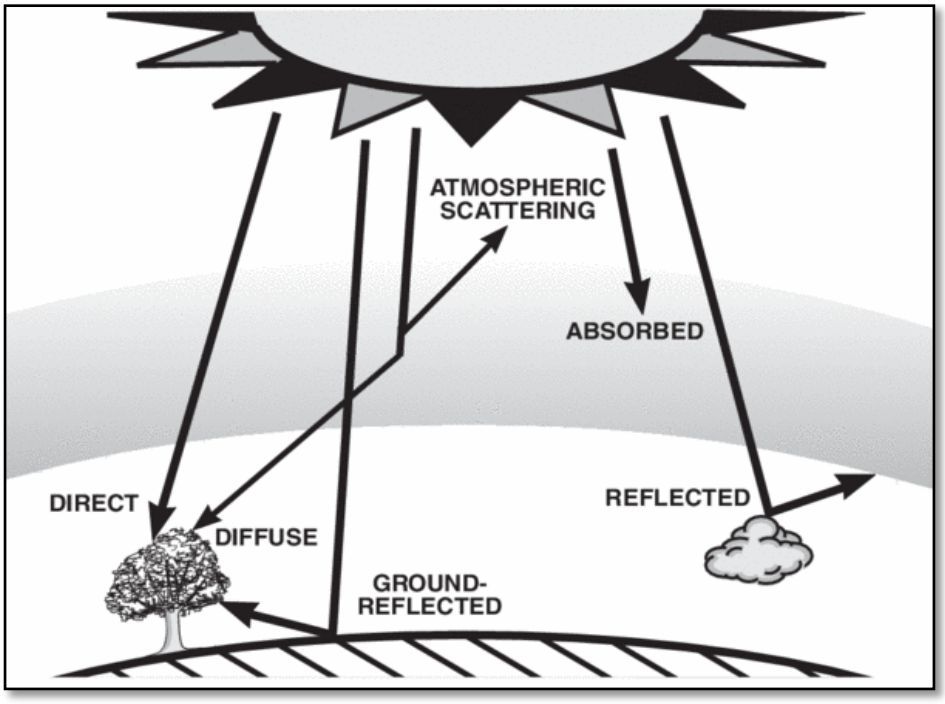

Fig. 1.1: Solar Radiation Distribution [8]

(a) Direct (or Beam) Radiation: Radiation which does not change its direction (in line with sun).
(b) Diffuse Radiation: Radiation reaches the surface of the earth from all parts of the sky (scattering).
(c) Reflected Radiation: Radiation reflected from nearby surfaces like ground, buildings etc.

Sunlight is freely available as a direct and permanent energy source which offers a fuel supply that is non-polluting. Around 1.8×10^{11} MW of Sun power is clog by earth [6], which is many thousand times higher than the current rate of consumption of all commercial energy on the earth [6]. This makes solar energy most auspicious non-conventional energy resource. However, its economic viability largely depends on its effective collection, processing and use [9].

1.2.1 Solar Energy Applications

The following list includes a few important applications of solar energy:

(i) Heating of Water
(ii) Heating of Space
(iii) Electricity Generation
(iv) Preservation of Food
(v) Drying of Agriculture Products
(vi) Green Houses
(vii) Food Cooking
(viii) Pumping of Water
(ix) Distillation of Water

Solar energy is a limitless, environment friendly energy source with low intensity [6]. However, its economic feasibility heavily relies on its effective gathering, storage, and use [9]. For which, generally solar collectors are employed.

1.3 Solar Energy Collectors

These are the devices used to collect radiation coming from sun and then transmit the energy that is collected to a heat transfer fluid [10]. It is necessary to have solar

collectors in order to make use of solar energy [11]. There are two overall categories [8] of these:

(i) Non concentrating solar collectors.

(ii) Concentrating solar collectors.

The solar energy collector, along with its corresponding absorber, is a crucial element in any system designed to convert solar radiation into a more practical form [6]. In the former type, collector area, which refers as radiation intercept area, is equivalent to the absorber area which is responsible for absorbing the radiation [12]. Whereas in concentrating collectors, the surface area that intercepts solar radiation is much larger, sometimes hundreds of times larger than the area of the absorber. Concentrating collectors allow for achieving much greater temperatures compared to non-concentrating collectors [13].

1.3.1 Non Concentrating Type

Non concentrating also called as flat plate, are especially advantageous where temperatures below around 90°C are sufficient [6]. Such systems are convenient for space and service water heating [8]. They are constructed in rectangular panels that range in size from around 1.7 to 2.9 sq. m, and they are built and erected in a pretty straightforward manner [8]. As a result of the fact that flat plates are able to gather and absorb both direct and diffuse solar light, they are able to be somewhat effective even on overcast days when there is no direct radiation [6]. Depending on the kind of heat transfer fluid that is used, flat-plate solar collectors may be classified into two primary categories according to their characteristics. The primary distinction between the two kinds is in the configuration of the conduits for the thermal exchange medium. It is common practice to use *liquid heating collectors* for the purpose of heating water and non-freezing aqueous solutions, and in certain cases, for heat transfer fluids that are not aqueous [14]. A glass-covered metal box with an absorber plate, many tubes connected to it, and thermal insulation below makes up the liquid heating collector [15]. Through these tubes, liquid coming from a storage tank absorbs heat before returning to the storage tank. Forced and thermosyphonic flow both are possible. Air or gas heating collectors are referred as s*olar air heaters* [16]. An absorber plate and a second parallel plate positioned below it provide a passageway

for air, in a typical solar air heating system [16]. In order to effectively transfer the heat, solar radiations penetrate through the transparent cover or coverings, impact on the blackened absorber plate, and are then transmitted to the air that flows underneath the absorber and makes contact with whole absorber surface. Figs. 1.2 and 1.3 shown below presents the working of these typical collectors.

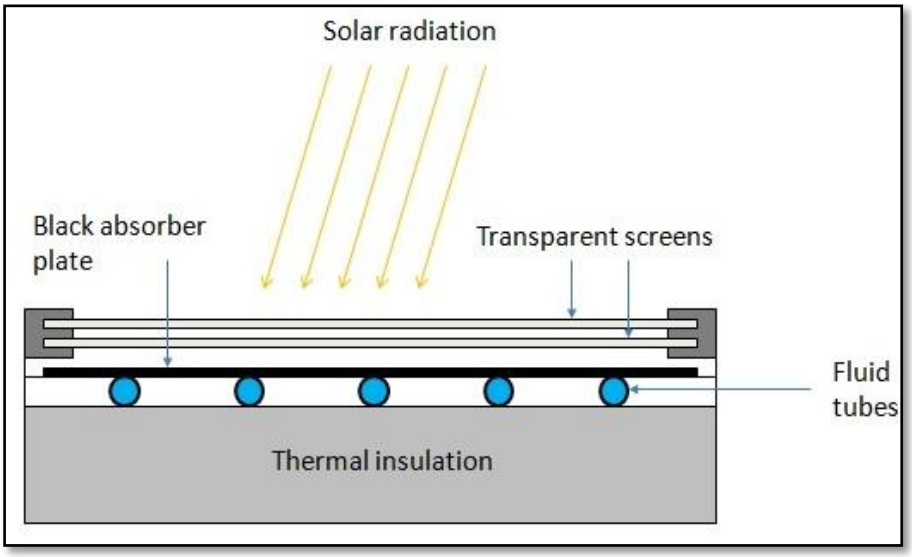

Fig. 1.2: Typical Liquid Heating Collector [6]

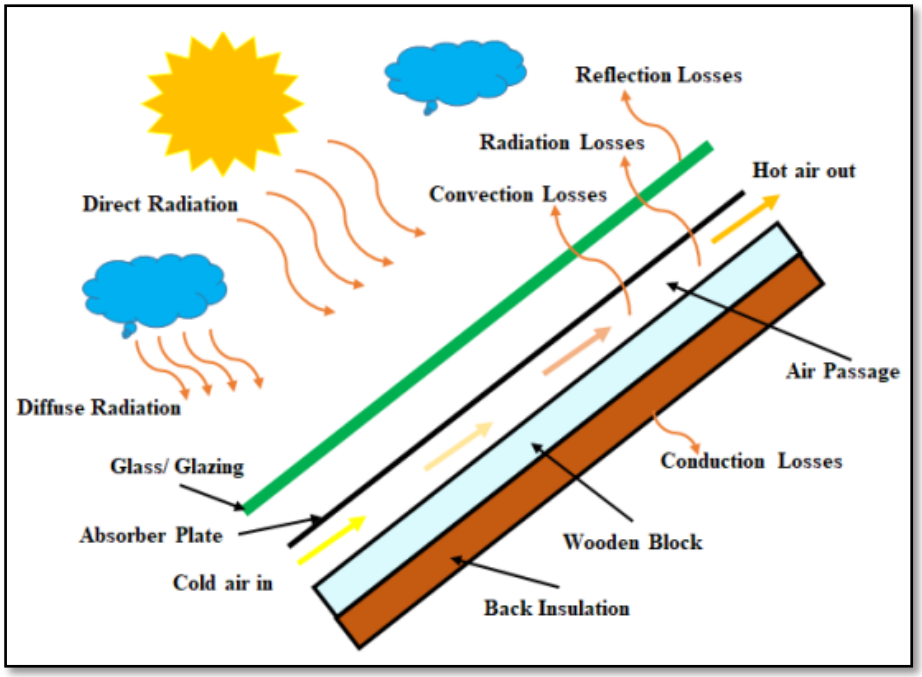

Fig. 1.3: Typical Air Heating Collector [16]

1.3.2 Concentrating Solar Collectors

Concentrating collectors typically include a receiver and a concentrator that facilitate the delivery of large volumes of solar insolation to its receiver. The high concentration enables high-temperature functioning and decrease in heat losses from the receiver [17]. These collectors are mostly employed for temperatures beyond 100°C, which are outside the operating range of flat technologies [17]. Further, the ratio of receiver area to the concentrator area [10], often called as concentration ratio determines the collector temperature level. Concentrating collectors having concentration ratio below 5 are classified as non-imaging type. These collectors are often employed for temperature levels up to 200°C [10]. In contrast, image concentrating collectors achieve greater concentrations, often exceeding 10, and operate at temperature ranges ranging from 200°C to 500°C [10]. The often used concentrating solar technologies are shown in Fig. 1.4. These are explained as follows;

(a) A CPC (*compound parabolic concentrator*) is a kind of non-imaging collector that achieves concentration ratio ranging from 1 to 15 and capable of operating for temperature range from 60°C to 300°C [18]. The concentrator is linked with variety of designs [6]. It is having cylindrical receiver. The functionality of it may be either with or without tracking [10].

(b) The PTSC (*parabolic trough solar collector*) is a line-focused concentrator and is considered as the well-established technology for concentration. It is capable of operating for temperature range upto 400°C to 500°C [19]. Its concentration ratio typically falls within the range of 10 to 50, with values around 25-30 being more common [10]. The PTSC has the capability to function with either a single-axis tracking system or, less often, a polar axis. The absorber's diameter ranges from 30 mm to 80 mm, with 70 mm being a common figure [20].

(c) The LFR (*linear Fresnel reflector*) is a type that operates on the same concept as the PTSC. Nevertheless, the LFR exhibits reduced operational complexities and decreased wind loads, resulting in a more affordable option. However, it exhibits worse optical performance in comparison to the PTC [21]. Its

concentration ratio ranges from 10 to 40 with working temperature range of 60°C to 250°C. Its receiver may consist of an evacuated tube including a secondary parabolic concentrator [22].

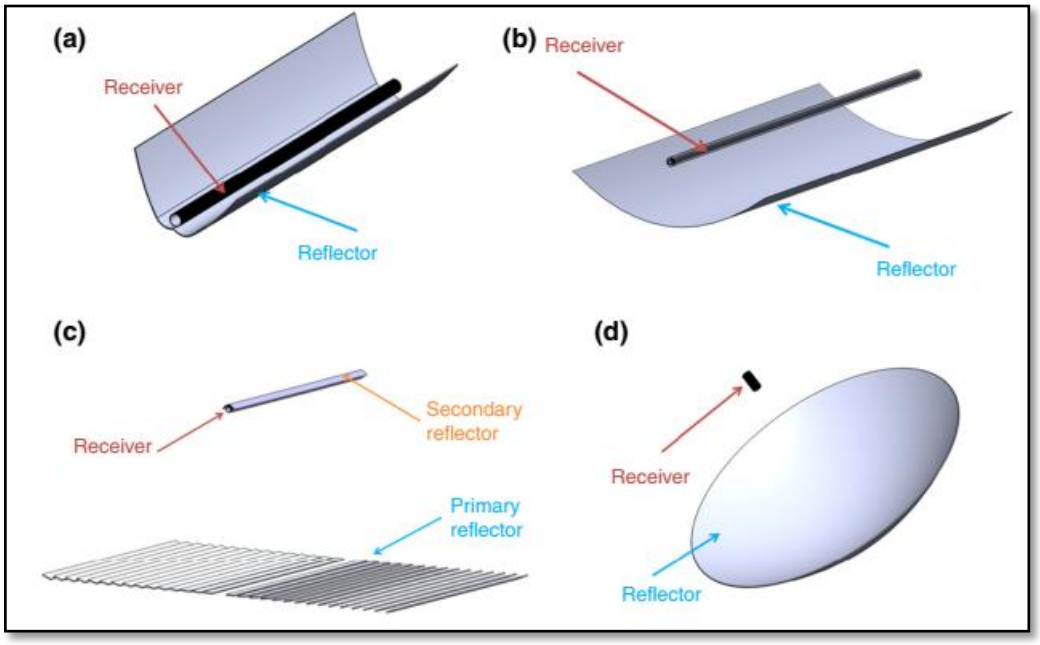

Fig. 1.4: Concentrating Techniques: (a) CPC, (b) PTSC, (c) LFR, (d) SDC [10]

(d) A SDC (*solar dish collector*) is a technology that focuses sunlight to a single point with concentration ratio of equals to 500 to 2000. Such systems are capable for working in the temperature range of 100°C to 2000°C. These are suitable for high-temperature applications, and they function with polar tracking method [18]. A wide range of designs are available, with cylindrical cavities being the common shape [23]. This method ensures a satisfactory level of electrical efficiency, but at a significant initial expense.

1.3.3 Methods of Performance Enhancement for Concentrating Collectors

Concentrating solar collectors are innovative technologies that aim to generate environment-friendly thermal energy. Their installation is linked to the enhancement of their performance and the reduction of their cost [24]. Considerable study has been dedicated to improving the performance of concentrating collectors in this field. The various performance enhancement techniques are;

(i) Enhancement for Optical Characteristics: In order to improve the optical characteristics, the concentrator design, and the tracking system has to be

improved. Both of these adjustments are taken into consideration. The purpose of these modifications is to increase the irradiation intensity onto the absorber in order to create a greater quantity of heat that may be put to beneficial use. Several concepts have been proposed by the researchers, and there has been a significant amount of progress made in this field [10].

(ii) Thermal Enhancements: The thermal enhancement techniques rely on enhancing the heat transmission between the receiver and the heat transfer fluid [7]. Thermal enhancement methods become more significant at elevated temperatures due to the amplified heat losses. These include modifications in receiver such as use of inserts or generating passive vortexes with the aim of creating turbulence. Utilization of different fluids such as nanofluids or gaseous fluids also counted in this category [20].

1.4 PTSC (Parabolic Trough Solar Collector)

It is a type of concentrated solar technology. The function of which is to soak up the arriving solar radiant energy and to convert this energy into heat energy, after that the converted energy is transferred to a flowing fluid through the receiver pipe [25]. This working fluid basically soaks up the heat flux from the pipe side's walls.

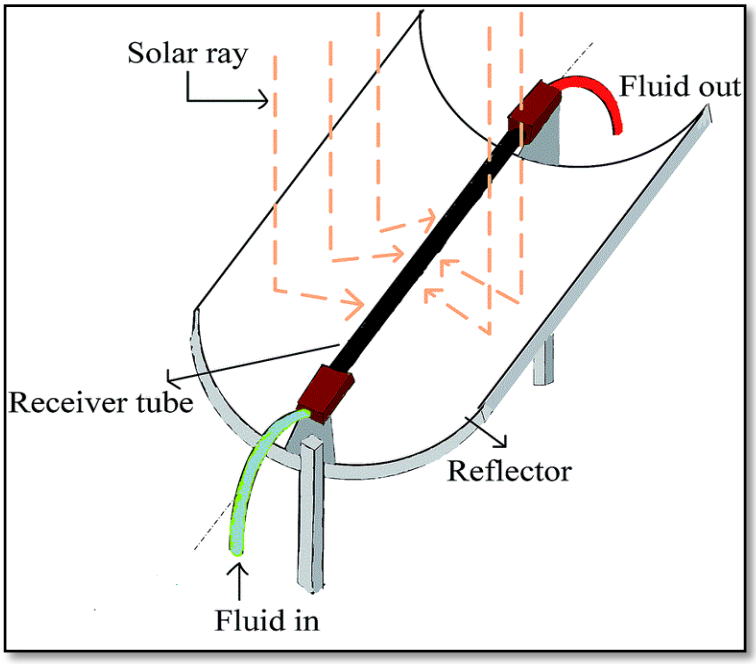

Fig. 1.5: Parabolic Trough Solar Collector [26]

In parabolic troughs, solar radiations are concentrated on the collector axis, that's why these are known as line focus collectors. It consist a receiver, which is permanently fixed at the concentrator focus, a concentric transparent cover and a reflector plate parabolic in shape and situated on rigid frame/structure. The schematic of parabolic trough solar collector is shown in Fig. 1.5. These are mainly used in those applications which demands low and high heat temperature [19]. In case of concentrated solar power plant applications, working fluid temperature with parabolic trough solar collectors can be increased by 500°C, which is helpful for the steam power cycles and in case of industrial process heat applications, 100°C to 250°C is the temperature range of heat transfer fluid, which is helpful in low temperature requirement like hot water supply for domestic purpose and heating of space etc. [2].

1.4.1 Passive Method of Heat Transfer Enhancement: Why?

The objective is to enhance the heat transmission from the receiver pipe to the working fluid by creating turbulence inside the flow path. It will lead to decrease in the receiver temperature which lowers down the heat losses and simultaneously increases the thermal performance of receiver pipe. Further, with fall of receiver temperature, a uniform distribution of temperature in its periphery occurred, due to which less thermal strains induced [27]. Due to the non-uniform concentration of heat flux on the receiver, the lower part becomes hotter. The passive techniques then makes its uniform distribution, by enhancing the heat coefficient [13].

1.4.2 Motivation

The impetus arises from the worldwide need to shift towards renewable energy sources in order to alleviate climate change and decrease reliance on limited fossil resources. The increasing worldwide need for energy requires the investigation and use of various and adaptable energy sources. Solar technologies, propelled by this need, provide a feasible alternative. Solar energy, including the use of parabolic trough collectors, provides a sustainable and eco-friendly option by decreasing greenhouse gas emissions and mitigating environmental harm linked to traditional energy sources. The objective is to bolster energy security via the diversification of the energy portfolio, reducing dependence on imported fossil fuels, and establishing a more robust energy infrastructure. The motivation for the development and

implementation of solar technologies, such as parabolic trough collectors, stems from the desire for technical innovation. Technological progress in these systems enhances productivity and cost-efficiency. Solar energy technologies, such as parabolic trough collectors, are essential for attaining a low-carbon and environmentally sustainable energy landscape. Government policies globally incentivize the use of solar energy technology. These efforts provide a conducive atmosphere for investment and development in the solar industry. Gaining insight into these incentives offers a framework for the solar energy technologies development, such parabolic trough collectors, as a component of a comprehensive plan for a sustainable and resilient energy future.

1.5 Structure of Thesis

This thesis is organized into six chapters, each of which addresses a specific aspect of the present work. The structure of the thesis is as follows:

Chapter 1 provides an overview of solar energy and its significance in the context of renewable energy sources. The focus narrows to parabolic trough solar collectors (PTSC's), highlighting their role in harnessing solar energy for thermal applications and elucidating the underlying reasons for the research endeavor. The chapter concludes with a summary of the thesis structure.

Chapter 2 presents a comprehensive review of existing literature related to solar parabolic trough collectors and receiver tubes. The research problem is defined; emphasizing the need for enhancing the thermal performance of receiver tubes in PTSC's. Special attention is given to previous studies on receiver tube design, material selection, and thermal performance analysis. This chapter also discusses various numerical methods and simulation techniques used in previous studies, highlighting the research gap that this thesis aims to address. The chapter concludes with the objectives of the study.

Chapter 3 outlines the numerical approach used to model the receiver tube. The chapter covers the development of the computational model. The governing equations for fluid flow and heat transfer are discussed, along with the assumptions and simplifications made for the numerical modeling. The geometry, boundary conditions,

and material properties used in the model are specified. The selection of numerical technique is justified and the computational tools employed are introduced.

Chapter 4 presents the results of the numerical simulations and analyzes the performance of the receiver tube. The simulation set up, including mesh generation and solver settings, is discussed in depth. The chapter also covers the validation of the numerical model by comparing simulation results with experimental and published data. Special attention is given to design of receiver tube, whereby the impact of different design parameters, and fluid flow rates, on the receiver tube's performance is explored.

Chapter 5 discusses the optimization of receiver tube design parameters using the RSM (response surface methodology) model. The process of identifying optimal settings for the input variables to achieve desired performance outcomes is explained. This section includes graphical tools like contour plots, response surfaces, and desirability functions to visualize the optimization results. The chapter concludes with a validation of the RSM model predictions against numerical simulations to ensure the reliability of the results.

The final Chapter 6 summarizes the key findings of the research, emphasizing the contributions made to the field of solar energy. The chapter also discusses the recommendations for future research to further enhance the energy efficiency of receiver tubes in solar parabolic trough collectors.

CHAPTER 2

LITERATURE REVIEW

2.1 Introduction

The exhaustion of fossil resources and concerning climate change has sparked worldwide attention towards the investigation of renewable energy. Solar energy is favoured due to its abundant and renewable nature, as well as its environmental impact. A CSP system harnesses solar energy and transforms into thermal energy for use [6]. CSP technology may be categorized as either point-focused or line-focused [28]. For high temperature applications, point focused collectors are designed [10] and line focused collectors are suitable for low-to-medium temperature applications [7]. There is a continuous implementation of four different forms of CSP technology. Fig. 2.1 illustrates the operational concepts of these technologies. Linear Fresnel reflectors use mirror strips to guide sunlight to a linear receiver [18]. The parabolic trough solar collector focuses solar radiation onto the collector axis [8] and is composed of three components. The first component is a fluid chamber known as receiver, second is concentric transparent cover that minimizing heat losses, and third is reflector mounted on a rigid structure [24]. Conversely, central receiver technology often referred to as solar tower technology [6], involves the use of a cavity point receiver positioned atop a tall tower [18]. This tower consists of curved or flat mirrors called heliostats [6], concentrating the sunlight onto the central receiver [18]. Heliostats are equipped with trackers to ensure that the redirected radiation consistently reaches the receiver [6]. This technique exhibits superior efficiency compared to line focused collectors [19]. Similarly, the parabolic dish collector functions within high temperature ranges. Additionally, it may be used for industrial heating processes [6].

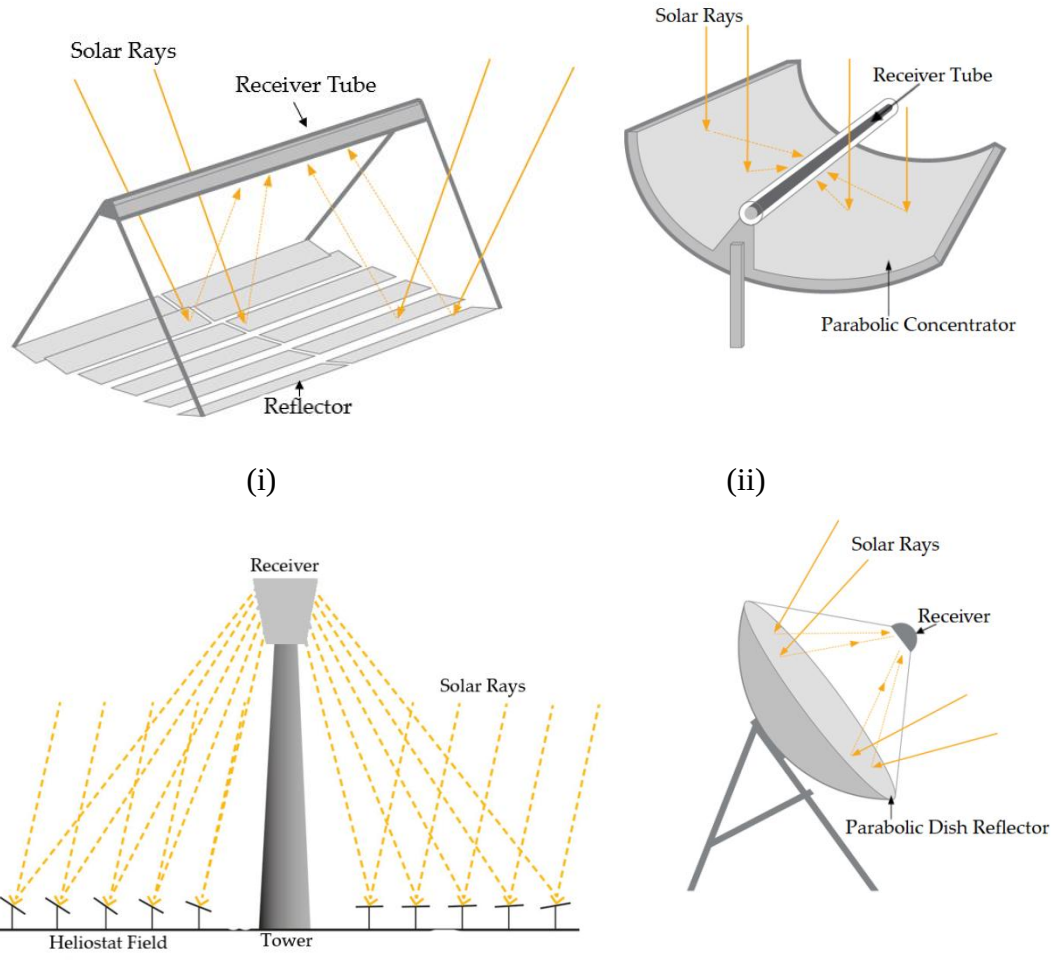

Fig. 2.1: CSP Technologies [29,30]

The parabolic trough technique widely used technology particularly for applications requiring medium temperatures [31]. Hence, this research primarily concentrates on this technology. In addition, this system provide several advantages such as substantial power capacity, exceptional performance, modularity, adaptability, and a prolonged life cycle [13]. Significant efforts have been undertaken to enhance infrastructure and make it compatible with corresponding energy systems via extensive research and development. This chapter explores numerous passive techniques for efficiently absorbing and dissipating heat, using a range of inserts and surface changes. Here, compilations of several quantitative and empirical investigations, providing an overview of passive techniques used are delineated. The accompanying sections show several current breakthroughs in thermal enhancement strategies of parabolic trough solar collectors.

2.2 Thermal Enhancement Methods

The feasibility of solar systems is heavily reliant on the conversion of solar input. The thermal losses from the receiver of PTSC have a significant impact on the overall system performance [32–34]. The system efficacy is greatly impacted by effectively reducing these losses. Various approaches have been developed to promote heat transmission, which may be categorized into three methods [7]:

(i) The *active approach* involves the implementation of external forces, like surface vibration and magnetic fields.
(ii) The *passive method* involves the use of inserts or surface changes on the receiver pipe to improve heat transmission.
(iii) *Compound approach*: This approach uses a mix of passive and active techniques to promote heat transmission.

The passive approach of thermal augmentation is widely used in PTSC, among other methods. The goal is to increase the heat transfer rate from the surface of the receiver pipe to the working fluid [20], resulting in a decrease in the pipe surface temperature. The decrease in temperature reduces heat losses, hence improving thermal performance. In addition, the achievement of a uniform temperature distribution results in a reduction in thermal strain [27]. The thermal strain is associated with the issue of deformation and the presence of significant temperature gradients. The bottom section of the receiving tube experiences increased temperatures as a result of uneven distribution of solar light [35]. This passive technique enhances heat transmission by achieving a homogeneous distribution, improving the heat coefficient, and establishing appropriate pathway for the heat to be received [13]. This technology reduces boundary layer thickness, increasing turbulence [36]. Furthermore, passive technologies operate without the need for an external power source. It only draws energy from inside the system, resulting in an increase in fluid friction [37]. Passive approaches include receiver profile modifications and insertion of inserts inside pipe. Several researchers have conducted extensive experiments on the employment of passive methods to promote heat transmission in the receiver pipe of line-focused PTSC. Researchers have suggested many types of direct inserts, including wavy type, internal fins, porous inserts, twisted type, and perforated plates

etc. Furthermore, the surface modification of the receiver is another way of passive method. The following sections demonstrate the progress made in the standard receiver pipe of PTSC.

2.3 Use of Inserts

This segment discusses the utilization of inserts used in flow channel of receiver. The evaluation has been structured to align with the geometric forms of the inserts, allowing for a clear demonstration of recent advancements. Several academics have conducted computer studies on the increase in heat transmission using inserts. The inserts are strategically placed inside receiver channel to disrupt the normal flow. The numerical studies rely on CFD algorithms, where researchers used several software packages. The numerous inserts may be grouped into four categories. All are discussed in the sub-sections ahead.

2.3.1 Porous/Circular Inserts

These inserts are placed in the fluid pathway of receiver pipe. The increase in heat transfer area and thermal conductivity of inserts [38,39] lead to the reconstruction of the velocity field resulting in improved thermal performance. Various inserts under this category include toroidal rings, porous configurations, and foams of metals.

Ahmed and Natarajan [40] conducted a investigation on the impact of internal toroidal rings. The rings used are shown in Fig. 2.2. They specifically focused on the influence of these rings under totally turbulent flow conditions. Nine distinct insert configurations in the receiver pipe, each characterized by various diameter ratios and pitch sizes were examined.

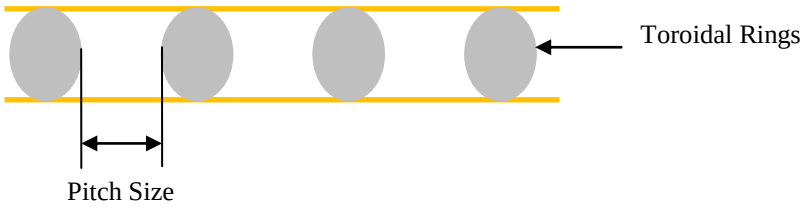

Fig. 2.2: Rings-Toroidal Insert [40]

The analysis was conducted via the finite volume approach, employing the realisable k-ε turbulence model. The model validation was conducted with the Gnielinski

relation [41]. The CFD analysis indicates that diameter ratio of 0.92 and a pitch of 132 mm is most suitable configuration. It was also mentioned that Nusselt number rises by a factor of 1.49 compared to the smooth receiver pipe.

The use of sieve-like arrangements, as seen in Fig. 2.3, is often favoured in the receiver pipe. Ghasemi and Ranjbar [38] conducted a CFD analysis on the PTSC receiver pipe equipped with porous rings insert as seen in Fig. 2.3(a). The study determined that the thermal efficiency improves when porous rings are used. The coefficient of heat transmission rises as the ring size grows and the distance among rings insert decreases. On contrary, increasing the distance among rings insert results in a decrease of friction factor. This is because there are fewer porous rings, which in turn decreases the pressure drop. Furthermore, it was determined that the ideal dimensionless size of the ring [expressed as the division of ring diameter (D_r) to the hydraulic diameter (D)] is 0.8 when the Reynolds number is 30,000 and the spacing (P) between two adjacent rings is 140 mm. The numerical model was validated with the investigations of Gnielinski [41] and Reddy et al. [42].

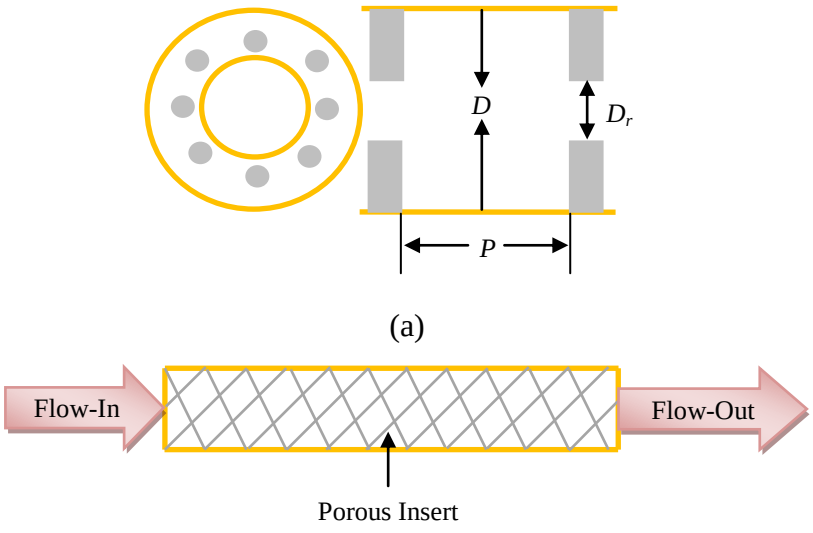

Fig. 2.3: Porous Inserts [38,43]

Another investigation examined the effects of such inserts, as seen in Fig. 2.3(b). Zheng et al. [43] conducted a numerical optimization with GA and FLUENT tools. Analysis conducted in order to determine the estimated thermo-hydraulic performance. The researchers have shown that the most efficient design was attained

at a Reynolds number of 90,000 and 0.951 of porosity value. In order to verify the accuracy of the simulated results, the Sieder-Tate [44] and Gnielinski [41] relations used for the smooth tube (without any insert). The comparison between these equations and the current model revealed a strong agreement. In addition, experimental outcomes of Huang et al. [45] was also used to validate simulated findings for a tube with an insert.

In addition, the receiver pipe of PTSC is examined for the presence of foam type porous inserts. Wang et al. [46] conducted a study using Computational Fluid Dynamics (CFD) to investigate the impact of metal foams, as depicted in Fig. 2.4(a). They examined various positions and layouts of the metal foams and observed that their presence enhanced heat transfer. This enhancement was attributed to the porosity of the foams, which affected thermal conductivity and resulted in the reconstruction of the velocity field. The heat augmentation was greater when metal foam is placed at the top position within a tube with a height-to-diameter ratio of 0.75. However, the most efficient thermo-hydraulic performance was seen when the foam insert was positioned near the bottom of the absorber tube, namely at a height that is 0.25 times the whole height of the tube. The introduction of heat augmentation results in a 45% drop in the maximum temperature differential throughout the tube's circumference, leading to a considerable reduction in thermal stresses. The model validation was conducted with the study of Huang et al. [45].

Kumar and Reddy [47] conducted a numerical investigation on the placement of circumferential metal foam [Fig. 2.4(b)] in the bottom half of pipe. According to investigators, the use of foam inserts is an excellent method for reducing temperature differences and improving the efficiency of heat transmission. A decrease in maximum circumferential temperature differential of around 47% to 72% was seen when comparing it to a smooth case. Furthermore, the greatest increase for net energy efficiency was determined to be 3.71%, while the maximum gain for exergy efficiency was discovered to be 2.32%.

In a particular experimental investigation, Jamal-Abad et al. [48] uses foams of copper, which serves to boost thermal performance. A study was conducted outdoors, following the ASHRAE 93 standard [49], to examine how the use of porous material,

as seen in Fig. 2.4(c), affects the thermal efficiency of PTSC. The research has shown that the placement of copper foam reduces the total heat loss coefficient by 45% compared to a smooth tube [48], resulting into efficiency gain.

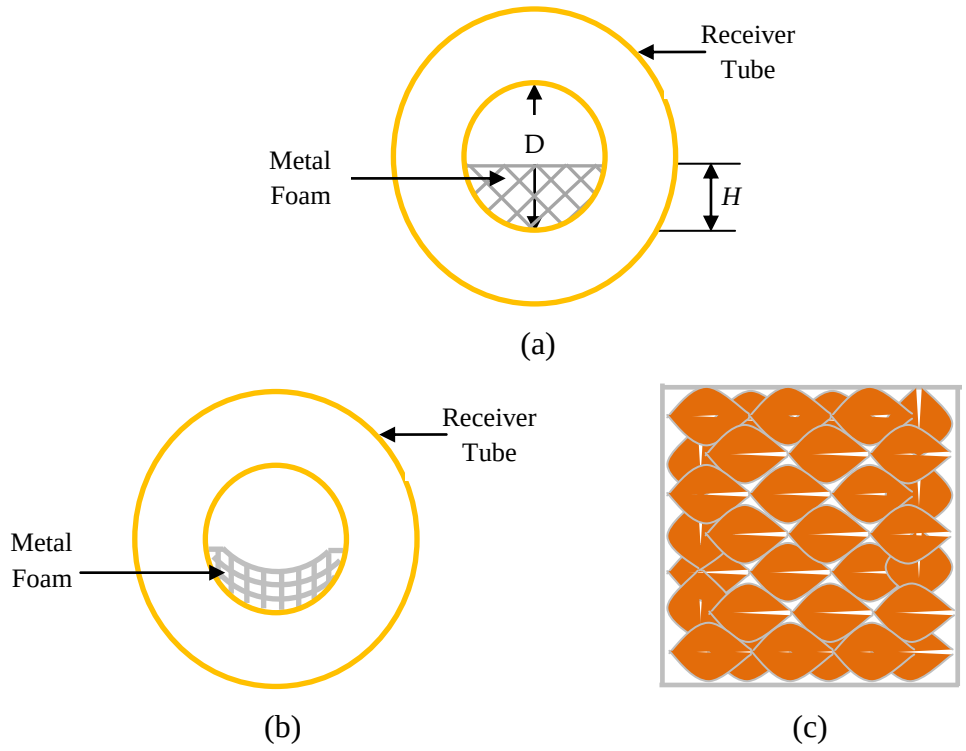

Fig. 2.4: Foams: (a) Metal [46], (b) Circumferential Metal [47], (c) Copper [48]

Valizade et al. [50] examined copper foams of lesser density (10 ppi) and 0.95 porosity. The investigators performed the test outdoors in accordance with ASHRAE 93 [49] guidelines. Three absorber tubes, namely a tube with complete porosity, a tube with partial porosity, and a tube with no porosity, were used. A range of working flow rates from 0.3 L/min to 1.6 L/min with input temperatures from 20°C to 40°C [50], was used. The thermal efficiency improves as the flow rate increases and the inlet temperature decreases. The thermal efficiency increased by 119.6% for semi insert and 171.2% for complete insert. The largest temperature changes observed were 3.3°C, 12.2°C, and 8.8°C, and for foamless, full foam, and half foam conditions respectively.

Kumar and Reddy [51] performed a numerical study on inclined porous discs. It is shown in Fig. 2.5(a). This work determines the most effective design parameters. The research includes five distinct instances for investigation: receiver with complete disc

case, bottom half disc case, top half disc case, alternative disc case and smooth tube case. Under these circumstances, the most favourable configuration was discovered, along with the impact of several characteristics such as the angle, disc height, and the distance among two discs. The validation was done using Dittus-Boelter [52], Sider-Tate [44], and Nasiruddin and Siddiqui [53] correlations. The findings indicate that heat transmission is enhanced as a consequence of improved area for heat transfer, thermal conductivity and turbulence. The top half disc case was determined to be the most effective. It was observed that the height of the said insert should be 0.5 times the hydraulic diameter. The angle of inclination should be around 30°, and the ideal spacing among two discs should be equal to the hydraulic diameter.

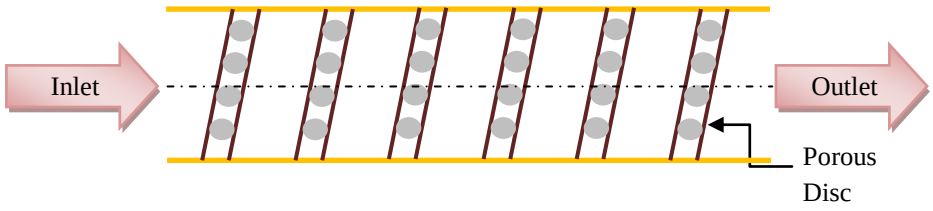

(a)

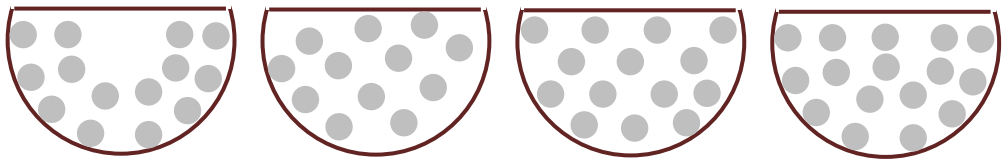

(b)

Fig. 2.5: Porous Discs: (a) Inclined [51], (b) U-Shaped, Inclined, Alternate, Bottom [42]

Reddy et al. [42] conducted an experimental analysis of six different pipe designs using comparable porous disc inserts. Among the six, two were traditional absorber pipes, namely unshielded and shielded ones. Four remaining porous discs were inserted as seen in Figure 2.5(b). A research comparing several factors was given. The receiver has an inner diameter of 54 mm and an external diameter of 60 mm. The size of hole in every discs kept is 5 mm. An experimental research based on the ASHRAE 93-1986 standard [49] was conducted in outdoor situations with varying flux ranging

from 500 - 900 W/m^2. The flow rate ranged from 1.6 L/min to 16.6 L/min. Upon completion of the trial, the alternate porous disc receiver had the most favourable outcome compared to all other categories. The installation of a porous insert clearly leads to an increase in the pumping power demand [42].

Mahmoudi et al. [54] investigated the impact of water, thermal oil and ethylene glycol as well as nanofluids, namely CuO-H_2O and TiO_2-H_2O, on an receiver equipped with perforated ring steps that have a triangular cross-section. It was revealed that the thermal efficiency ranged from 67% - 76.5% when using CuO-H_2O nanofluid (4% particle concentration) flowing through receiver with inserts. The efficiency of the receiver with inserts only, while operating with water as HTF, ranged from 66% - 73%. The model was verified using the Gnielinski correlation [41].

Bozorg et al. [55] conducted a numerical study for receiver equipped with porous material. The working fluid used in the study was a combination of Al_2O_3 and synthetic oil. This study investigates the effects on heat transfer, pressure drop, and thermal efficiency. The findings indicate that when the Reynolds number exceeds 30 $\times 10^4$, the Darcy number is 0.3. Additionally, the heat coefficient improved by 20% and 7%, the pressure penalty enhances by 42% and 42.5%.

Hatami et al. [56] conducted a finite element method (FEM) analysis using FlexPDE software to examine the impact of porosity and nanoparticles. A porous insert is filled leads to formation of semi-circular cavity. The nanofluids employed in this study were water-based and consisted of several volume fractions ranging from 0.02 to 0.08. The nanofluids included copper (Cu), aluminium oxide (Al_2O_3), iron oxide (Fe_3O_4), and titanium dioxide (TiO_2). The copper based nanofluid exhibited the best mean Nusselt number due to its superior thermal characteristics.

Ahmed and Natarajan [57] conducted an energy and exergy study by evaluating the performance of three gaseous fluids: helium, air and carbon dioxide. These fluids were allowed to flow through pipe equipped with toroidal rings insert. According to the findings, helium (He) gas is the most optimal choice in terms of exergetic performance.

2.3.2 Fin Type Inserts

Researchers conducted numerical examinations on several types of fin inserts, as depicted in Fig. 2.6. This segment is dedicated to such studies.

Burak Kurşun [58] conducted a study on the impact of flat and sinusoidal internal longitudinal fins on the thermal efficiency. Fig. 2.6(a) displays the sinusoidal geometrical model. The analysis was conducted via the finite volume method employing the realisable k-ε turbulence model [59].

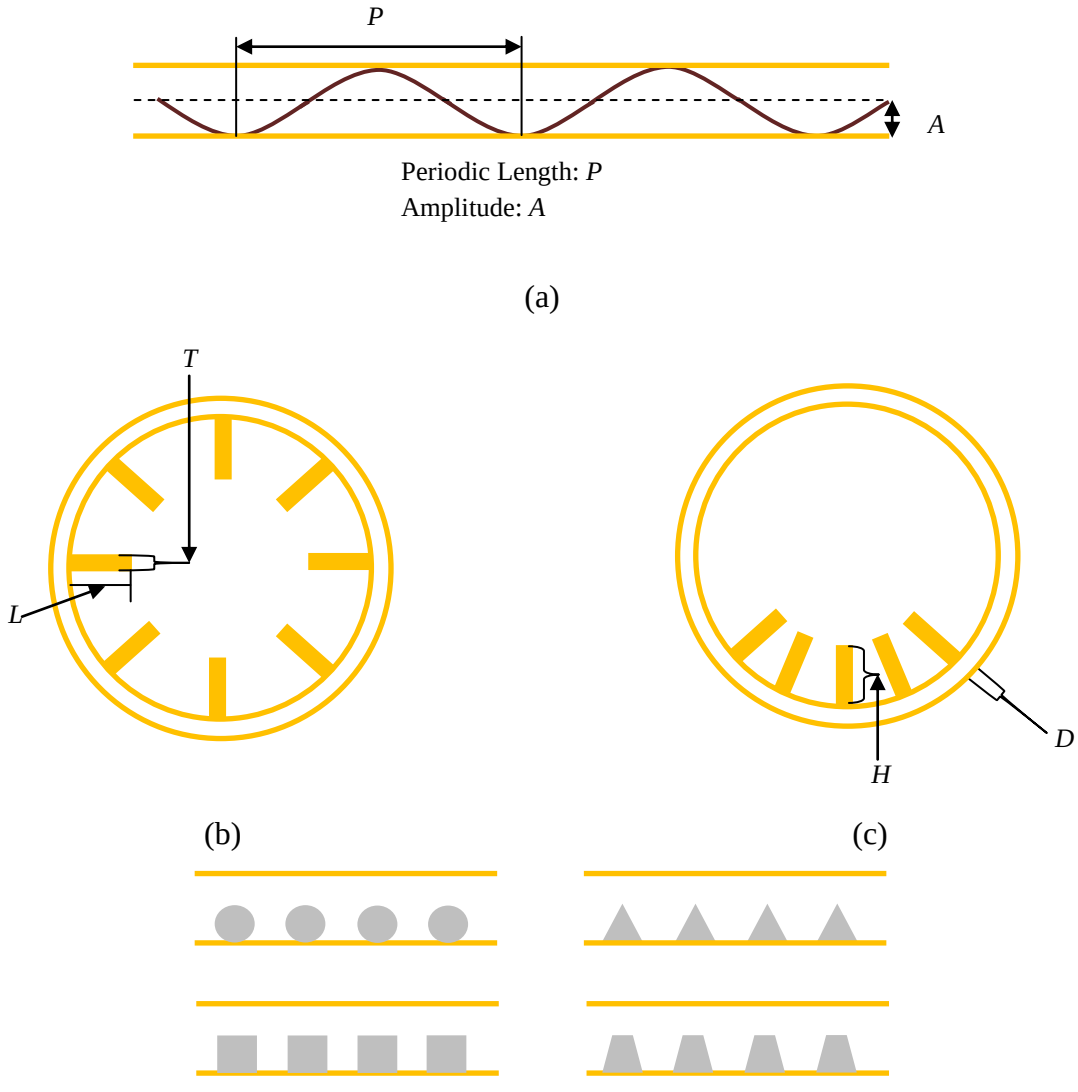

Fig. 2.6: Fin Inserts: (a) Sinusoidal [58], (b) Longitudinal [60], (c) Array: Pin Fin [61], (d) Circular, Triangular, Square, Trapezoidal Porous [39]

The validation was conducted by employing the Petukhov [62] and Gnielinski [41] correlations, as well as referencing previous studies [63,64]. The CFD analysis shows that the Nu increases by 25% for flat fin and by 78% for sinusoidal one.

Bellos et al. [60] investigated internally finned receiver, as shown in Fig. 2.6(b), using the solidworks flow simulation programme. Validation of numerical model is carried out with previous investigation conducted by Dudley et al. [65] and Jensen and Vlakancic [63]. The investigation involved twelve longitudinal fins of varying length and thickness, positioned evenly in eight numbers. The purpose of the research is to determine the optimal fin, resulting in the most efficient operation. The simulated findings indicate that fin geometry having thickness (T) equals to 2 mm and 10 mm length (L); Nu improved by 65.8%. Additionally, the friction factor also enhances by 99.4%.

Zhao et al. [66] executed an experimental study employing air in a internally pin finned receiver tube. The selected fin height is 3 mm and 3.5 mm, with longitudinal pitches of 1 mm and 1.8 mm. An increase in thermal efficiency of 10.4% to 14.5% was seen when comparing to a smooth tube, along with an exergetic boost of 2.55% to 4.29%. The tube with 3.5 mm fin height and an axial pitch of 1.8 mm [66] achieved the maximum exergy efficiency, which was measured at 16.6%.

In a different study, Xiangtao et al. [61] examined a scenario with array of pin fin, as depicted in Fig. 2.6(c), which was positioned at the bottom edge of the absorber where the highest concentration of flux occurs. The study aimed to evaluate the heat transfer efficiency and flow parameters through a CFD-based examination. The numerical results were validated with the results of DISS test facility [67] and by comparing the heat flux distribution with the findings of Hachicha et al. [68]. The objective was accomplished by reducing the temperature gradient around receiver tube and inducing turbulence. The study demonstrates that average Nusselt number (Nu) reaches its maximum value of 9% when the fin height (H) is 2 mm, the diameter (D) is 4 mm, and the Reynolds number is 4036. The optimal number of fins is determined to be 5.

Reddy and Satyanarayana [39] examined the porous fins. The CFD investigation was conducted for four nos. configurations as depicted in Fig. 2.6(d). The study

investigated the optimal geometry under free convective conditions, as well as the impact of different fin factors such as the tip to base thickness ratio and the spacing between neighboring fins. In order to validate, Dittus-Boelter correlation [52] has been used. The simulation findings indicate that the trapezoidal fin configuration achieved the highest level of heat transmission. The most favourable outcomes were achieved when the tip to base thickness of the trapezoidal fin was 0.25 [39]. The appropriate thickness was determined to be 4 mm. The ideal distance between two fins be equal to hydraulic diameter. The heat transfer rate is increased by 13.8% compared to a smooth tube with no inserts when the flow rate is 6.4 kg/s.

In addition, Benabderrahmane et al. [69] conducted an analysis employing various nanoparticles in thermal oil. The study focused on investigating the enhancement of heat transfer using four different nanoparticles (Al_2O_3, Cu, C, SiC) mixed with Dowtherm-A. The mixture is inserted in a longitudinal finned pipe. The findings revealing that 1.6 - 1.85 time's enhancement in friction factor and 1.3 - 1.8 times rise in the Nusselt number. Furthermore, copper based nanofluid and insert together resulted in an enhancement factor ranging from 1.3 to 1.68.

In another investigation conducted by Benabderrahmane et al. [70], CNT were utilized together with Therminol VP-1 in baffles equipped receiver. The study revealed that the use of CNT resulted in a 3.5-fold increase in Nusselt number (*Nu*) to that of smooth absorber.

Bellos et al. [71] conducted a comparison of identical gases running through a finned receiver. The analysis revealed that greatest exergy efficiency for He was determined to be 42.70% when the length of fin was 10 mm. At a fin length of 15 mm, the reported percentages for CO_2 and air were 41.97% and 40.76% respectively. Both of these tests have demonstrated that helium gas exhibits superior performance. Here, the temperature ranging from 500 K - 700 K. However, at elevated temperatures, CO_2 exhibits greater performance [71].

Kasperski and Nems [72] utilize an multiple fin array tube provided with air. The experiment yielded a thermo-hydraulic improvement of 14% and 3.31% when using double & single glass envelope tubes, respectively.

2.3.3 Inserts: Twisted Tape

Being one of the most effective heat transfer enhancers [37], twisted tapes improve the pace and fluid combination while supplying a fluid spinning along the receiver wall [37]. The clearance between tape and walls as well as the twist ratio are crucial factors. The ratio of length to diameter in a single twist is the twist ratio [73]. The heat transmission reduces as the clearance increases, resulting in the creation of bypass flow and reduced fluid rotation. Several inquiries have been conducted utilizing these inserts, which will be addressed in the next sections.

Jaramillo et al. [74] introduced a twisted tape: wall-attached, depicted in Fig. 2.7(a). The investigation encompasses a range of flow rates, from 1 L/min to 6 L/min. The suggested insert has twist ratios of 1, 2, 3, 4, and 5. The study has determined that the thermal performance was improved while using a firmly fitted insert, specifically at lowest twist ratio. The boost happened as a result of an increase in swirl flow, generating turbulence. It is further supported by Borunda et al. [75], where the PTSC performance is examined through the use of identical inserts. The optimization is performed by employing the genetic algorithm technique to assess the efficiency of both the first and second laws.

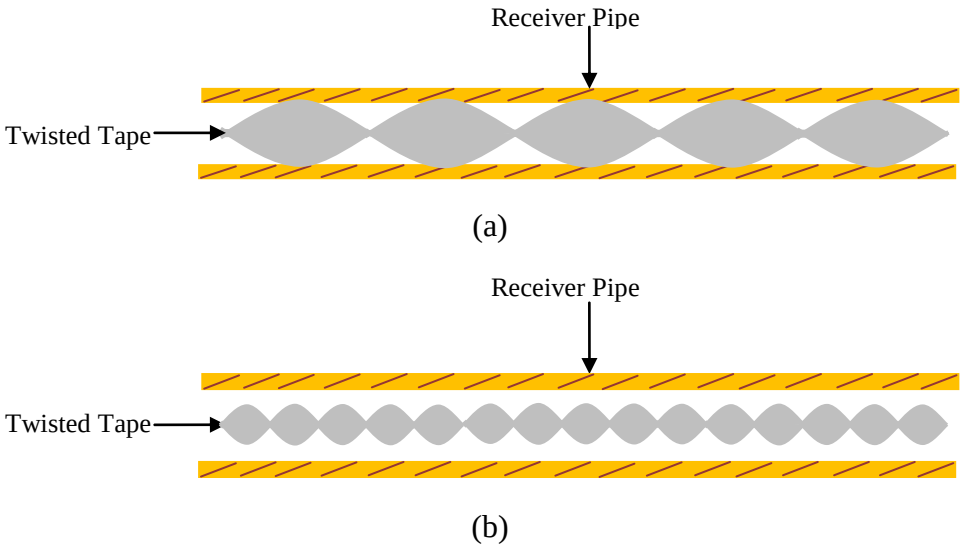

Fig. 2.7: Twisted Tape: (a) Attached with Wall [74], (b) Wall Apart [76]

Mwesigye et al. [76] analyzed another type of twisted tape called wall detached as depicted in Fig. 2.7(b). A CFD analysis was implemented to examine the effects of several twist ratios (0.5-2). The findings reveal that with the reduction in twist ratio,

thermal performance increases. Furthermore, it is stated that the utilization of such inserts results in a decrease of 4 to 68% in the peripheral temperature difference, hence enhancing the thermodynamic efficiency.

Chang et al. [77] also conducted a study using a plain twisted tape, as depicted in Fig. 2.8(a), by numerical analysis. The results once again demonstrate that reducing the twist ratio leads to better heat transmission. However, the friction factor also enhances simultaneously. The ideal twist ratio was determined to be 2.5, whereas the clearance ratio was found to be 0.

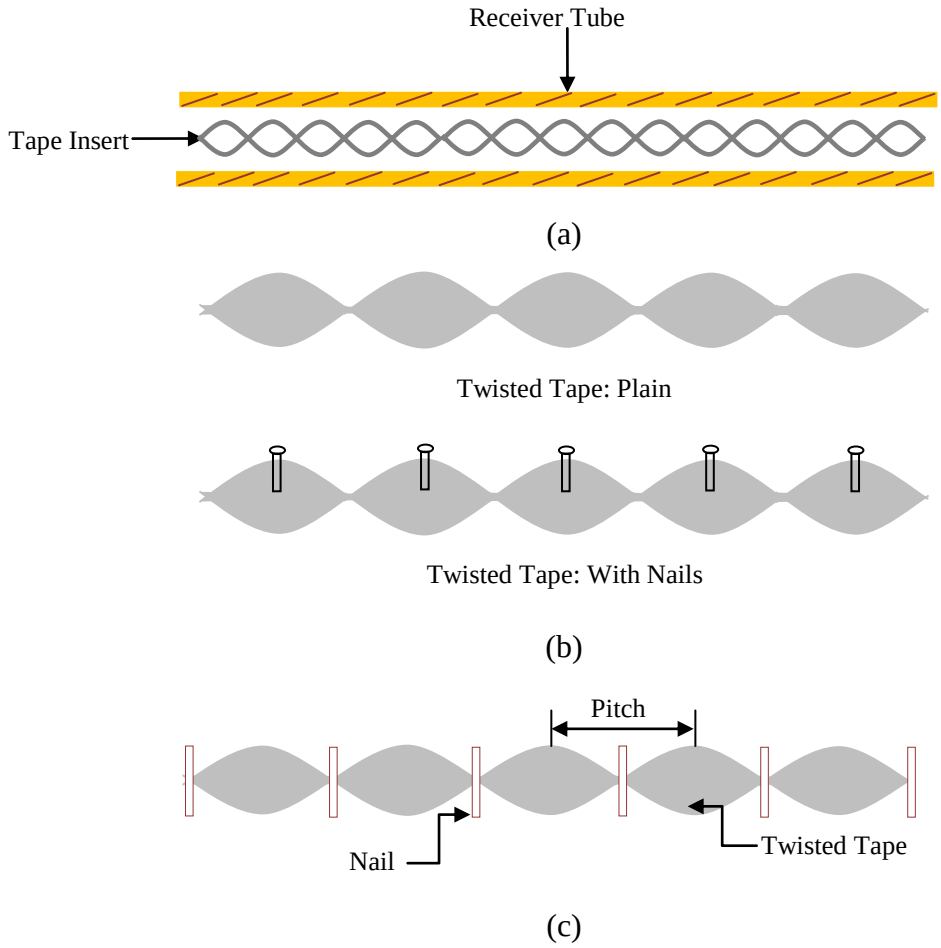

Fig. 2.8: (a) Twisted Tape: Plain [77], (b-c) Twisted Tape: Nailed [73,78]

Jafar and Sivaraman [73] employed nailed twisted tape, as depicted in Fig. 2.8(b), into the receiving tube. An experimental examination was conducted to compare the water heating efficiency under outdoor situations. Three absorbers, namely tube with nail twisted tape, plain twisted taped tube and smooth tube were tested. The collector was exposed to insolation ranging from 350 W/m^2 to 780 W/m^2. It was stated that “using a

twist ratio of 2, the Nusselt number (*Nu*) increases by 10%-15% for plain tape, while the enhancement is 20%-30% for nail type twisted tape". Correspondingly, friction factor is increased by 10.12% for nail type and 9.01% for plain tape.

In addition, Bhakta et al. [78] conducted experimental investigations with headless nail-twisted tape inserts, as depicted in Fig. 2.8(c). The investigators examine the influence of the nail twist pitch ratio. Three distinct ratios (9.042, 6.914 and 4.787) were examined. The most optimal outcomes were observed for the scenario with a twist ratio of 4.787. Furthermore, the aforementioned metrics exhibited similar patterns, with an initial increase at the start of the day, reaching their highest point at midday, and thereafter declining. The greatest total efficiency exhibits a 12.027% improvement in contrast to smooth pipe.

Ghadirijafarbeigloo et al. [79] accomplished a 3D modelling study in which they enhanced the coefficient of heat transfer by employing a perforated louvred twisted tape having twist ratios of 5.33, 4 and 2.67. The perforation is having 30° angle of attack. The optimal twist ratio found was 2.67 at Re: 5000. The proposed insert's configuration is depicted in Fig. 2.9(a).

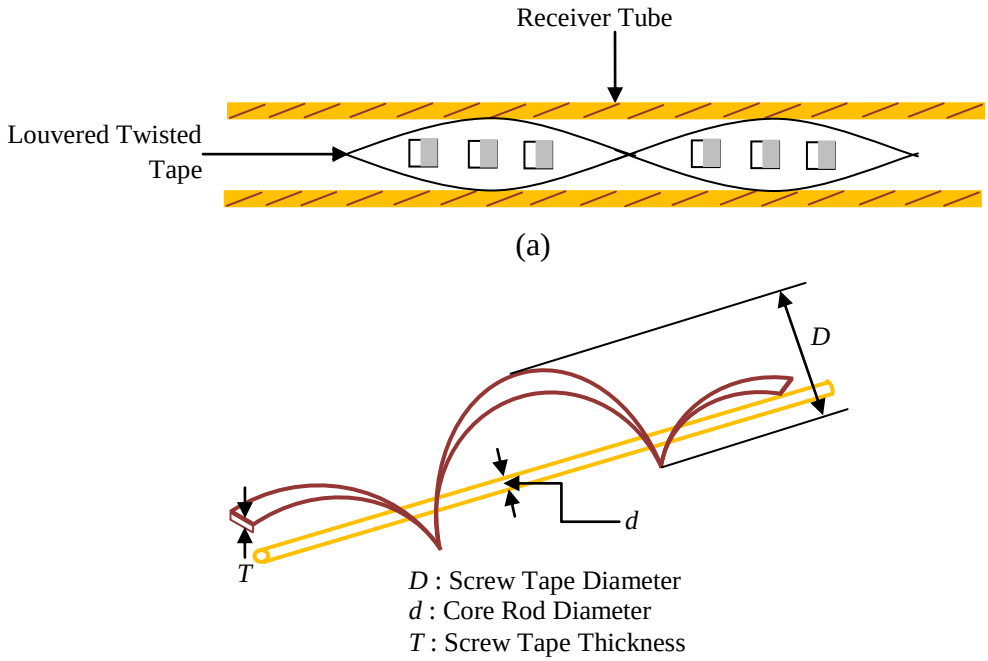

Fig. 2.9: (a) Twisted Tape: Perforated Louvered [79], (b) Screw Tape: Helical [80]

A comparison was made between the results of the suggested insert and a tube deployed with plain twisted tape with equal twist ratios [79]. The study indicated a rise of 37% in the *Nu* (Nusselt number) & 72% enhancement in friction factor. In order to establish the credibility of the simulated outcomes, the authors conducted a validation process by comparing the outcomes with Dittus-Boelter relation [52], Blasius equation [52], and relations of Eiamsa-ard et al. [81].

Song et al. [80] conducted a study on the PTSC absorber tube, specifically focusing on the impact of a twisted insert. The insert used in the study was a helical screw type, as illustrated in Fig. 2.9(b), which was attached to a connecting rod. A computational fluid dynamics (CFD) analysis was employed. The aim is to investigate the impact of solar incidence angle [80] on heat transfer rate and to examine the influence of an insert on this process. The simulated findings show that the transversal angle has a greater impact compared to longitudinal angle. Furthermore, suggested insertion significantly impacts heat loss, reducing it by around 3 to 6 times as compared to a smooth tube. The validation process involved comparing the proposed model with previous research conducted by Gnielinski [41], Dittus-Boelter [52], Petukhov et al. [62] and Eiamsa-ard. S and Promvonge P [82].

Rostami et al. [83] investigated the impact of a hybrid-nanofluid: Cu/SBA-15 on the exergy and energy efficiency with turbulators as inserts. The CFD analysis indicates that there is a reduced enhancement in heat transfer for Reynolds numbers below 3500. In addition, the average Nusselt number increases in comparison to a smooth case. The exergy and energy efficiencies reached their peak values of 5% and 65% respectively during noon hours, surpassing the conventional case by 1% and 2% respectively.

The combined impact of Fe_3O_4-H_2O nanofluid and twisted insert was examined by Bilal et al. [84]. The work demonstrates that the absorber equipped with nanofluid, water + insert, and nanofluid plus insert had significant increase of 56%, 59%, and 63% - 87%, respectively, as compared to the smooth case.

Waghole et al. [85] conducted trials in controlled indoor conditions to study the performance with twisted tape that contained silver-nanofluid. The measurements for efficiency, thermal performance and friction factor were documented. According to

this, the Nusselt number (*Nu*) and friction factor (*f*) rise by a factor of 1.25 to 2.10 and 1.0 to 1.75 respectively [85] compared to a smooth absorber. Furthermore, the test yielded a significant increase in efficiency, ranging from 135% to 205%.

2.3.4 Other Inserts

In addition to the aforementioned investigations, there are a few other studies focused on utilizing direct inserts in the flow channel of absorber tubes to boost thermal performance. These inserts are examined separately in this category since they have different geometrical shapes.

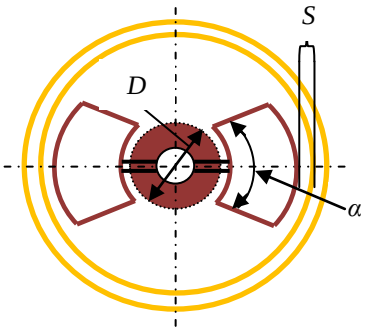

D : Insert's Hollow Diameter
S : Space among Insert and Inner Wall
α : Insert Central Angle

(a)

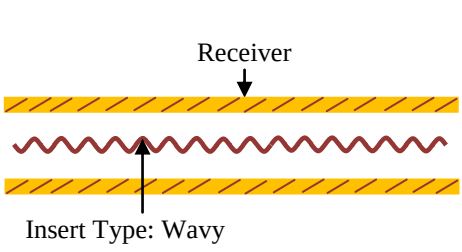

(b)

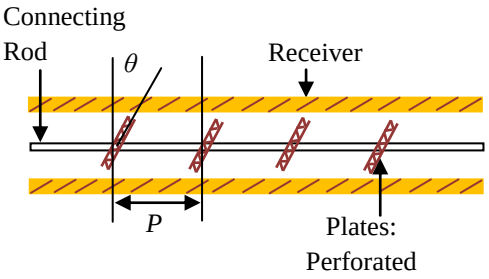

(c)

Fig. 2.10: Inserts: (a) Conical Strip [86], (b) Wavy Type [87], (c) Centrally Placed Perforated Plate [88]

Liu et al. [86] analyzed the impact of conical strip inserts, as depicted in Fig. 2.10(a). An assessment has been conducted on the effects of geometrical elements. The CFD analysis indicates that the Nusselt number (*Nu*) experiences a rise ranging from 45% to 203%, resulting in a maximum reduction in heat loss of 82.1%. As a result, there

was a 5.04% gain in thermal efficiency and a 5.7% improvement in exergetic efficiency. The validation was done with Gnielinski's [41], Petukhov's correlations [62], and Dudley et al. [65] and Deshmukh and Vedula [89] studies.

A CFD study has been conducted by Zhu et al. [87] with the use of a wavy-type insert in the absorber tube of a parabolic trough solar collector (PTSC). The geometric representation of the object is shown in Fig. 2.10(b). The researchers have conducted a comparative investigation, i.e., with and without insert. The use of an insert resulted in a considerable increase in the Nu, ranging from 261% to 310%, which in turn led to a reduction in heat loss by 17.5% to 33.1% within the investigated range.

Mwesigye et al. [88] introduced a design consisting of perforated plates positioned at the centre and attached to a connecting rod (without considering the influence of the rod). This design is illustrated in Fig. 2.10(c). The research conducted focused on three specific geometrical parameters as shown in above figure. The validity of the smooth case was confirmed through extensive literature reviews, including studies by Gnielinski's correlation [41], Petukhov's correlation [62] and Dudley et al. [65].

The aforementioned evaluation was supported by Mwesigye et al. [90] study, in which they conducted multi-objective and thermodynamic optimization utilizing DOE, RSM, GA and CFD. According to reports, there is a decrease in entropy formation when the orientation angle increases at a specific Reynolds number. The application of thermodynamic optimization results in the generation of an optimal Re, which drops as plate size increases and plate separation decreases.

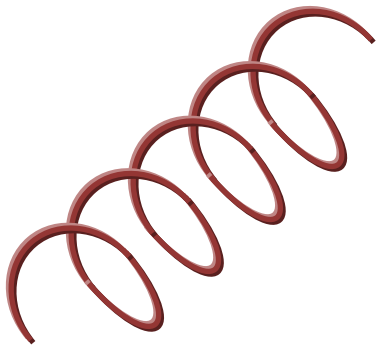

Fig. 2.11: Wire-Coil Insert [91]

Diwan and Soni [91] conducted an numerical investigation of the wire coil inserts depicted in Fig. 2.11. At various flow rate settings (0.01388 kg/s to 0.099 kg/s), the properties of heat transfer and pressure drop were examined. According to this, the Nu increases by 104% - 330% depending on the pitch values of the insert. The optimal pitch value for lower flow rates ranges from 6 mm to 8 mm. However, under greater flow rate conditions, the claimed optimum pitch is 8 mm. Correspondingly, the pressure drop ranges from 55.23 Pa - 1311.79 Pa.

Additionally, Yilmaz et al. [92] performed a computational fluid dynamics (CFD) study utilizing equilateral triangular wire-coil inserts. This investigation resulted in an improvement in thermal efficiency (increased from 0.4% - 1.4%). The study validation is done using the Gnielinski [41], Petukhov [62], and Gunes et al. [93] equations.

Kalidasan et al. [94] performed an experiment for tube equipped with hinged blades, as depicted in Fig. 2.12. The experiment utilized distilled water as the working fluid. The researchers demonstrated that the new absorber tube has an efficiency range of 67.97% - 70.82%, whereas the conventional tube has an efficiency range of 58.77% - 61.70% under same conditions.

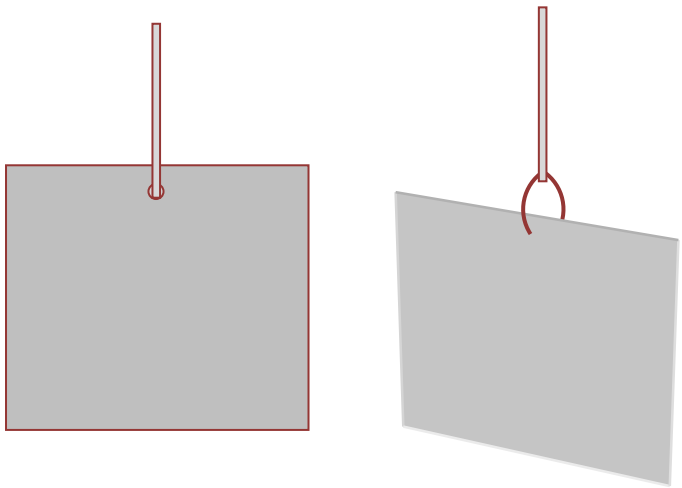

View-Front View: Isometric

Fig. 2.12: Insert: Blade Type [94]

2.4 Surface Modifications of Receiver Pipe

In contrast to direct inserts, this passive technique for improving heat transmission modifies the PTSC receiver pipe's wall profile. This implies that rather than employing a smooth surface for the reception tube, a typical pipe designs with non-uniform cross-sectional areas are utilized. This technique is utilized to optimize heat transfer efficiency, a concept that has been extensively studied and supported by researchers, as outlined below:

Li et al. [95] conducted a study on the design of a linear cavity receiver with an arc form, as depicted in Fig. 2.13(a). Effect of variables such as aperture width, inclination angle, arc emissivity and surface temperature on heat loss was investigated. Copper alloy, known for its exceptional thermal conductivity, was chosen as luncate channel [95]. It was stated that "radiation losses were mostly influenced by the temperature and emissivity of the collecting surface". Additionally, the inclination angle has a significant effect on free convection losses. It was additionally mentioned that the impact of aperture width on thermal losses is directly related. In order to demonstrate the dependability of the simulated outcomes, validation is conducted using the literature by Yasuaki et al. [96].

Huang et al. [97] examine the 'dimpled receiver tube', as shown in Fig. 2.13(b). CFD analysis was conducted on the impact of dimple's depth. The results suggest that dimple's at lower portion significantly contributes to thermal rise. The impingement impact and reattachment in the top dimple are observed to be insufficient [20]. Nevertheless, side dimples redirect the fluid in an upward direction. An increase in the Nusselt number ranging from 1% to 21% was seen for dimples with a high depth of 0.007 m. In contrast, for dimples with a depth of 0.001 m, the enhancement was limited to 18%. For deep dimples, the friction factor ranges from 1% to 34%, whereas for shallow dimples, it can reach up to 28%. The proposed model was validated using the Gnielinski equation [41].

Munoz and Abanades [98] analyzed the internal helical finned receiving tube, as depicted in Fig. 2.13(c). This study utilized a CFD programme for investigation. The numerical model was verified using existing literature [44]. Following code validation, a comparison was conducted between the proposed receiver tube and the

traditional tube of PTSC. The investigators have determined that increasing the number of fins and their helix angle leads to an increase in pressure loss. Nevertheless, thermal losses and a decrease in temperature gradient result in an increase in thermal efficiency.

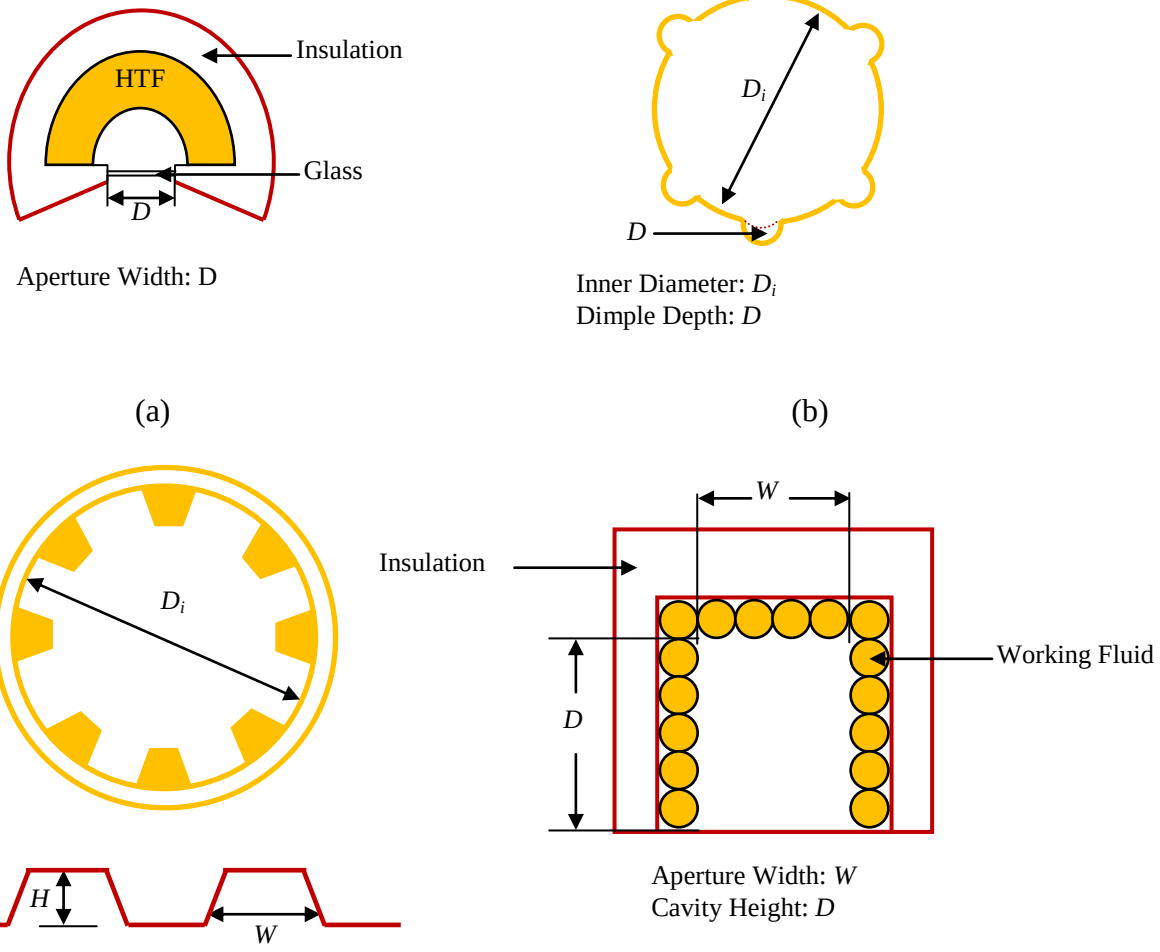

Fig. 2.13: Receiver: (a) Arc Type Cavity [95], (b) Dimpled [97], (c) Internal Finned: Helical [98], (d) Rectangular Type Cavity [99]

Loni et al. [99] conducted a computational analysis on a rectangular cavity receiver, as depicted in Fig. 2.13(d). An analysis was conducted for parameters as shoen in figure. Study indicates that cavity position should be situated precisely along the parabolic focal line. Moreover, the optimal aperture width is equal to the depth of the

cavity and is 5 mm, which is also the optimal diameter for the cavity tube. The highest recorded efficiency was 77.26%, with heat value of 618.09 W. The validation is conducted with Kasaeian et al. [100].

Bellos et al. [64] presented a study that focused on altering the peripheral surface. The study specifically examined a situation involving a receiver tube with a converging-diverging design. Fig. 2.14(a) displays the surface of the tube. The model dimensions were chosen according to the commercial IST-PTC specifications. The study demonstrates a 4.55% enhancement in the average efficiency through the alteration of the receiver tube. Nevertheless, there was a decrease in pressure, ranging from 160 Pa to 330 Pa. The research explicitly stated that "the improvement happened under high temperature conditions". Therefore, they recommended this modification specifically for high temperature applications.

Akbarzadeh and Valipour [101] conducted an experimental investigation on the helical corrugated pipe seen in Fig. 2.14(b) in outdoor conditions. The purpose here was to examine the impact of height and pitch. The PTSC thermal performance and exergy efficacy are enhanced by reducing the pitch and increasing the corrugation height. The thermal and exergy efficiencies reached their highest values at 65.8% and 7.97%, respectively.

Fuqiang et al. [102] examined asymmetric outward convex corrugated pipe, as depicted in Fig. 2.14(c). They established an optical-thermal-structural technique to investigate the efficiency of heat transport and the thermal stress. Several approaches viz. Monte Carlo ray tracing, FVM and FEA were employed. The examined model was compared to the DISS facility [67] and Hachicha et al. [68]. The study determined that the overall heat transfer performance factor increased by 148% and the highest Von-Mises strain was 26.8% [102].

Biswakarma et al. [103] conducted an analysis for Al_2O_3-water nanofluid in a internal helical grooved receiver. When the volume concentrations of nano-particles grow from 3% - 8%, there is a corresponding 14.5% increase in pressure drop. In addition, as the Re increases, the pressure drop and heat transfer coefficient also increases by 76.5% and 41.3% respectively. It was also found that the maximum enhancement was achieved at a concentration of 8% Al_2O_3, resulting in a 9% improvement.

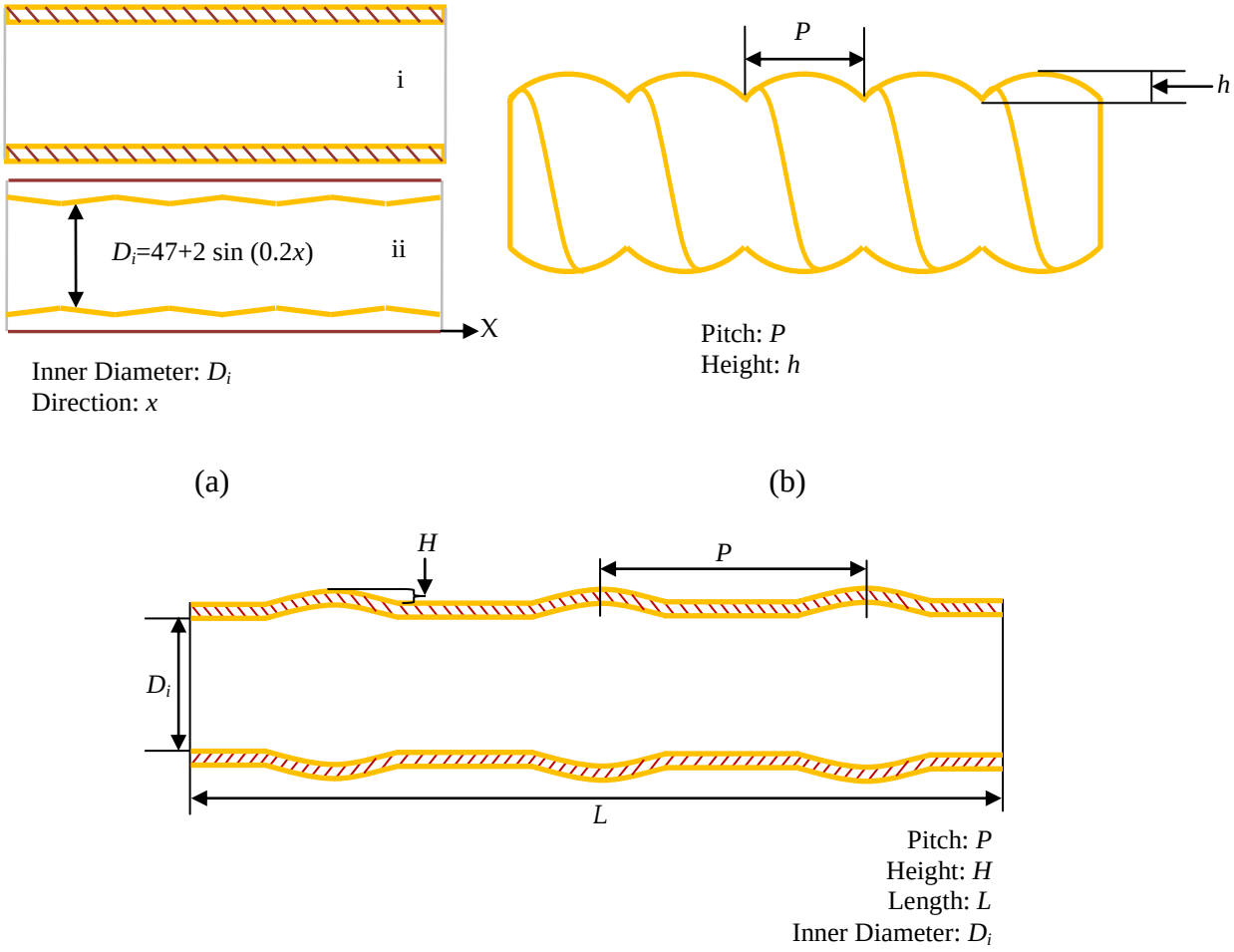

Fig. 2.14: Receiver's: (a) (i) Smooth, (ii) Converging-Diverging [64]**,** (b) Helical Corrugated [101], (c) Asymmetric Outward Convex Corrugated [102]

2.5 Comparison of Investigations

Using a passive technique is an effective method for enhancing heat transmission by creating turbulence inside the receiver tube of PTSC. Pertaining to shape, arrangement, and orientation, turbulators-also known as surface modifiers or inserts-used in PTSC can take on a variety of shapes. The heat transfer improvement mechanisms within the receiver region are thoroughly analyzed in the aforementioned sections. Tables 2.1 to 2.3 display the comparison of the several tactics discussed in the preceding sections.

Table 2.1: Comparison of Insert Based Numerical Studies

Insert Kind	Dimension: Insert	Receiver Dimension (mm) Outer Dia. (OD), Inner Dia. (ID), Length (*L*)	Fluid	Flow Conditions / *Re*	Optimum Findings	
					Thermal Efficient	Energy Efficient
Circular Toroidal Rings [40]	Dia. Ratio : 0.88 - 0.94, Size of Pitch (mm) : 132 - 264	OD : 70, ID : 66, *L*: 7800	Syltherm 800	Turbulent	Diameter ratio : 0.88; Pitch size : 132 mm; Increase in *Nu* : 2.33 times	Diameter ratio : 0.92; Pitch size : 132 mm; *TEF* : 1.20; Increase in *Nu* : 1.49 times
Porous Rings [38]	Thickness (mm) : 3, Dia. (mm) : 42 - 63	OD : 76, ID : 70, *L* : 2000	Syltherm 800	30×10^3 – 251×10^3	*Re* : 30 x 10^3 and for 56 mm insert diameter, *TEF* : 0.78	
Porous [43]	Porosity : 0.975, 0.967, 0.951	OD : 70, ID : 66	Steam	5×10^4 – 9×10^5	66% - 68%: energy conversion efficiency	*TEF* : 2.72: *Re* : 9 x 10^5; Porosity : 0.951
Foams : Metal [46]	Porosity : 0.9132, 0.9546, 0.9726 , Height (mm) : 0 - 54	OD : 70, ID : 54	Steam	Turbulent	*TEF* : 1.1 - 1.5, increase in friction factor : 400 - 700 times: Height of insert : 40.5 mm; Increase in *Nu* : 10 - 12 times	*TEF* : 1.4 to 3.2; increase in friction factor : 10 - 20 times; Height of insert : 13.5 mm; Increase in *Nu* : 5 - 10 times
Metal Foams [47]	Porosity : 0.9132, 0.9546, 0.9726	OD : 70, ID : 50	Steam	0.1 kg/s - 1 kg/s	Maximum gain in exergy efficiency : 3.71%; Increase in *Nu* : 10 times	Maximum gain in exergy efficiency : 2.32%; *TEF* increases 5 times

Inclined Porous Disc [51]	Thickness (mm) : 2, Distance Between Two Porous Discs Distance (mm) : 49.5 - 132, Height (mm) : 14.52 - 49.5	OD : 70, ID : 66, *L* : 2000	Therminol-VP1	31845 – 254765	Insert inclination : 30°; Distance between porous discs : 66 mm; *Nu* increase : 64.2% at *Re* : 31845 alongwith 457 Pa pressure penalty; Insert height : 33 mm	
Longitudinal Fins with Sinusoidal Lateral Surfaces [58]	Periodic Length (mm) : 10 - 14, Length (mm) : 7800 , Amplitude (mm) : 2 - 6	OD : 70, ID : 66, *L* : 7800	Syltherm 800	2×10^4 – 8×10^4	Max. increase in *Nu* : 78% for sinusoidal & 25% for flat fin	*TEF* : 0.85 to 2.32; Periodic length : 10 mm; Amplitude : 2 mm
Fins : Internal [60]	Length (mm) : 5 - 20, Thickness (mm) : 2 - 6	OD : 70, ID : 66, *L* : 7800	Syltherm 800	50 L/min. - 250 L/min.	*Nu* increase : 1.652 times, friction factor: doubled; Compared to smooth tube, 0.82% enhancement occurred	*TEF* : 1.317 at inlet temperature : 600 K & flow rate : 150 L/min. ; Fin Thickness : 2 mm ; Fin Length : 10 mm
Fin Array : Pin [61]	-----	OD : 70, ID : 67, *L* : 4060	Thermal Oil D12	1979.5 - 11151.6	For insert height : 2 mm, insert diameter : 4 mm, increase in average *Nu* = upto 9%	Compared to smooth pipe, increase in *TEF* = upto 12% for insert height : 2 mm, insert diameter : 4 mm
Porous Fins [39]	Thickness (mm) : 2 - 8	OD : 70, ID : 66, *L* : 2000	Therminol-VP1	Turbulent	Trapezoidal fin, *h* : 400 to 2100 W/m^{2}K along with Δp : 50 - 1850 Pa; Fin thickness : 4 mm	
Twisted (Wall Fitted) [74]	Twist Ratio : 1 - 5	OD : 25.4, ID : 23.2, *L* : 4880	Water	1350 - 8350	Thermal efficiency : 39% - 65%; Twist ratio : 1	Exergy efficiency : 28% - 44%; Twist ratio : 1

Twisted (Wall Fitted) [75]	Twist Ratio : 1 - 5	OD : 25.4, ID : 23.2, *L* : 4880	Water-Liquid	1 - 6 L/min.	Twist ratio : 1	
Twisted (Wall Separated) [76]	Thickness (mm) : 1, Width Ratio : 0.53 - 0.91, Twist Ratio : 0.5 - 2.0	OD : 70, ID : 66, *L* : 7800	Syltherm 800	10260 - 1353000	Thermal efficiency increases : upto 10%	Maximum reduction in entropy generation rate : 58%; *TEF* : 0.74 - 1.27
Twisted [77]	Clearance Ratio : 0 - 1, Twist Ratio : 2.5 - 41.7, Thickness (mm) : 0 & 1	OD : 24, ID : 20, *L* : 1000	Molten Salt	7485 - 30553	*Nu* increase: 2.9 times & friction factor increase: 2.5 times than smooth pipe, Twist ratio : 2.5	
Perforated Louvered Twisted [79]	Length and Width (mm) : 10, Twist Ratio :5.33, 4, 2.67 Thickness (mm) : 0.9	ID : 17, *L*: 1000	Behran Thermal Oil	5×10^3 - 25×10^3	*Nu* increase: 150%, friction factor increase: 210%, Twist ratio : 2.67	Increased *TEF* : 26%
Screw Tape : Helical [80]	Core Rod Dia. (mm) : 5, Length of 1 Twist (mm) : 18 , Dia. (mm) : 17, Thickness (mm) : 1	OD : 25	Dowtherm-A	10×10^3 - 80×10^3	Pressure loss increases from 4 - 23 times at inlet temperature : 373 K	
Strips : Conical [86]	Central Angle : 40° - 90°, Pitch Ratio : 0.5 - 2	OD : 70, ID : 66, *L* : 7800	Syltherm 800	5×10^3 - 791×10^3	*Nu* increases by 45% - 203%, thermal efficiency increase: 0.02% - 5.04%; friction factor : 6.17 - 17.44 times	Max. increase in exergetic efficiency : 5.7%, *TEF* : 0.70 - 1.33; Max. reduction in entropy generation rate : 74.2%

Wavy [87]	Amplitude (mm) : 3.2, Width (mm) : 28.55, Pitch (mm) : 128	OD : 70, ID : 67, *L* : 4096	Syltherm 800	7.20×10^4 - 2.16×10^5	Friction factor increases by 382% - 405%, *Nu* increases by 261% - 310%	Entropy generation rate : reduces by 30.2% - 81.8%, *TEF* : 2.11 - 2.43 times
Perforated Plate : Centre [88]	Spacing (mm) : 40 - 200, Orientation : -30° - 30°, Porosity : 0.65, Dia.(mm) : 30 - 60 ,	OD : 70, ID : 66, *L* : 7800	Syltherm 800	1.02×10^4 - 7.38×10^5	friction factor increases: 1.40 - 95 times: Thermal efficiency enhances : 1.2% - 8%; *Nu* increases : 8% - 133.5%	Max. reduction in entropy generation rate : 52.7%; *TEF* : 0.44 - 1.05
Wire Coils [91]	Mean Dia. (mm) : 17, Pitch (mm) : 6 - 20, Wire Dia.(mm) : 1.2	OD : 26.5, ID : 19.5, *L* : 250	Water-Liquid	0.01388 - 0.0999 kg/s	*Nu* increase : 104% - 330%, max. friction factor : 12.6%; Pitch : 6 mm - 8 mm	
Equilateral Triangular Wire Coils [92]	Pitch (mm) : 76, 114, 152, Width (mm) : 30, 33, 36,	OD : 80, ID : 76	Therminol-VP1	15×10^3 - 11.6×10^5	Avg. increase in friction factor : 14.41 times ; Avg. *Nu* increases : 183%	Max. decrease in entropy generation rate : 100%; *TEF* : 0.68 - 0.82

Table 2.2: Experimental Investigations Comparison having Inserts

Insert Kind	**Dimensions: Insert**	**Receiver Dimension (mm) Outer Dia. (OD), Inner Dia. (ID), Length (*L*)**	**Fluid**	**Flow Conditions**	**Outcomes**
Foam : Copper [48]	Density : 30 ppi Porosity : 0.9	OD : 28, *L* : 1280	Water-Liquid	0.5 L/min. - 1.5 L/min.	Overall eff. : 45% -55%; Overall loss coefficient decreases by 45%

Metal Foam : Copper [50]	Density : 10 ppi Porosity : 0.95	OD : 26, ID : 22, *L* : 1400	Water-Liquid	0.3 L/min. - 1.6 L/min.	Thermal efficiency complete porous : increases by 171.2%; for semi porous : 119.2%; Friction factor : 126 times for complete porous and 60 times : for semi porous; Overall efficiency : 49.42% - 60.23%
Porous Discs [42]	Porosity : 0.3 and 0.5 Thickness : 2 mm	OD : 60, ID : 54, *L* : 3000	Therminol and Water	100 L/h - 1000 L/h	Alternate porous disc is optimal arrangement: efficiency lies in the range of 61.18% - 69.03%; Max. ΔP at 1000 L/h as 550 Pa; Overall efficiencies : 63.9% - 66.66%
Fin: Pin Type [66]	Height : 3 mm, 3.5 mm, Axial Pitch : 1 mm, 1.8 mm	OD : 40, ID : 36, *L* : 8000	Air	40 Nm^3/h - 130 Nm^3/h	fin height : 3.5 mm, fin pitch : 1.8 mm; overall collector efficiency : 10.4%-14.5% higher, exergy efficiency : 2.55%-4.29% higher; Pressure penalty 10 - 20 times more
Twisted Insert: Nail [73]	Twist Ratio : 2, 3, 5	OD : 12.5, ID : 12, *L* : 2000	Water-Liquid	*Re*: 710 – 2130	Twist ratio : 2, Nu increases by 20% -30%; At *Re* : 2130, friction factor : 10.12%; efficiency increases by 27%; Overall collector efficiencies : 70%-80%
Twisted: Nail [78]	Thickness : 1.2 mm, Width : 20 mm, Twist Ratio : 4.787, 6.914, 9.042,	OD : 25, ID : 23, *L* : 1220	Water-Liquid	----	Nail twist ratio : 4.787; Max. overall efficiency enhances by 12.027%; Max. instantaneous efficiency : 61.639%-64.280%
Hinge Blade [94]	Height : 7 mm, Pitch : 50 mm, Drill Holes : 2 mm, Length : 7 mm	OD : 15, ID : 14, *L* : 1500	Water-Distilled	0.89 L/min - 1.22 L/min	Thermal efficiency : 69.33% (9.05% more than smooth); Overall efficiency lies : 67.97% - 70.82%

Table 2.3: Comparison of Studies Involving Modified Receiver (Surface Modifications) Pipe

Receiver Type	Geometrical Parameters Outer Dia. (OD), Inner Dia. (ID), Length (*L*)	Fluid	Flow Condition	Outcomes
Linear Cavity (Lunate Channel) [95]	OD : 140 mm, ID :100 mm	-----	Laminar	Optimum width of aperture : 50 mm - 70 mm
Dimpled [97]	ID : 27 mm, Dimple Depth : 1 mm and 7 mm *L* : 20 mm Thickness : 7 mm	Therminol-VP1	Turbulent	*Nu* increases : 1% - 21%; friction factor increases : 1% - 34%
Helical Finned [98]	ID : 66 mm, *L* : 7795 mm, Helix Angle : 16°, 25° Fin Height : 2 mm	Syltherm-800	0.68 kg/s - 0.71 kg/s	Efficiency increases : 3%; 2% increase in plant performance
Cavity: Rectangular [99]	Dia. : 5 mm, 10 mm, 25 mm	Thermal Oil	30 ml/s, 210 ml/s, 530 ml/s	Optimal dia. = 5 mm; Max. thermal efficiency : 77.26%; Max. absorbed heat : 618.09 W
Converging - Diverging [64]	OD : 51 mm, ID : 47 mm, *L* : 6100 mm	Thermal Oil	Turbulent	Avg. efficiency improvement : 4.55%; ΔP : 160 Pa - 330 Pa; Exergy efficiency : 7% - 35%
Corrugated : Helical [101]	OD : 28 mm, ID : 25 mm, *L* : 2000 mm, Corrugated Pitch : 3 mm, 5 mm, 7 mm, Corrugation Height : 0.5 mm, 1 mm, 1.5 mm	Water-Liquid	5×10^3 - 10×10^3	Optimum corrugation pitch = 3 mm and height = 1.5 mm, thermal efficiency : 61.7% - 65.8%; max. exergy efficiency : 7.97%; Friction factor increases : 35.5% - 84.8%
Convex Corrugated : Asymmetric Outward [102]	OD : 70 mm, ID : 67 mm, *L* : 4060 mm	D12 Thermal Oil	Turbulent	At pitch/dia. : 1.11, *Nu* increase : 59%; Max. *TEF* : 2.48 at Re : 67,120

2.6 Research Gaps

The receiver tube is a critical component of parabolic trough solar collectors, playing a central role in the conversion of solar energy into thermal energy. Despite extensive

research, several keys gaps remain in the understanding and optimization of receiver tubes for enhanced thermal performance:

(i) Research on receiver tube geometries has primarily focused on traditional cylindrical designs, with minimal exploration of alternative shapes that could enhance heat transfer and reduce thermal losses. Advanced geometries, such as corrugated or grooved surfaces, may offer significant improvements in thermal performance but have not been extensively studied. The potential of these novel designs to improve the efficiency of solar energy capture and transfer remains underexplored, particularly under varying operational conditions.

(ii) Over the past decades, solar energy research has used location specific tools and techniques to optimize the performance. System operation enhancement requires the regression model to assess or optimize the performance. In the reported literature above, no such work has been found where findings are utilized to develop model using RSM (response surface methodology). RSM uses statistical design to establish an improved operational parameter for achieving optimized design in specified trials.

(iii) It is also established from literature survey that impact of double corrugations on receiver's surface of parabolic trough solar collector has not been examined in the past. The extensive study using double corrugated receiver pipe has not been carried out.

Addressing these research gaps will be critical in advancing the development of energy efficient receiver for parabolic trough solar collectors, ultimately contributing to more effective solar energy systems.

2.7 Objectives of the Present Study

The primary objective of this thesis is to investigate and develop modified receiver tube for parabolic trough solar collector that enhances the thermal performance. To achieve this, the research has been focused on the following objectives;

1. Design and development of modified receiver tube for solar parabolic trough collector.
2. Thermo-hydraulic performance analysis of developed receiver tube for solar parabolic trough collector.
3. To compare the performance of new receiver tube with conventional plain tube of solar parabolic trough collector.

2.8 Summary of the Chapter

This chapter covers the different studies taken for improving the heat transmission through receiver of parabolic trough solar collector. The usage of inserts and customized receiver surfaces boost heat transfer, generates secondary flows and improvised heat transfer area. From above, it can be stated that passive method is an effective technique of heat transfer enhancement for parabolic trough solar collector.

CHAPTER 3

METHODOLOGY

3.1 Introduction

The literature review found that one of the feasible strategies of enhancing convective heat transfer is the deployment of passive techniques in the PTSC receiver pipe. The objective of this is to increase the heat transfer rate from the receiver pipe to the working liquid. A better thermal performance is the end consequence of this temperature drop since less heat is wasted. Furthermore, the bottom part of the receiver pipe becomes hotter due to the uneven concentration of solar radiation. A more consistent distribution is achieved by the passive techniques of heat transmission. Passive techniques for thermal enhancement include changing the receiver's profile or inserting direct inserts or turbulators in the fluid flow path. Although inserts may increase turbulence intensity and thereby heat transfer, they are more material intensive. In addition, compared to methods that include surface alteration, the pressure drop associated with inserts is much higher. Consequently, the alteration of the PTSC receiver pipe's shape is much more practical. Previous research indicates that extensive investigations have been conducted to assess the impact of modifications. Various configurations of receiver's wall modifications have been examined. Nevertheless, the assessment of double corrugations on receiver surface (symmetrical convex-concave corrugations) has been largely overlooked. This study addresses the research gap by investigating PTSC receiver having several arrangements of double corrugations.

3.2 Physical Model

A CFD (computational fluid dynamics) based analysis has been conducted to evaluate the thermal-hydraulic performance of the receiver pipe by considering different geometric characteristics. The characteristics of corrugation design such as pitch (P), height (e), and flow rate are varied in order to assess the performance under non-uniform heat flux condition. A comparative analysis has been conducted between a

modified receiver pipe and a regular (smooth/conventional) receiver pipe. The schematic design for receiver pipes alongwith PTSC is shown in Fig. 3.1. Here, it is seen that the concentrator redirects solar energy onto the pipe positioned at the focal axis of the concentrator. The heat transfer fluid is allowed to flow through the receiver. The receiver pipe of 316L steel is having an configurations [65] with exterior diameter of 70 mm, inner diameter of 66 mm, and 7.8 m length. Fig. 3.1 (c) shows the schematics of double corrugated receiver pipe. The corrugation design consists of corrugation pitches varied as 4 mm, 6 mm, 8 mm, and 10 mm, and 1.5 mm, 2 mm, and 2.5 mm are the corrugation heights. The receiver wall has double (symmetrical convex-concave corrugations) that extend longitudinally and come into contact with the working fluid. The detailing of receiver pipe alongwith working fluid is shown in Tables 3.1 and 3.2.

Table 3.1: Pipe Geometrical Characteristics [104]

Particulars	**Detail**	
	Smooth	**Double Corrugated**
Material	316L Steel	316L Steel
Inner Diameter (D_{ri})	66 mm	66 mm
External Diameter (D_{ro})	70 mm	70 mm
Length (L)	7.8 m	7.8 m
Height of Corrugations (e)	-----	1.5 mm, 2 mm, 2.5 mm
Pitch of Corrugations (P)	-----	4 mm, 6 mm, 8 mm, 10 mm

Table 3.2: Thermo-Physical Characteristics

Parameter	**Detail**	
	Receiver Pipe [58]	**Heat Transfer Fluid** [59]
Type	316L Steel	Liquid-Water
Specific Heat	0.50248 kJ/kg-K	4.182 kJ/kg-K
Thermal Conductivity	24.92 W/m-K	0.6 W/m-K
Density	8030 kg/m^3	998.2 kg/m^3
Dynamic Viscosity	-----	0.001003 kg/m-s

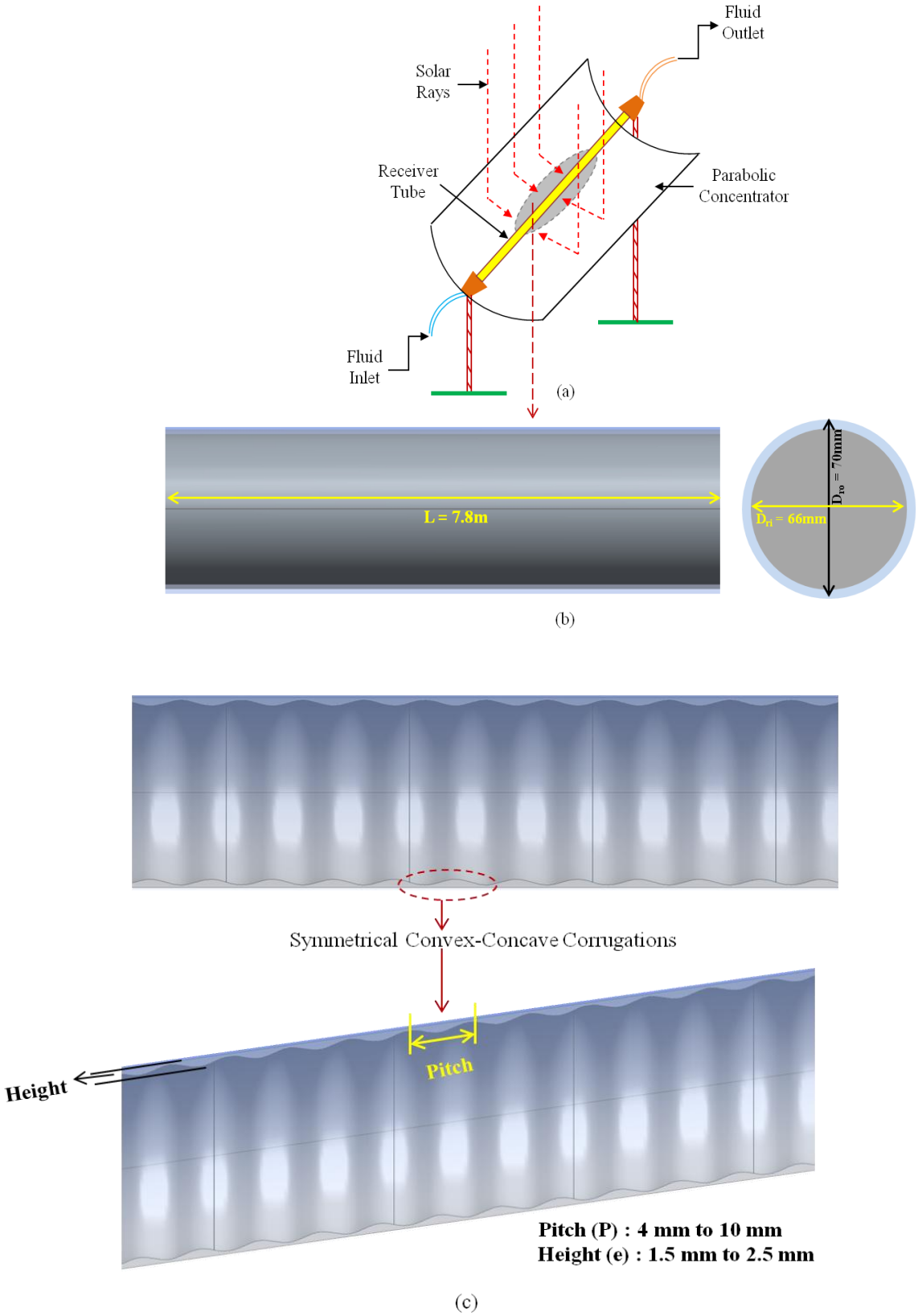

Fig. 3.1: Configurations: (a) PTSC, (b) Smooth, (c) Double Corrugated

The thermal-hydraulic performance of receiver has been evaluated for non-uniform heat flux condition and varying flow rates. For which, Nusselt number, pressure drop (friction penalty) and thermal enhancement factor (*TEF*) have been used to assess the impact of corrugation design. The velocity variations, pressure variations, and turbulent kinetic energy are also used to present the thermal characteristics.

3.3 Principal Equations

The investigation is carried out for both turbulent flow and steady state conditions. There are several different formulas [59] involved, which are as follows:

Continuity equation:

$$\frac{\partial}{\partial x_i}(\rho u_i) = 0 \tag{3.1}$$

Momentum equation:

$$\frac{\partial}{\partial x_j}\left(\rho u_i u_j\right) = -\frac{\partial P}{\partial x_i} + \frac{\partial}{\partial x_j}\left[\mu\left(\frac{\partial u_i}{\partial x_j} + \frac{\partial u_j}{\partial x_i}\right) - \frac{2}{3}\mu\frac{\partial u_i}{\partial x_i}\delta_{ij} - \rho\overline{u_i' u_j'}\right] \tag{3.2}$$

Energy equation:

$$\frac{\partial}{\partial x_j}\left(\rho u_j c_p T\right) = -\frac{\partial}{\partial x_j}\left(K\frac{\partial T}{\partial x_j} + \frac{\mu_t}{\sigma_{h,t}}\frac{\partial (c_p T)}{\partial x_j}\right) + u_j\frac{\partial P}{\partial x_j} + \left[\mu\left(\frac{\partial u_i}{\partial x_j} + \frac{\partial u_j}{\partial x_i}\right) - \frac{2}{3}\mu\frac{\partial u_i}{\partial x_i}\delta_{ij} - \rho\overline{u_i' u_j'}\right]\frac{\partial u_i}{\partial x_j} \tag{3.3}$$

In this equation, ρ is the density of the fluid, time-averaged velocities in the *i* and *j* directions are represented as u_i, and u_j, x_i and x_j are spatial coordinates, averaged pressure is denoted by *P*, *T* is its averaged temperature, thermal conductivity is presented as K, viscosity is denoted by μ, $-\rho\overline{u_i' u_j'}$ are the Reynolds stresses, and δ_{ij} is rate of linear deformation tensor (1/s). Further,

$$-\rho\overline{u_i' u_j'} = \left[\mu_t\left(\frac{\partial u_i}{\partial x_j} + \frac{\partial u_j}{\partial x_i}\right) - \frac{2}{3}\mu_t\frac{\partial u_k}{\partial x_k}\delta_{ij} - \frac{2}{3}\rho k\delta_{ij}\right] \tag{3.4}$$

In this case, *k* represents turbulent kinetic energy (*TKE*) expressed per unit mass. It can be determined by,

$$k = \frac{1}{2}(\overline{u'^2} + \overline{v'^2} + \overline{w'^2}) \tag{3.5}$$

As a result of the implantation of SST k-ω turbulence model, two more equations of 'turbulent kinetic energy (*k*)' and 'dissipation rate (*ω*)' are there and provided as follows:

k-equation:

$$\frac{\partial}{\partial x_i}(\rho k u_i) = \frac{\partial}{\partial x_j}\left(\Gamma_k \frac{\partial k}{\partial x_j}\right) + \widetilde{G_k} - Y_k \tag{3.6}$$

ω-equation:

$$\frac{\partial}{\partial x_i}(\rho \omega u_i) = \frac{\partial}{\partial x_j}\left(\Gamma_\omega \frac{\partial \omega}{\partial x_j}\right) + G_\omega - Y_\omega + D_\omega \tag{3.7}$$

Where,

$$\Gamma_k = \mu + \frac{\mu_t}{\sigma_k} \tag{3.8}$$

$$\Gamma_\omega = \mu + \frac{\mu_t}{\sigma_\omega} \tag{3.9}$$

are the 'effective diffusivities' of turbulent kinetic energy (*k*) and specific dissipation rate (*ω*).

Here, μ_t is 'turbulent viscosity' and is expressed as;

$$\mu_t = \frac{\rho k}{\omega} \frac{1}{\max\left[\frac{1}{\alpha^*}, \frac{SF_2}{\alpha_1 \omega}\right]} \tag{3.10}$$

To further elaborate, the 'turbulent Prandtl numbers' for *k* and *ω* are denoted by σ_k and σ_ω. Additionally, the model coefficient and model constant are denoted by α^* and α_1, respectively. The blending function is denoted by F_2, and the modulus of the mean rate of strain tensor is denoted by *S*. As the production of specific dissipation rate (*ω*) and turbulent kinetic energy (*k*) are represented by G_ω and $\widetilde{G_k}$ respectively, the dissipation of specific dissipation rate (*ω*) and turbulent kinetic energy (*k*) are represented by Y_ω and Y_k respectively. The cross-diffusion term is denoted by D_ω. These all are given as;

$$G_\omega = \frac{\alpha_\infty}{\nu_t} \widetilde{G_k} \tag{3.11}$$

$$\widetilde{G_k} = \min\left(\mu_t S^2, 10\rho\beta^* k\omega\right) \tag{3.12}$$

$$Y_\omega = \rho\beta_i \omega^2 \tag{3.13}$$

$$Y_k = \rho\beta^* k\omega \tag{3.14}$$

$$D_\omega = 2(1 - F_1)\rho\sigma_{\omega,2}\frac{1}{\omega}\frac{\partial k}{\partial x_j}\frac{\partial \omega}{\partial x_j} \tag{3.15}$$

Where, $\sigma_{\omega,2}$ is model constant, β^*, α_∞, β_i are model coefficients, and F_1 is blending function, for those SST k-ω theory gives, $\sigma_{\omega,2}$ = 1.168, β^* = 0.09, α_∞= 0.52, and β_i = 0.075.

3.4 Boundary/Thermal Conditions

Fig. 3.2 provides a visual representation of the various boundary conditions that are utilized in the surrounding area of the receiver pipes.

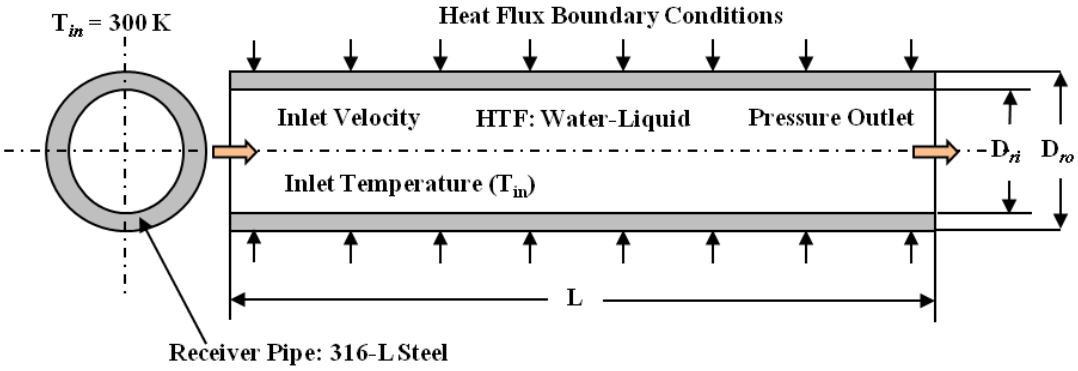

Fig. 3.2: Receiver Pipe with Boundary/Thermal Conditions

(i) At inlet: the temperature of HTF (heat transfer fluid) is T_{in} = 300 K, and the inlet velocity corresponds to *Re*, which can range from 5×10^3 to 50×10^3.

(ii) Outlet boundary condition: The usage of a zero pressure gradient.

(iii) On the receiver pipe wall: to the inlet and outlet faces adiabatic condition is applied, and the no-slip condition is applied to the solid surfaces that are in the fluid domain. In addition, the heat flow boundary condition, which is depicted in Fig. 3.3, is administered in the following manner at the receiver outside surface:

(a) The top half portion of the pipe is exposed to I_b (W/m^2) = *DNI* value;

(b) The bottom half portion of the pipe is provided with $CR \times I_b$ (W/m^2).

Here, *CR* is the concentration ratio and is equals to 22.74 [65], *DNI* is the direct normal irradiance, solar irradiance of a town named as Sundernagar (longitude 76.8889°E, latitude 31.5299°N), Himachal Pradesh, India received on 31st March, 2021 [105]. Both conduction-convection losses from the receiver's wall has been neglected because of the vacuumed cover glass [46,58,97]. Like earlier studies [46,58,97], radiation heat loss from the receiver is disregarded as the focus of present investigation is on the maximization of heat transfer performance.

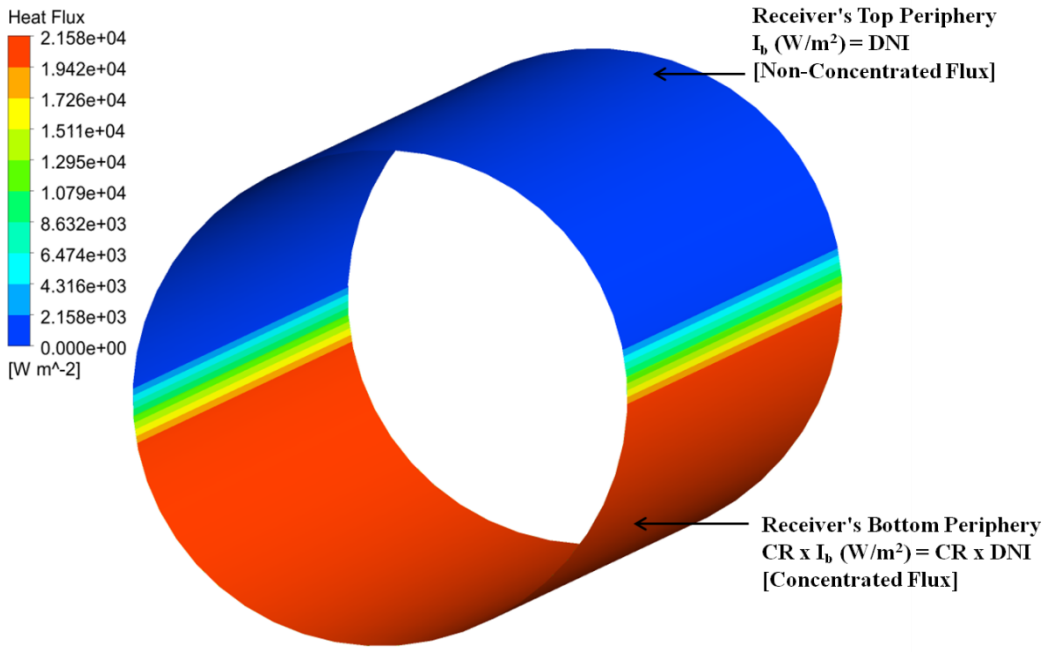

Fig. 3.3: Heat Flux Boundary Condition

(iv) Symmetrical boundary condition has been used about the vertical plane since the model geometry is symmetrical.

3.5 Solar Radiation Data

The local radiation data is used to apply the boundary conditions for the heat flux. It pertains to Sundernagar, District Mandi, Himachal Pradesh, India (longitude 76.8889°E and latitude 31.5299°N). The Solcast PT30M radiation data set for March 31, 2021 [105] is used. The Sun's variation for the chosen day is shown in Fig. 3.4, where it can be seen that the its intensity rises from 0800 hours to midday, then progressively rises till 1400 hours and falls sharply from 1400 hours to 1800 hours.

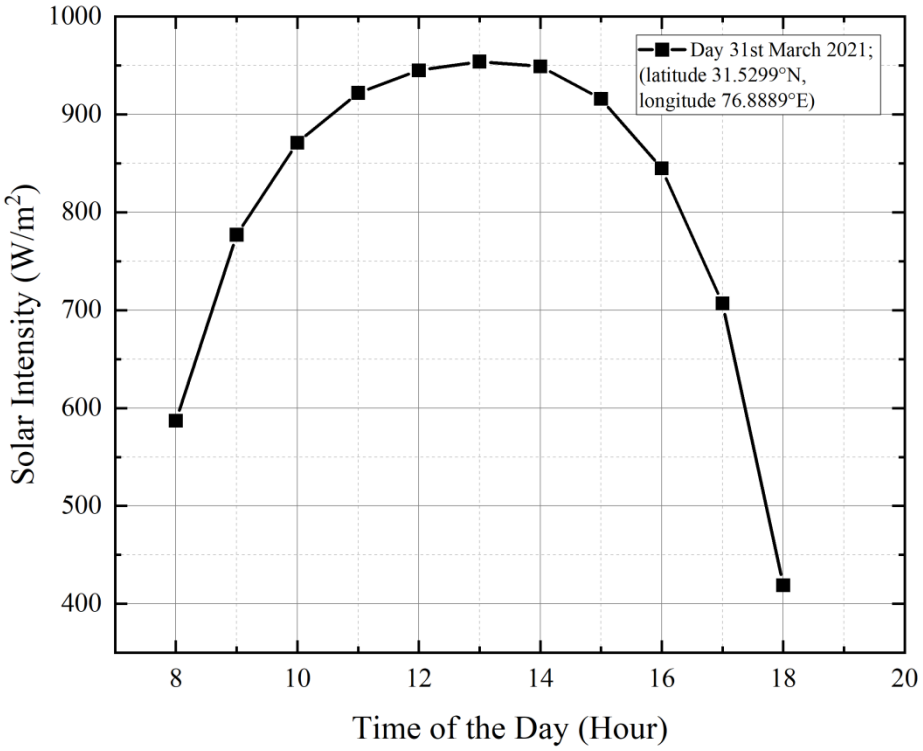

Fig. 3.4: Solar Intensity Variation [105]

3.6 Data Reduction

In the present study, the impact of various heat conditions and flow rates on the parabolic trough's receiver pipe is examined. It entails assessing a number of parameters [52], as listed below;

Reynolds number (*Re*) [52] is determined by

$$Re = (\rho V D_{ri})/\mu \tag{3.16}$$

Here, D_{ri} is inner diameter of pipe (serves as hydraulic diameter) and V is velocity of fluid.

The turbulent intensity (I) for fully developed pipe flow is given by [59]

$$I = 0.16\mathrm{Re}^{-(1/8)} \tag{3.17}$$

To evaluate the dimensionless Nusselt number (*Nu*) [52], use

$$Nu = (hD_{ri})/K \tag{3.18}$$

Where, h is convection coefficient [52]and is

$$h = q/(T_{wall} - T_{bm}) \quad (3.19)$$

Here, the average inner wall temperature of the receiver is T_{wall}, average heat flux on the receiver wall is q, T_{bm} is the average fluid temperature.

Further, the friction coefficient (f) is obtained as;

$$f = 2\Delta p D_{ri}/\rho V^2 L \quad (3.20)$$

To evaluate the thermal-hydraulic performance of receiver, an indicator known as the thermal enhancement factor (*TEF*) is used, expressed as;

$$TEF = (Nu/Nu_S)/(f/f_S)^{1/3} \quad (3.21)$$

3.7 Summary of the Chapter

Table 3.3 presented below depicts the summarized form of methodology and tools utilized to carry out the present investigation;

Table 3.3: Methodology/Tools Used

Objective	Step	Tool
Design and development of modified receiver tube for solar parabolic trough collector	Designing/ Modeling of conventional (smooth) receiver tube and modified receiver tube	3D Modeling Software-ANSYS Design Modeler
Thermo-hydraulic performance analysis of developed receiver tube for solar parabolic trough collector	Effect of varying flow rates and thermal conditions on thermo-hydraulic performance	Numerical investigation using software ANSYS FLUENT. In addition, optimization of corrugation design has been carried out using response surface methodology (RSM) technique
To compare the performance of new receiver tube with conventional plain	Comparative analysis between conventional (smooth) and	A performance evaluation criterion [thermal enhancement factor (*TEF*)] has been adopted

tube of solar parabolic trough collector	modified receiver tube

CHAPTER 4

HEAT TRANSFER & HYDRAULICS FOR DOUBLE CORRUGATED RECEIVER PIPE

4.1 Introduction

The abundant and continuous availability of sunlight serves as an environment friendly and inexhaustible source of energy, offering a clean and sustainable fuel resource. An optimal method for harnessing solar energy is to transform it into thermal energy through the use of solar collectors, which is both straightforward and very effective for varied purposes. A concentrated solar power (CSP) system is one that makes use of solar energy in order to transform it into different types of energy that may be used including thermal energy. Among CSP's systems, parabolic trough is the most economical and economically feasible CSP technology for medium-temperature applications [31]. In this, the receiver pipe is an essential component since it is responsible for absorbing the solar radiation that is coming in and converting it into thermal energy that can be used. Processing and utilization of the solar heat is very important to the economic sustainability of this system [2]. The total performance of the system is significantly impacted by the losses that occur from the receiver pipe [13]. Effective reduction of such thermal losses increases the effectiveness of the system. The passive method of thermal enhancement is one of the many strategies [20] that have been created for the purpose of effectively absorbing and dissipating heat. It is the goal of this endeavour to enhance the heat transmission from the wall to heat transfer fluid, resulting in a reduction of pipe's surface temperature. This decrease in temperature reduces the amount of heat that is lost, which ultimately results in an improvement in thermal performance [17]. Additionally, since the concentration of solar light is non-uniform, the bottom half portion of the receiver pipe acquires a higher temperature. The implementation of passive method helps in creating a uniform distribution of temperature by enhancing the heat coefficient [47]. Both, the alteration of the receiver's profile and implementation of inserts in the flow channel are considered to be passive strategies

for thermal augmentation. Insert insertion and receiver wall geometric alteration are both passive methods. Inserts may enhance heat transmission by increasing turbulence intensity; however this comes at the price of higher material consumption. Another way for improving PTSC thermal performance is receiver pipe modification. Furthermore, the pressure drop is substantially larger with insert deployment than that of surface modification case. As a result, geometric modification of PTSC receiver pipe is much more feasible. Prior studies show that a significant work has been carried out to examine the impact of different changes to PTSC receiver pipes. Different pipe profiles have been studied. However, the influence of double (symmetrical convex-concave) corrugations has received no attention. The present study bridges this research gap by examining the various kinds of PTSC receivers. This chapter presents the heat transfer and hydraulic characteristics of double corrugated receiver pipe. To fulfill the desired objective, a CFD investigation has been conducted with the use of software package ANSYS FLUENT v 19.3. Various corrugation parameters such as pitch (P), height (e) and flow rate, all varied to get the best form and flow properties. A comparison of modified receiver pipe has also been carried out with that of conventional receiver pipe having smooth wall surface.

4.2 Simulation Technique

For the purpose of solving the mathematical equations associated with the model, a commercially available CFD tool known as “ANSYS FLUENT 19” has been used. For the purpose of solving the governing equations, ‘SST k-ω turbulence model’ has been implemented. This is because to its greater accuracy in estimating flow separation and unfavourable pressure when compared to the k-ε model. [80,106]. When it comes to the momentum and turbulent kinetic energy equations, second order upwind approach is used to discretized the convective variables. Pressure, is discretized using the second order scheme. A discretization of the energy equation is also accomplished by the use of the second order upwind approach. In addition, SIMPLE algorithm is used to discretized the pressure-velocity coupling. Further, the interface between the pipe surface and fluid domain as a coupled interface before the initialization process begins. The convergence criteria for momentum equations, continuity equation, turbulent dissipation rate, and turbulent kinetic energy are

established in the residuals conditions on the order of 10^{-5}. Additionally, higher order of 10^{-8} is utilized for the energy equation. These criteria are utilized in order to get exact conclusions. It has been determined that the convergence has been achieved within the range of residual values mentioned above.

4.3 Grid Creation and Grid Independent Test

For each of the instances that are being investigated in this study, a hybrid mesh is being constructed. A tetrahedral type mesh/grid is employed to represent the fluid domain within the pipe, while a receiver pipe is provided with hexahedral type grid/mesh. The density of the grid is enhanced in the areas of the receiver that are located near the interior wall. Incorporating inflated layers in close proximity to the contact region between the pipe and the fluid is a necessary step in the process of creating the fine mesh. This makes it possible for the wall $y+$ average value to remain continuously close to 1. The grid structures that were used for the receivers that are being considered are shown in Fig. 4.1. Furthermore, a grid independent test has been performed on both kinds of receivers, which are referred to as smooth and modified receivers. The data is acquired in terms of Nusselt number (Nu) and friction factor (f) values. The determined data during this analysis for various grid sizes are displayed in Table 4.1. It has been determined by the aforementioned study that the cases number 3 and 4 exhibit the least amount of variance in Nu and f, which is indicative of grid/mesh independence. This is the case for both types of pipe receivers. Because of this, mesh 3 has been selected as the final grid for future testing in order to reduce computational time and cost.

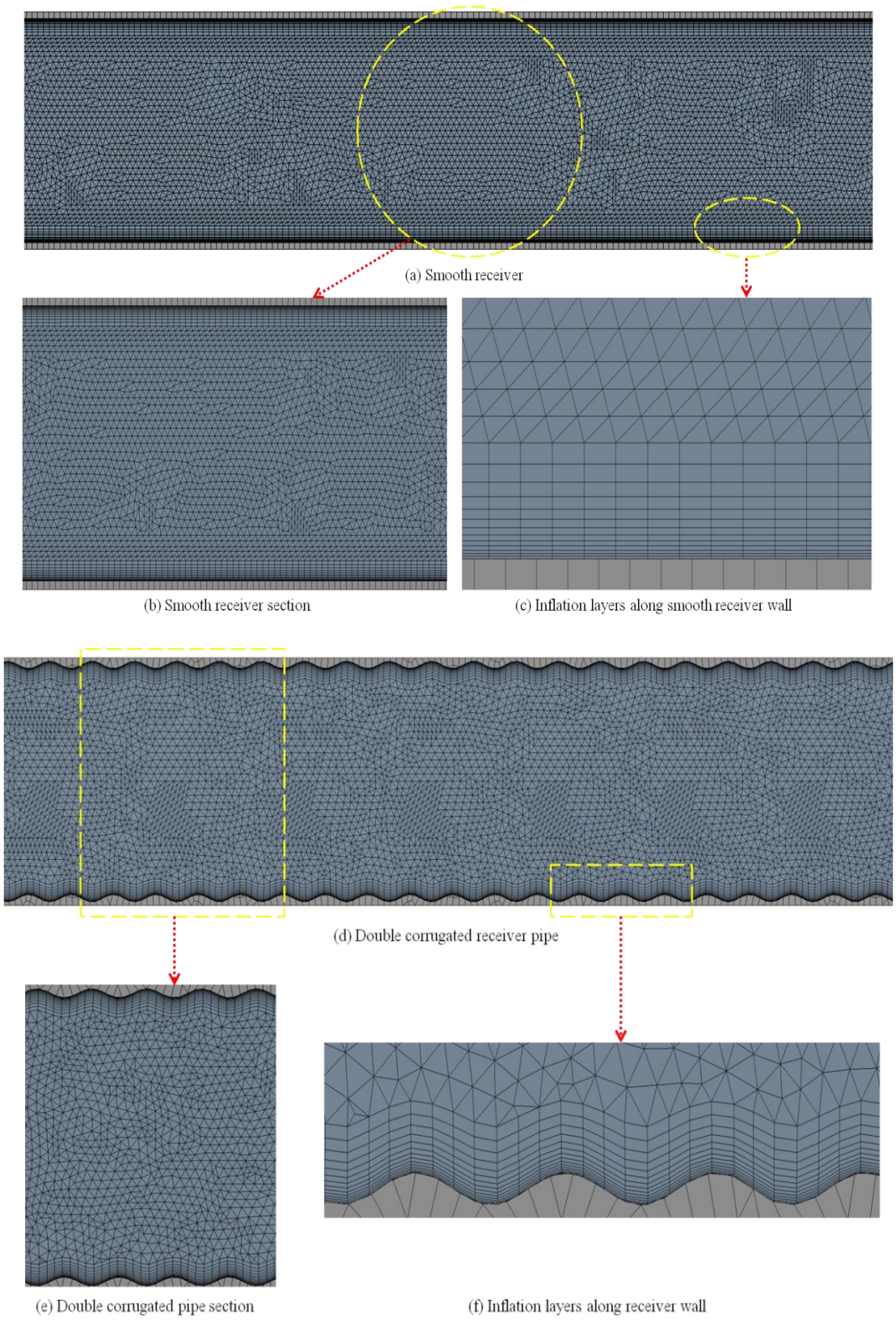

Fig. 4.1: Grid Domains for: (a-c) Smooth Case, (d-f) Modified Case

Table 4.1: Grid Independent Test (T_{in} = 300 K, Re = 4 × 10^4, I_b = 1000 W/m^2)

Pipe	Mesh / Grid No.	Elements Count	Nu	$\left\|\frac{Nu_{i+1}-Nu_i}{Nu_i}\right\|$ %	f	$\left\|\frac{f_{i+1}-f_i}{f_i}\right\|$ %
Smooth	1	755769	265.776	---	0.023107	---
	2	1277750	261.071	1.770	0.022524	2.523
	3	1431724	260.027	0.399	0.022406	0.524
	4	2316401	259.025	0.385	0.022394	0.054
Double Corrugated	1	1329949	319.86	---	0.062093	---
	2	2863367	331.793	3.731	0.061330	1.229
	3	3419201	333.843	0.618	0.060147	1.929
	4	5587732	334.376	0.159	0.059295	1.417

4.4 Model Validation

The current work involves the model validation in two distinct phases. The initial stage involves validating the implemented model by comparing it to the existing correlations in literature [41,52,62]. The relations employed for comparison are

Gnielinski's relation [41]: $Nu = [(f/8)(Re - 1000)Pr]/[1 + 12.7(f/8)^{0.5}(Pr^{2/3} - 1)$ (4.1)

Dittus-Boelter relation [52]: $Nu = 0.023Re^{0.8}Pr^{0.4}$ (4.2)

Petukhov relation [62]: $f = (0.79lnRe - 1.64)^{-2}$ (4.3)

Filonenko relation [52]: $f = (1.79logRe - 1.55)^{-2}$ (4.4)

A plot is created to compare the values of Nusselt number and friction factor. Nusselt numbers derived from computational analysis are being compared to the Gnielinski and Dittus-Boelter relations [41,52] within the analyzed *Re* range. Fig. 4.2 (a) displays the comparison curve, indicating the mean deviation among *Nu* values. It has been observed that for the current CFD model average deviation with Gnielinski and Dittus-Boelter relations is 5.96% and 7.06% respectively. In addition, the friction factor values obtained from the CFD analysis are compared to the correlations developed by Filonenko [52] and Petukhov [62]. According to Fig. 4.2 (b), the average deviation using Filonenko's correlation is 3.80%, whereas using Petukhov's

correlation, it is 3.25%. These data demonstrate that the current numerical model aligns well with turbulent relations, affirming its reliability and consistency.

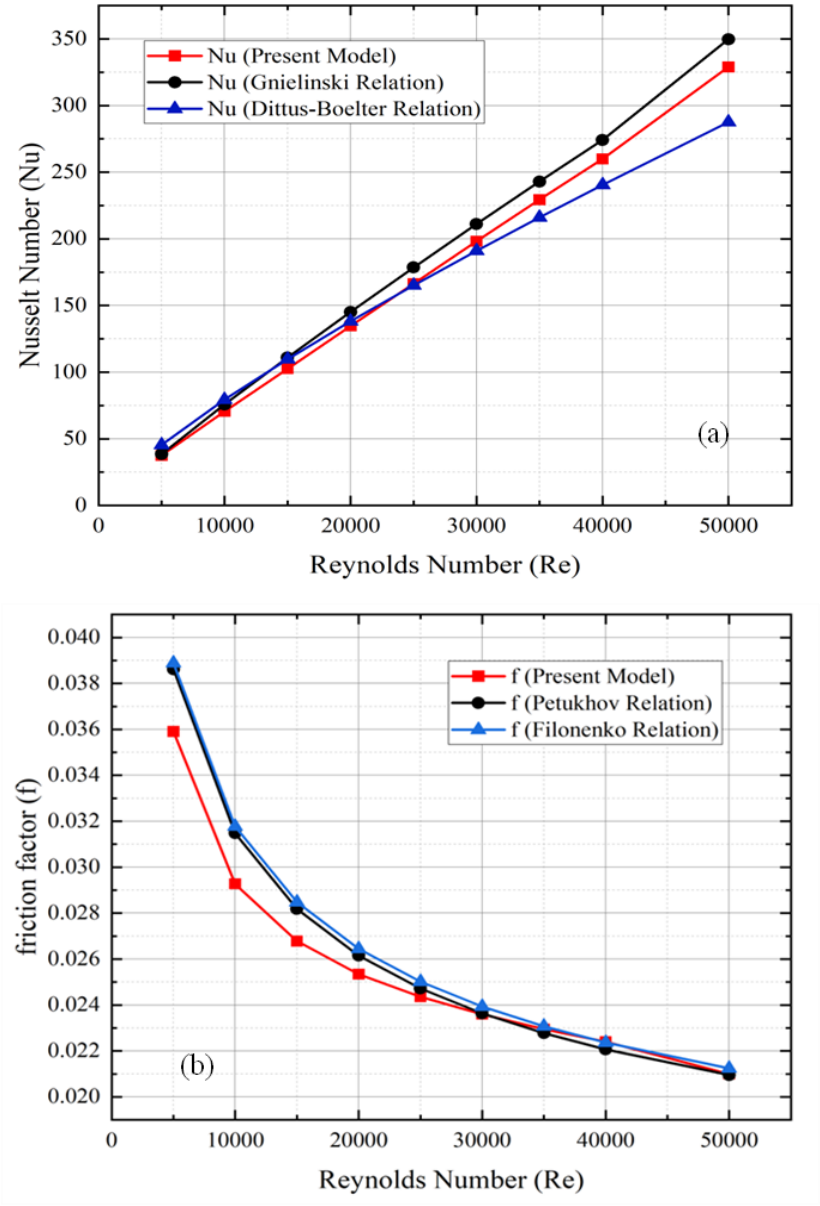

Fig. 4.2: Validation Plots: (a) Nusselt Number (*Nu*), (b) Friction Factor (*f*)

The second phase involved validating the computational model by comparing its outputs with the experimental test results. The experimental tests have been carried out during December 2021, from 10:00 hrs to 14:00 hrs, at Sundernagar (longitude 76.8889°E, latitude 31.5299°N). These tests has been conducted on a set up similar to prior study [78] fabricated by 'Ecosense Sustainable Solutions Pvt. Ltd.', based in New Delhi, India. The set up model used is named as 'EcoSCTS 2.2'. Fig. 4.3

displays the specific arrangement of the test.

(1) Light Dependent Resistor, (2) Stainless Steel Receiver Pipe, (3) Water Inlet, (4) Acrylic Mirror, (5) Control and Display Unit, (6) Digital Anemometer, (7) Solar Flux Meter, (8) Water Flow Sensor, (9) Water Storage Tank, (10) Pump, (11) Sun Tracking Actuator, (12) Power Supply, (13) Hydraulic Hose Pipes, (14) Parabolic Trough, (15) Water Outlet

Fig. 4.3: Experimental Test Rig

The test rig comprises a trough with rim angle of 67.24°, equipped with a highly reflective acrylic mirror with a reflectivity of 0.90. The focal length of the mirror is 0.6065 m. The parabolic reflector has a total aperture area of 2.068 m^2. It focuses the incoming solar radiation onto a long receiver pipe of 1.2 m length made up of steel, which is coated with nickel black. It has an inner diameter of 23 mm and external diameter of 25 mm. The test rig is equipped with an automated solar tracking system that accurately detects and follows the Sun rays as it falls onto it. The system concentration ratio is around 23.44. A water pump is positioned in the lower portion of the experimental arrangement, facilitating the circulation of water in a closed loop from a storage tank to receiver pipe. The storage tank is covered with rexene cover and provided with glass wool insulation to ensure the decrease of heat losses. The storage tank and receiver pipe is connected with suitable water hose pipes. A fluid

flow sensor ('Model: YF-S201, Make: Seametrics Inc., USA') is fitted between receiver pipe's inlet and the pump's outlet to determine the rate at which water is flowing. The control-cum-display unit consists of flow regulator and digital indicators for displaying the inputs and outputs. There are five numbers digital temperature indicators and one number flow rate indicator. Thermocouples are also fixed at the receiver pipe's entrance and exit location, inside the storage tank, at the storage tank entrance, and on the wall surface of the pipe to measure the working fluid's temperatures. The solar intensity impinging at the test location is measured using Tenmars solar power meter having model number TM-207. Table 4.2, shows the percentage divergence of output values among the CFD responses and experimental outputs is less than 5%. This shows the consistency and reliability of the CFD model.

Table 4.2: Experimental Validation of Computational Model

I_b (W/m^2)	Mass Flow Rate (kg/s)	T_{in} (K)	Temperature: Outlet (K)			Efficiency (%)		
			Exp.	CFD	Deviation (%)	Exp.	CFD	Deviation (%)
825	0.12	285.95	287.61	287.68	0.024	48.94	51.01	4.219
645	0.12	287.75	289.15	289.09	0.021	52.76	50.49	4.304
551	0.12	290.05	291.22	291.19	0.010	51.59	50.27	2.559
1001	0.12	292.55	294.53	294.6	0.024	48.03	49.73	3.528
1001	0.15	292.25	293.8	293.88	0.027	47.00	49.43	5.162
1068	0.15	294.25	295.91	295.98	0.024	47.17	49.16	4.218
970	0.15	296.15	297.75	297.71	0.013	50.03	48.78	2.508
1115	0.15	297.95	299.68	299.74	0.020	47.06	48.69	3.453
Mean	-	-	-	-	**0.020**	-	-	**3.744**

In above, thermal efficiency [6] is computed as;

$$\eta_{thermal} = mc_p(T_{out} - T_{in})/A_{ap}I_b \quad (4.5)$$

4.4.1 Uncertainty Analysis

In spite of the precautions that are taken, there is always the possibility of making mistakes while doing any kind of scientific inquiry. For this reason, it is essential to

conduct an analysis in order to ascertain the greatest inaccuracy that is conceivable and, therefore, the validity of the experimental data. Uncertainty calculations are conducted using the methodology developed by Kline and McClintock [107]. The standard uncertainty, derived from manufacturer specifications and calibration data, guarantees accurate outcomes by considering the constraints of the device and inaccuracies in calibration. The measurement is quantified as an extended uncertainty or standard deviation, usually accompanied by a coverage factor. The uncertainties for the solar irradiation, temperature, flow rate, length of aperture, and width of aperture are provided in Table 4.3. The uncertainty of thermal efficiency from Eq. 4.5 is calculated using these values.

Table 4.3: Measurement Uncertainties

Parameter	Uncertainty
Solar Irradiation	±1 W/m^2
Temperature	±0.1°C
Flow Rate	±4.1%
Length of Aperture	±0.01 mm
Width of Aperture	±0.01 mm

The uncertainty associated with the aforementioned variables, which is used to calculate the efficiency, is determined by taking the square root of the variance of the statistical distributions of each component as given below [50];

$$\Delta\eta = \sqrt{\left\{\left[\frac{\partial\eta}{\partial m}\Delta m\right]^2 + \left[\frac{\partial\eta}{\partial T_{out}}\Delta T_{out}\right]^2 + \left[\frac{\partial\eta}{\partial T_{in}}\Delta T_{in}\right]^2 + \left[\frac{\partial\eta}{\partial A_{ap}}\Delta A_{ap}\right]^2 + \left[\frac{\partial\eta}{\partial I_b}\Delta I_b\right]^2\right.} \quad (4.6)$$

The thermal efficiency has been determined with an overall uncertainty of 4.27%.

4.5 Pressure Variation

To understand flow mechanics, corrugated pipes flow is presented across a wide geometric range. Fig. 4.4 displays the variations in the static pressure within a pipe section.

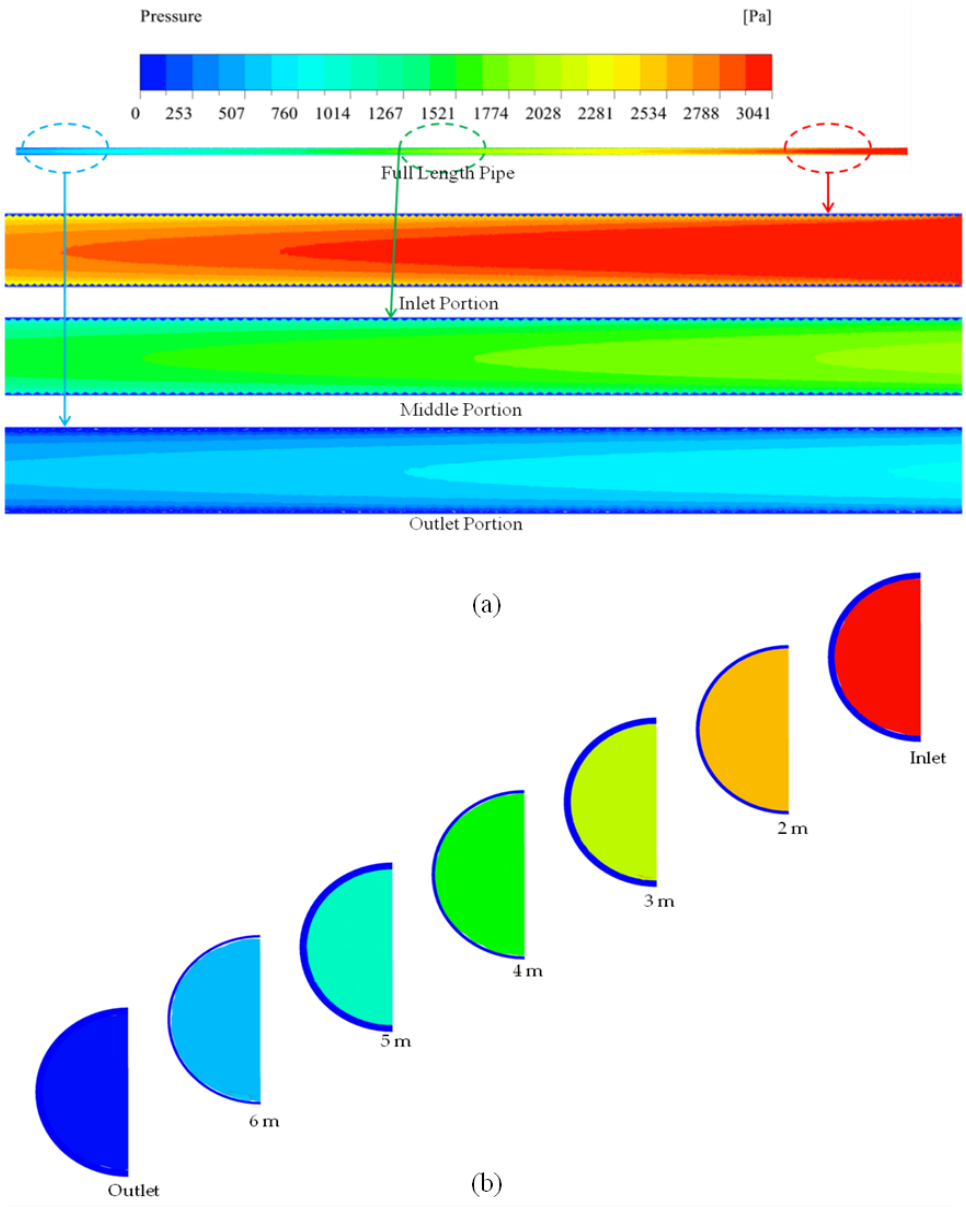

Fig. 4.4: Static Pressure Variation in Corrugated Case: (a) Full Length, (b) In Different Sections

It is evident that the pressure within the pipe decreases as the length of the pipe increases. Three different zones of flow are shown in this picture. Initial, located at the pipe inlet exhibits high pressure, while the middle one positioned in the centre

experiences lower pressure compared to the inlet. Lastly, the outflow section indicates lowest pressure.

To examine the impact of geometric parameters, Figs. 4.5-4.6 represent the variations of dynamic pressure along the axial sections of the receiver pipes. It has been observed that the dynamic pressure exhibits a consistent pattern across all situations. The highest pressure is found in the centre of the pipe, and it gradually decreases as it moves towards the outer wall, eventually reaching a lowest value at the pipe wall. The increased pressure at the centre region compared to the outside pipe wall requires a higher pressure gradient to counteract the centrifugal force caused by the corrugations. This may result in increased circulation, secondary flows, and mixing. Moreover, it has been noticed that as the corrugation pitch changes from 4 mm to 8 mm, dynamic pressure increases and on further increase in pitch size it gets reduces. And in the same way when the height of corrugations is altered from 1.5 mm to 2 mm then it is found that dynamic pressure increases inside the pipe and further change I height value to 2.5 mm, it gets reduces.

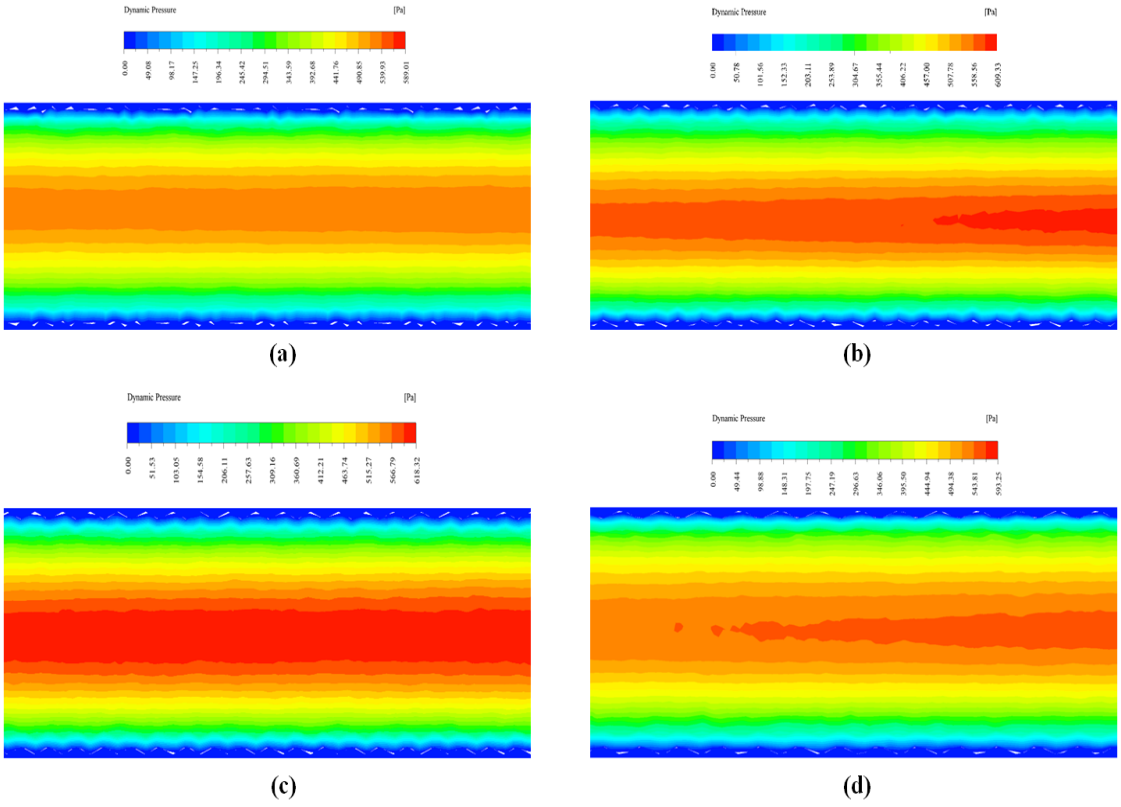

Fig. 4.5: Dynamic Pressure [*DNI*: 949 W/m^2 (1400 hrs.), Corrugation Height: 2 mm]: Corrugation Pitch: (a) 4 mm, (b) 6 mm, (c) 8 mm, (d) 10 mm

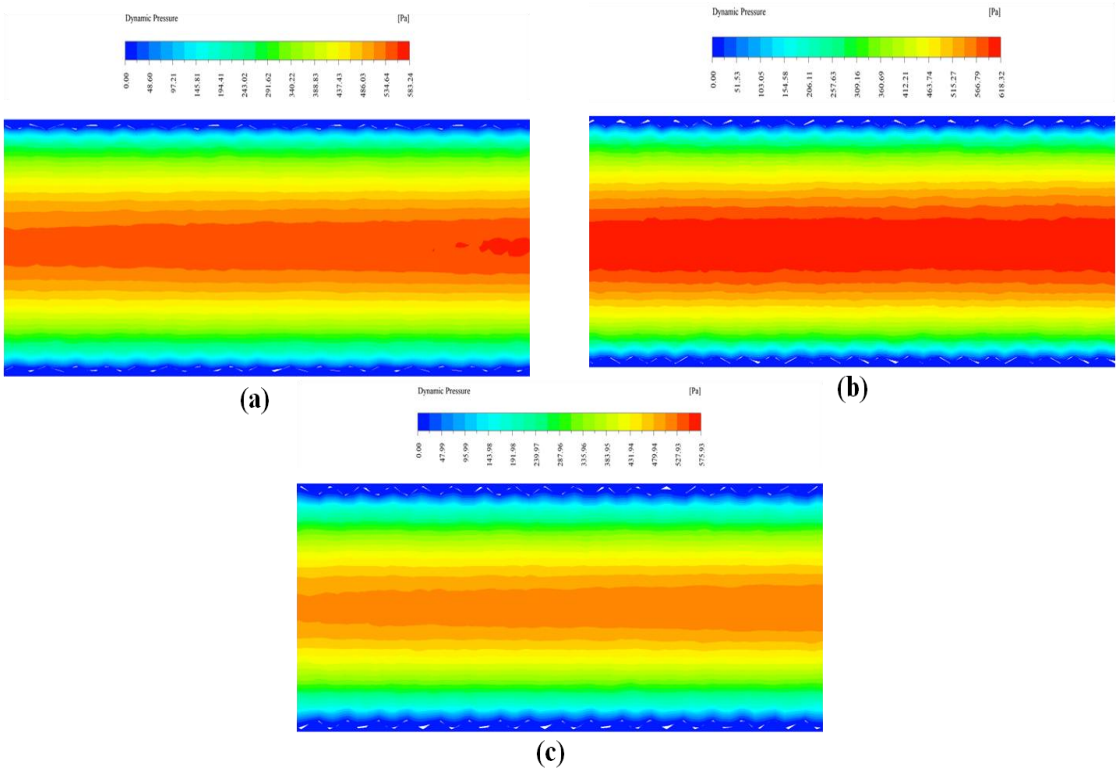

Fig. 4.6: Dynamic Pressure [*DNI*: 949 W/m^2 (1400 hrs.), Corrugation Pitch: 8 mm]: Corrugation Height: (a) 1.5 mm, (b) 2 mm, (c) 2.5 mm

4.6 Velocity Pattern

The study focuses on analyzing the impact of corrugations on flow behaviour by examining twelve different types of double corrugated pipes. These pipes experiencing same flow rates and has similar hydraulic diameters too. Velocity surface streamlines for various configurations are displayed in Fig. 4.7 in order to distinguish the behaviour from inside. The observed streamlines as a sample one are created at 5 m location from intake side and for Reynolds number (*Re*) = 50 × 10^3. Local velocity exhibits a gradual increase towards the centre of the pipe and a subsequent decrease towards the pipe wall in all configurations. This alteration in the velocity of the flow generates periodic flow along the entire length of the pipe. When a liquid flow comes into contact with corrugated surfaces, the direction of the flow is altered and vortices are generated as a result of the obstruction and stimulation caused by the corrugations in the direction of the flow. Consequently, the occurrence of axial spinning and vortexes led to a heat transfer enhancement.

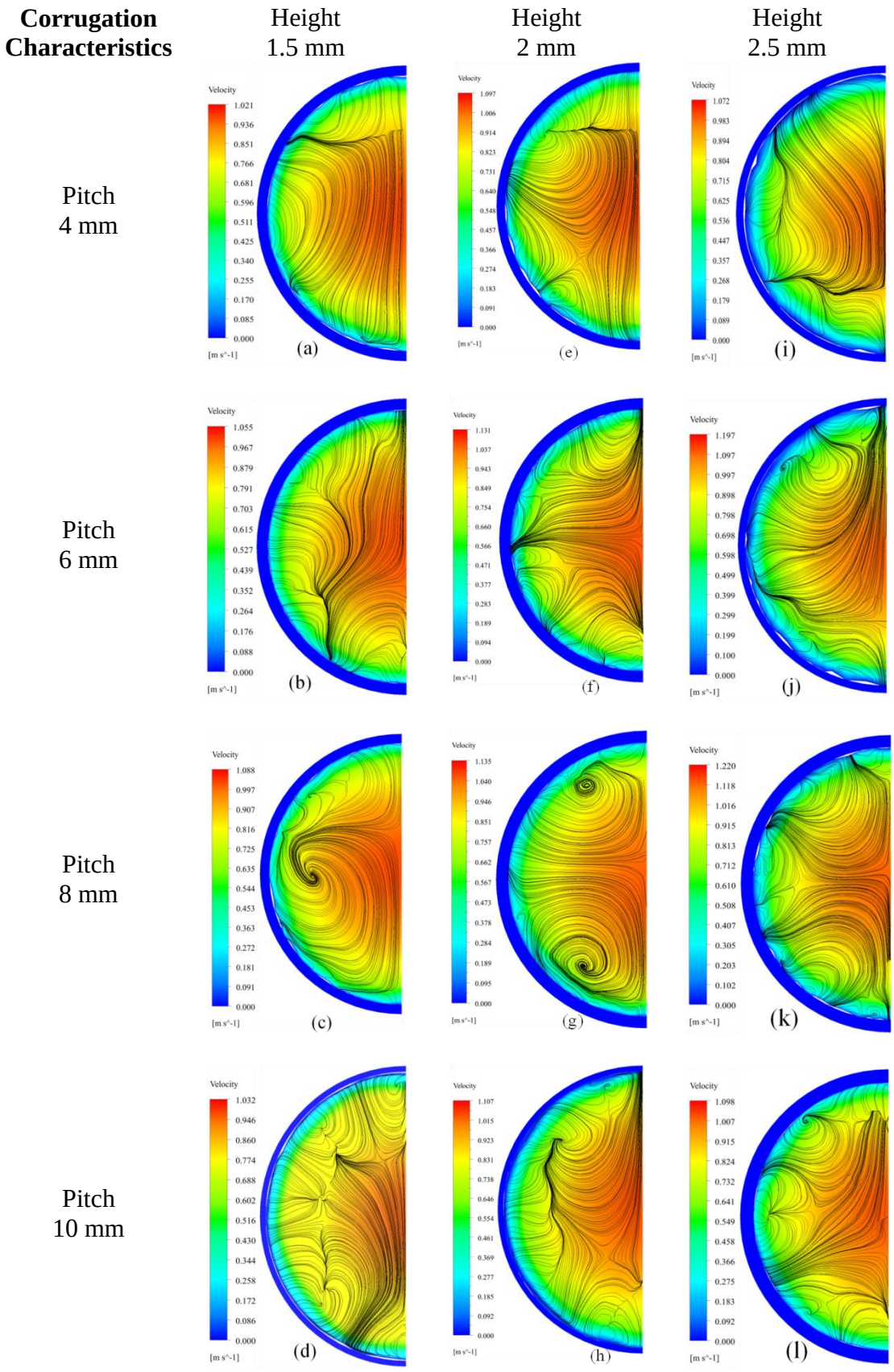

Fig. 4.7: Surface Streamlines of Velocity [*DNI*: 949 W/m^2 (1400 hrs.), *Re*: 50,000]

Furthermore, Fig. 4.7 illustrates that corrugated pipe having 8 mm pitched and 2 mm heighted corrugations exhibits greater mixing flow regions and recirculation size compared to the other instances. To gain a deeper understanding of this pattern, the whole pipe is sectioned into four sections, i.e. at 2-meter interval among them. It is shown in Fig. 4.8 for different examined cases. These figures provides a clear understanding that vortex formations and axial spinning goes on increasing as the fluid flow advances within the pipes. The presence of the vortex distribution is evident in the radial cross sections, as noted earlier.

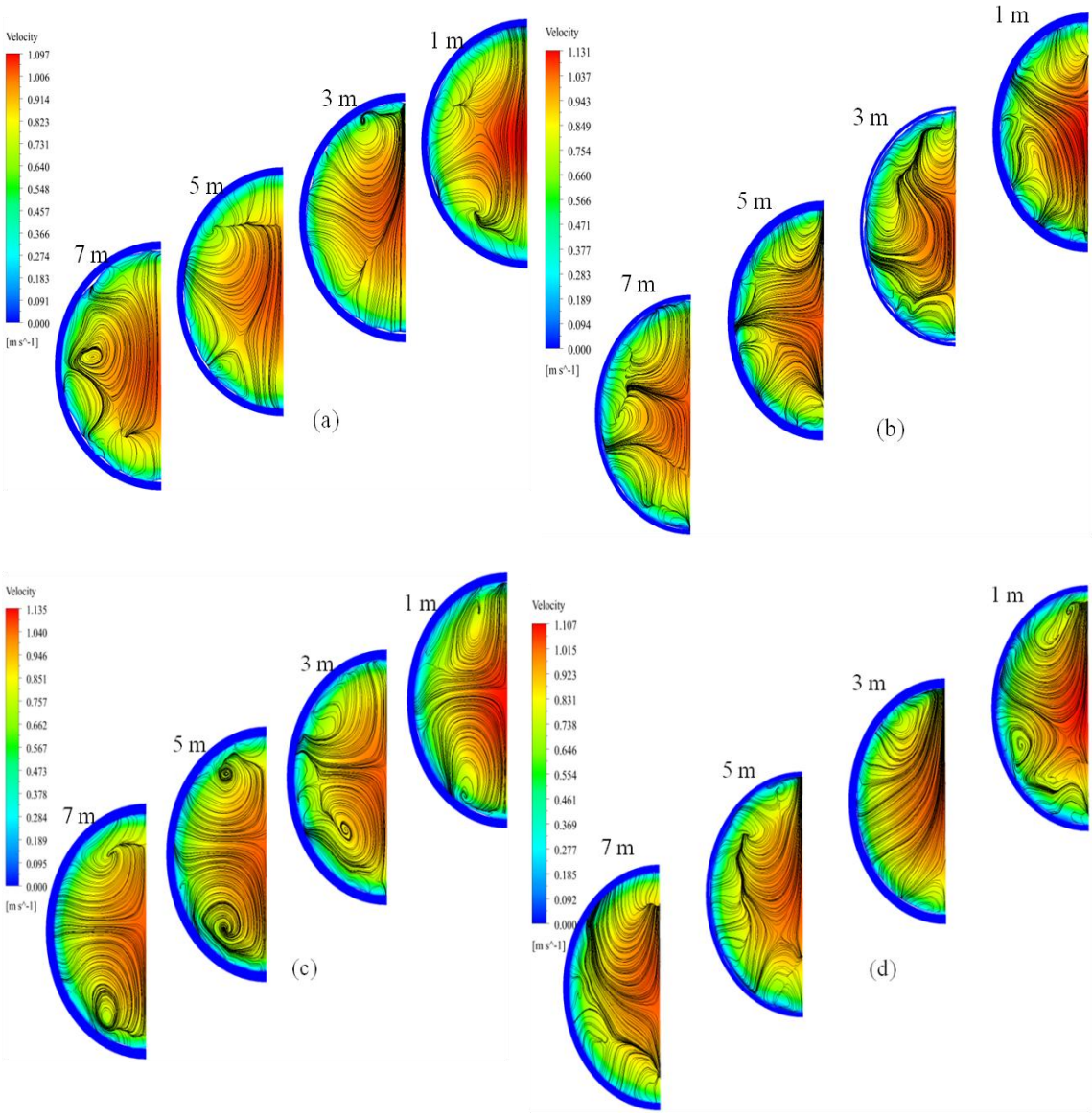

Fig. 4.8: Velocity Variations along Axial Length [*DNI*: 949 W/m^2 (1400 hrs.), *Re*: 50,000, Corrugation Height: 2 mm]: Pitch (a) 4 mm, (b) 6 mm, (c) 8 mm, (d) 10 mm

Fig. 4.9 displays the contours of *TKE* for several cases with corrugation heights ranging from 1.5 mm to 2.5 mm, while the pitch remains unaltered at 8 mm. It is noticeable that the *TKE* undergoes significant changes when the configurations vary. Moreover, as a result of vortex interactions, there is a significant amount of *TKE* in close proximity to the wall. As a result, the corrugated surfaces and the core sections disrupt the thermal barrier layer in close proximity to the corrugated faces. This has the potential to greatly enhance turbulence. Therefore, the incorporation of double corrugations (symmetrical convex-concave) increases turbulence in comparison to smooth case, thus increases the heat transfer. Furthermore, it is apparent that changing the height of corrugations from 1.5 mm to 2 mm results in an increase in *TKE*. Conversely, further increase in height from 2 mm to 2.5 mm, there is a drop in the intensity of *TKE* due to reduction in swirl tendency. Therefore, it can be concluded that corrugation height of 2 mm exhibits superior intensification compared to others. For further in-depth information regarding the *TKE* variation, Fig. 4.10 is displayed, with a corrugation height of 2 mm and different pitch values ranging from 4 mm to 10 mm. This figure clearly demonstrates that increasing the pitch from 4 mm to 8 mm results in an increase in *TKE*. However, further increase in the pitch value (from 8 mm to 10 mm) leads to a reduction in *TKE*.

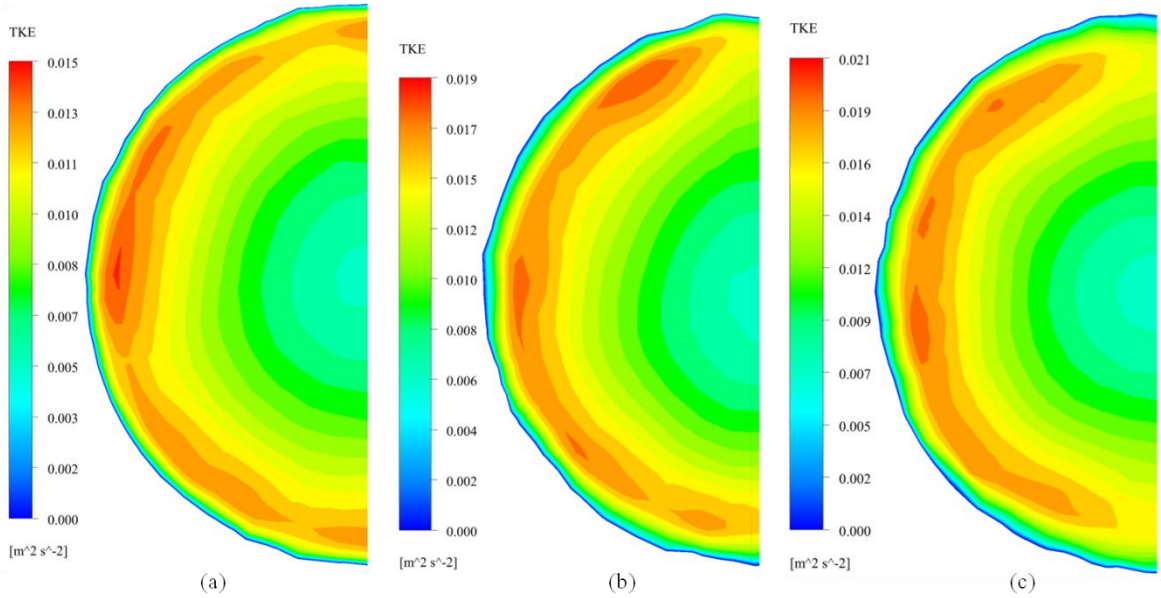

Fig. 4.9: *TKE* (Turbulent Kinetic Energy) [*DNI*: 949 W/m^2 (1400 hrs.), *Re*: 50,000, Corrugation Pitch: 8 mm]: Height (a) 1.5 mm, (b) 2 mm, (c) 2.5 mm

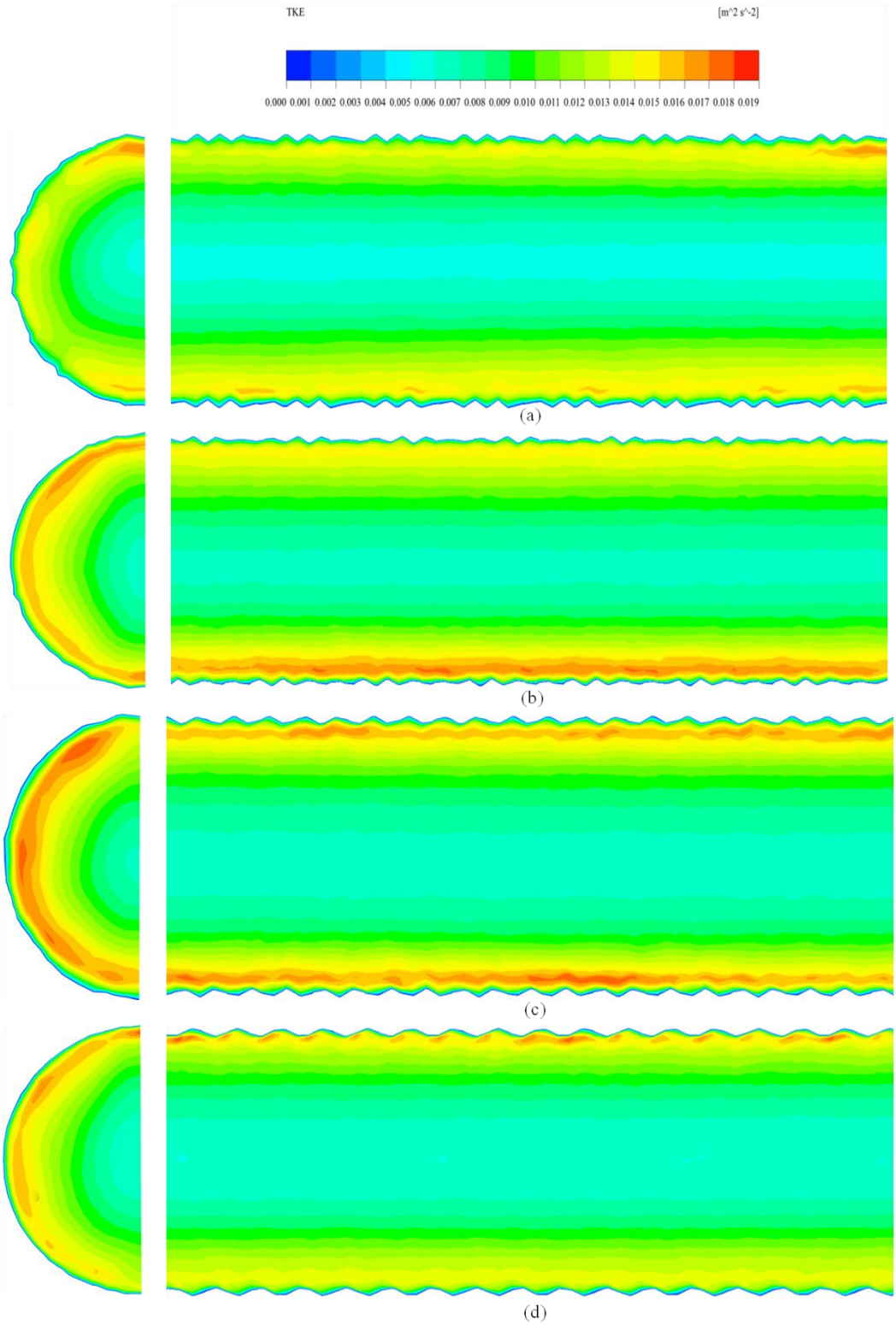

Fig. 4.10: *TKE* (Turbulent Kinetic Energy) [*DNI*: 949 W/m^2 (1400 hrs.), *Re*: 50,000, Corrugation Height: 2 mm]: Pitch (a) 4 mm, (b) 6 mm, (c) 8 mm, (d) 10 mm

4.7 Heat Transfer Characteristics

Numerical investigation has been conducted to evaluate the characteristics of heat transfer for cases under examination. The geometric and flow characteristics impact has been assessed under turbulent flow circumstances. From the data presented in Figs. 4.11-4.13, it can be seen that the *Nu/Nus* (Nusselt number) ratio values for all corrugated pipes are consistently higher than one at different *Re* (Reynolds number). This indicates that corrugated pipes have superior heat transmission capabilities as compared to smooth (conventional) pipe. The existence of thermal boundary layer inhibits the heat flow between the wall and the fluid. This typical configuration disrupts the said layers and increases the turbulence. This means that layers that served as a barrier to heat transfer are eliminated, enabling more effective heat transfer. Moreover, when a liquid flow comes into contact with corrugated surfaces, the direction of the flow is altered and swirling patterns are generated as a result of the obstruction and stimulation caused by the corrugations in the same direction as the flow.

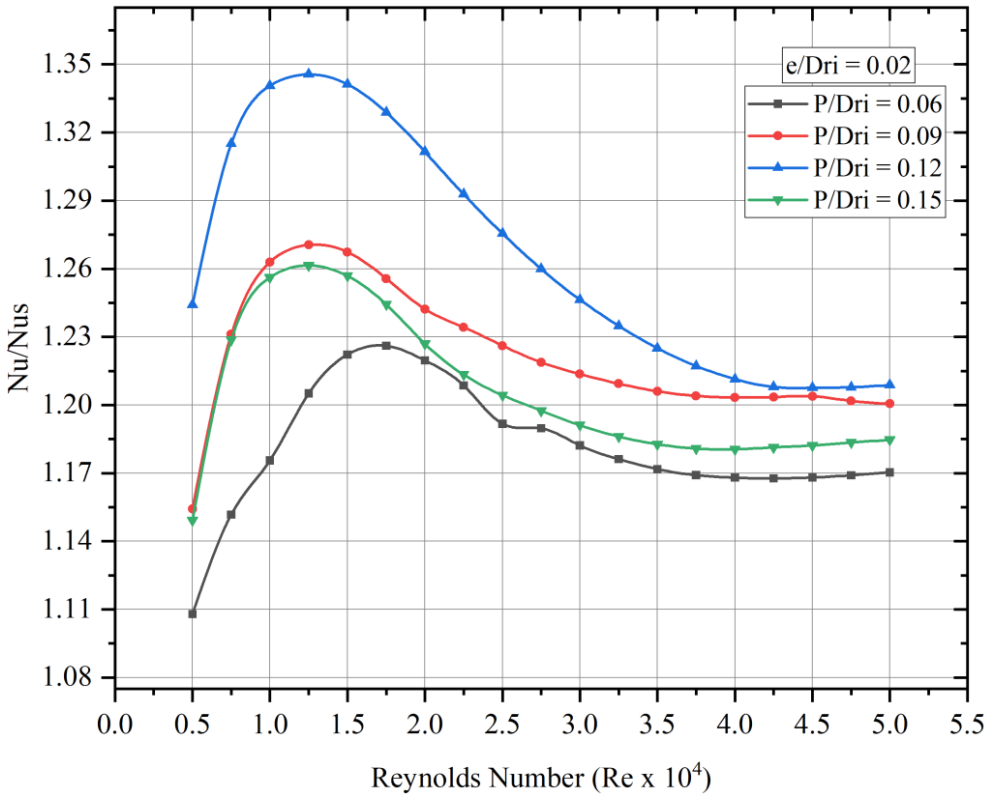

Fig. 4.11: Effect of Corrugation Pitches for Corrugated Height: 1.5 mm

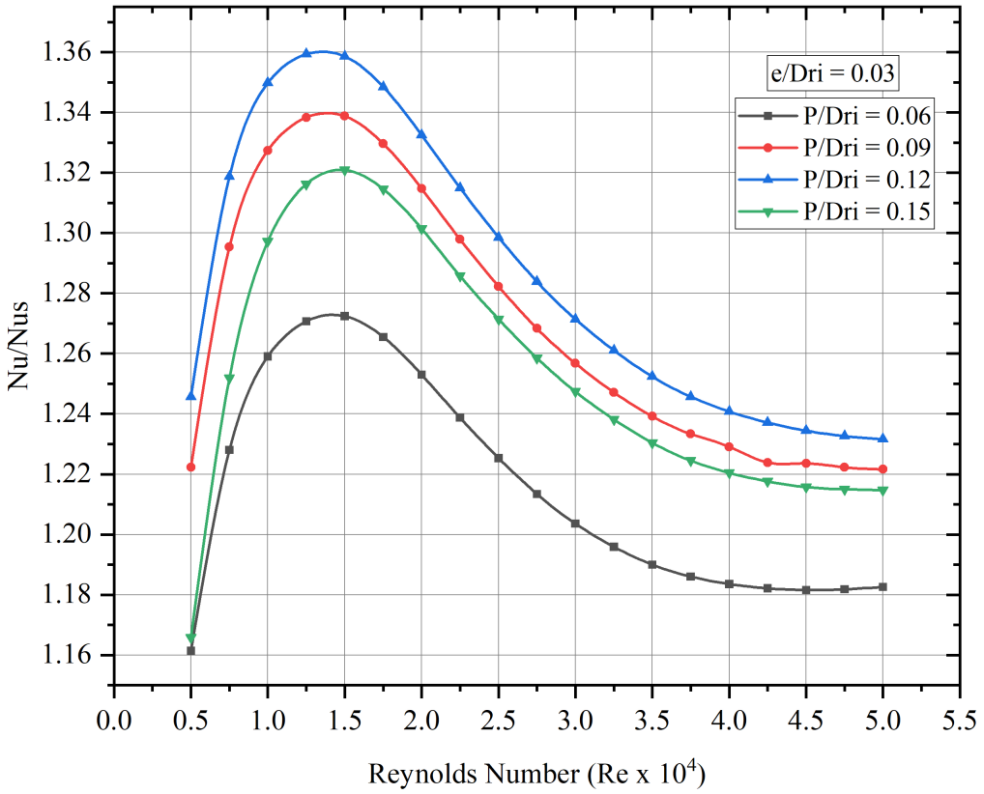

Fig. 4.12: Effect of Corrugation Pitches for Corrugated Height: 2 mm

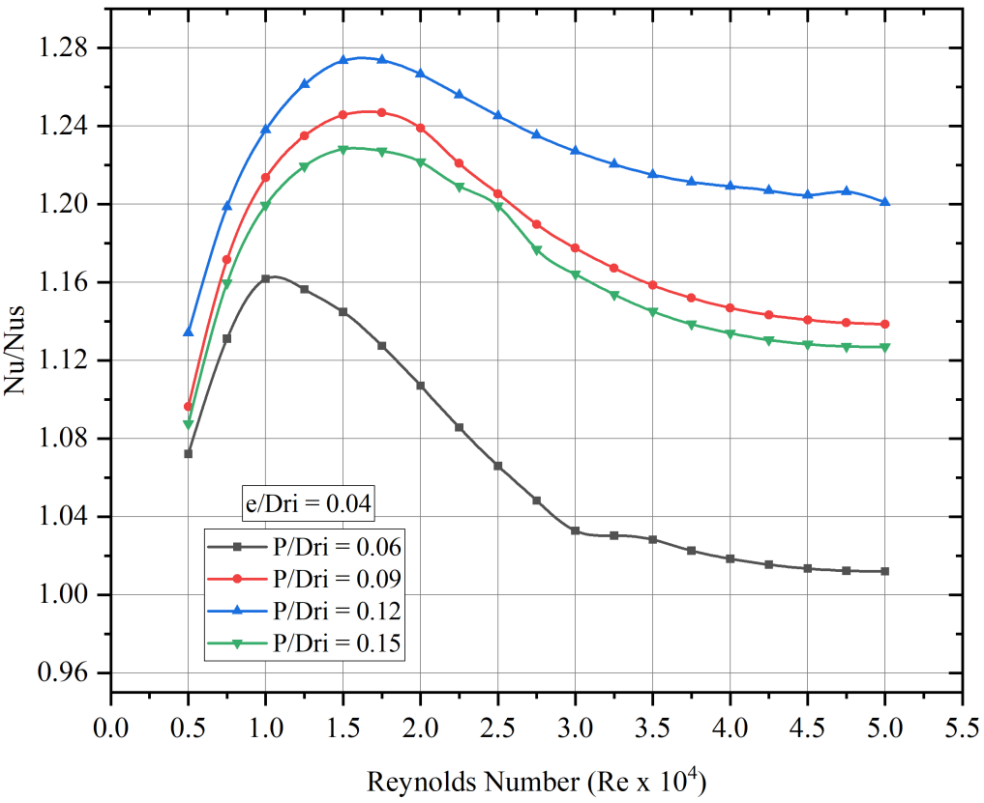

Fig. 4.13: Effect of Corrugation Pitches for Corrugated Height: 2.5 mm

Consequently, the occurrence of vortexes, axial whirling, and higher inflow velocity led to an improvement in heat transfer. By utilizing increased flow mixing, the suggested pipe configurations exhibit an average *Nu* increase ranging from 6.77% to 28.51% compared to a conventional case. Furthermore, *Nu* gets increases for pipe having a corrugation pitch of 8 mm compared to a corrugation pitch of 4 mm. However when the pitch size is increased from 8 mm to 10 mm, the value of *Nu* falls. This may be due to the fact of reducing swirling tendency, recirculation size or mixing area inside the receiver pipe. Hence, it can be stated that corrugated pipe of 8 mm pitch case exhibits the most optimal heat transmission features compared to all other scenarios. Moreover, the data indicates that change in corrugation height as 1.5 mm to 2 mm leads to an improvement in *Nu*. However, beyond that point, *Nu* decreases. The axial whirling and vortex formations inside the pipe significantly affect the turbulence and hence thermal performance. The aforementioned effect can be seen in Figs. 4.7, where it is plainly visible that the swirling tendency of the heat transfer fluid flowing through the receiver pipe increases when the height of corrugation changes from 1.5 mm to 2 mm, and then decreases on further increment in corrugations height from 2 mm to 2.5 mm. This is a clear indication of the effect (recirculation size and mixing flow areas) that was mentioned earlier. Therefore, the greatest increase in *Nu* is observed when using a pitch of 8 mm and corrugations height of 2 mm. Also, within the investigated range of *Re*, the *Nu* enhancement for corrugations with a 2 mm height and 8 mm pitch is determined as 23.16%-34.98% greater than that of conventional pipe. Since, thermal boundary layer thickness is more pronounced at low value of Reynolds numbers (*Re*), the presence of used corrugation design leads to the highest level of thermal enhancement in the lower *Re* range.

4.8 Hydraulic Characteristics

It is important to note that the rise in pressure drop caused by enhanced heat transfer is inevitable. Figs. 4.14-4.16 illustrate the impact of double corrugated pipes in contrast to smooth pipes. These graphs illustrate the variation among *Re* and the ratio of friction factor for various receiver designs. The friction factor ratio rises with an increase in pitch length for all corrugated heights. This phenomenon could be

attributed to the increased occurrence of rotating flow and turbulence within the pipe. This turbulence, which is the consequence of the corrugations, causes the creation of a vortex inside and around the corrugations, increased flow separation, as well as causes the fluid to encounter more friction. It is unsurprising that all of these factors together lead to an escalation in the pressure drop. Note that depending on the corrugation pitches and heights, the *f/fs* ratio can range from 1.08 to 4.46. When e/D_{ri} (ratio of corrugation height to pipe diameter) is equal to 0.02 and P/D_{ri} (ratio of corrugation pitch to pipe diameter) is varying (0.06, 0.09, 0.12 and 0.15), the average friction factor is accordingly 2.20, 2.53, 2.51 and 2.30 times higher than conventional case. For e/D_{ri} equals to 0.03 and again P/D_{ri} is changed (0.06, 0.09, 0.12 and 0.15) the friction factor is accordingly 1.74, 2.11, 1.85 and 1.77 times greater than conventional case. And finally, for 0.04 e/D_{ri} and P/D_{ri} equals to 0.06, 0.09, 0.12, 0.15, the value is respectively 2.50, 3.51, 3.39, and 2.85 times more than conventional one. In addition, pipe with 6 mm corrugations pitch (P/D_{ri} = 0.09) and 2.5 mm (e/D_{ri} = 0.04) corrugations height exhibits the greatest frictional loss as compared to other used pipe configurations. It may be attributed to the fact that the fluid experiences more frictional resistance as it navigates the tighter and more frequent undulations, leading to a greater loss in pressure. Conversely, a larger corrugating pitch results in more widely spaced corrugations, which create less frequent disturbances in the fluid flow. This reduces the frictional losses, leading to a lower pressure drop. On the other hand, increase in the corrugation height results in higher viscosity losses along the pipe wall surface. The peaks and troughs cause the fluid to accelerate and decelerate repeatedly, which increases the energy dissipation in the form of frictional losses, resulting in greater pressure drop.

Based on the data outcomes, the utilization of double corrugations on the wall surface of pipe would greatly enhance the *Nu* (Nusselt number). Nevertheless, the enhancement has led to an escalation in the frictional penalty. Investigating *TEF* as described in Equation 3.21 is thus advantageous for conducting a comprehensive evaluation of heat transfer enhancement. The data values obtained by calculating *TEF* for the examined geometric characteristics and flow conditions corrugation are plotted in Figs. 4.17-4.19.

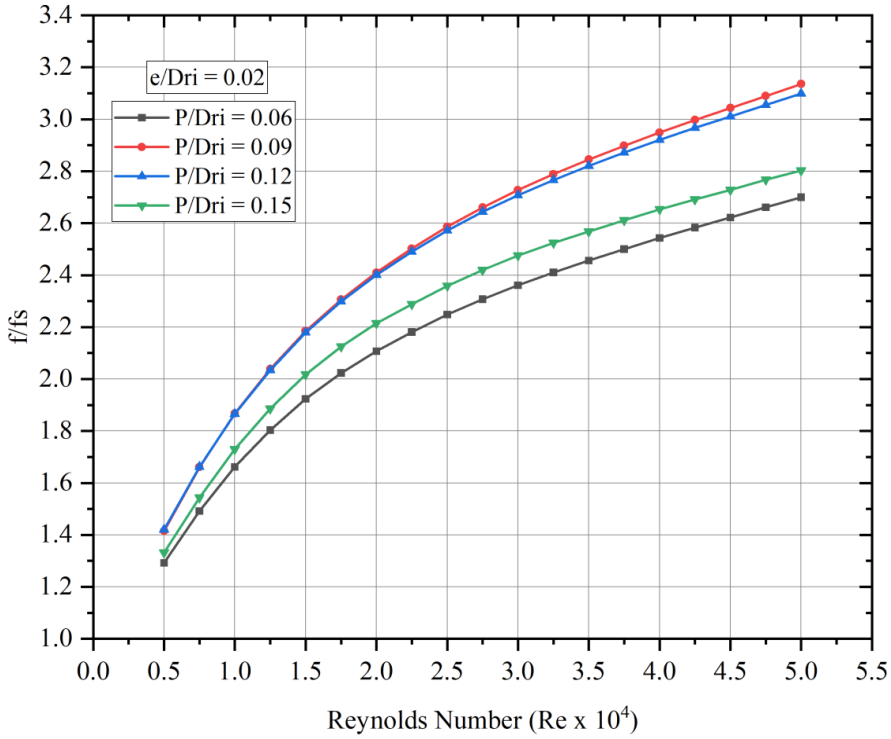

Fig. 4.14: Effect of Corrugation Pitches for Height: 1.5 mm

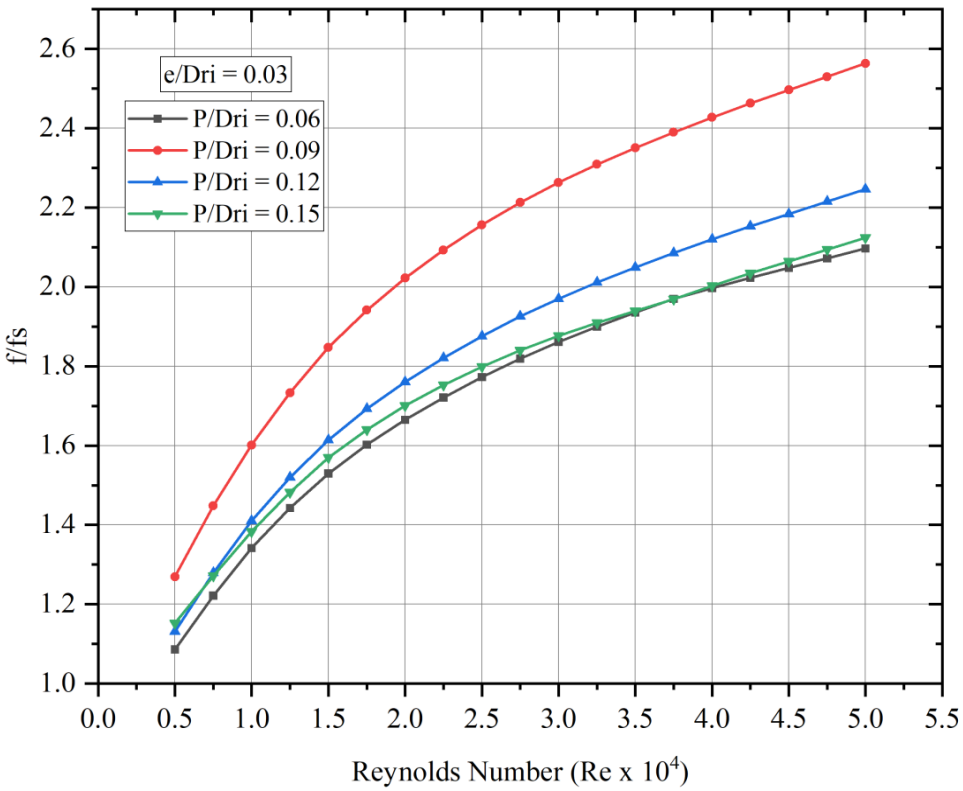

Fig. 4.15: Effect of Corrugation Pitches for Height: 2 mm

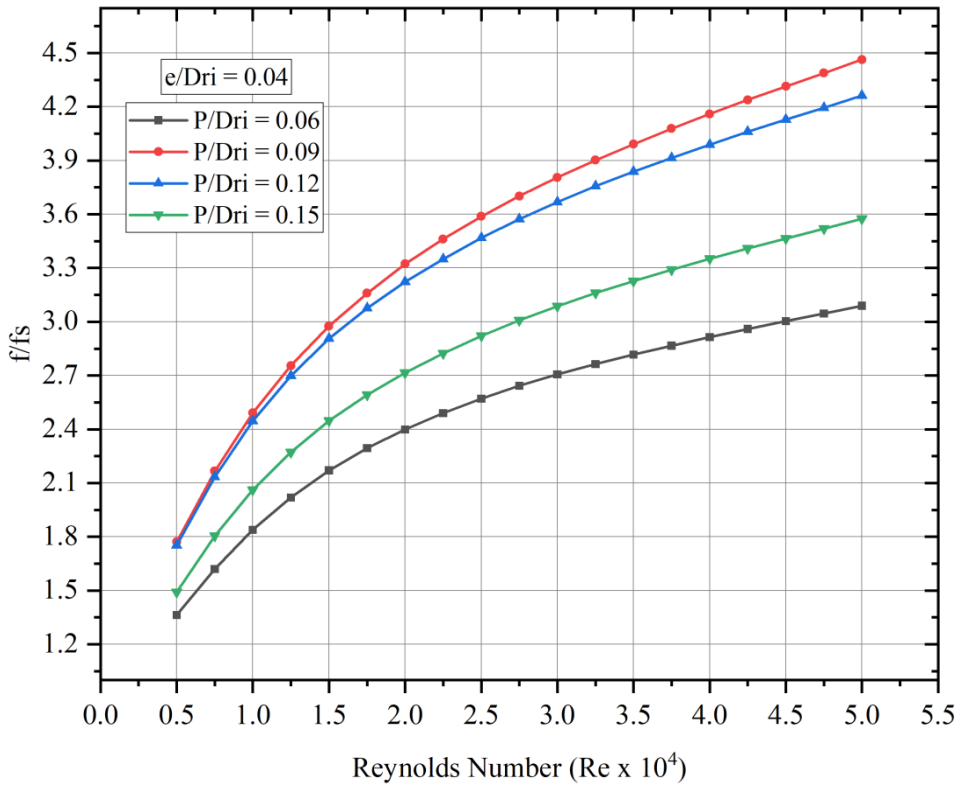

Fig. 4.16: Effect of Corrugation Pitches for Height: 2.5 mm

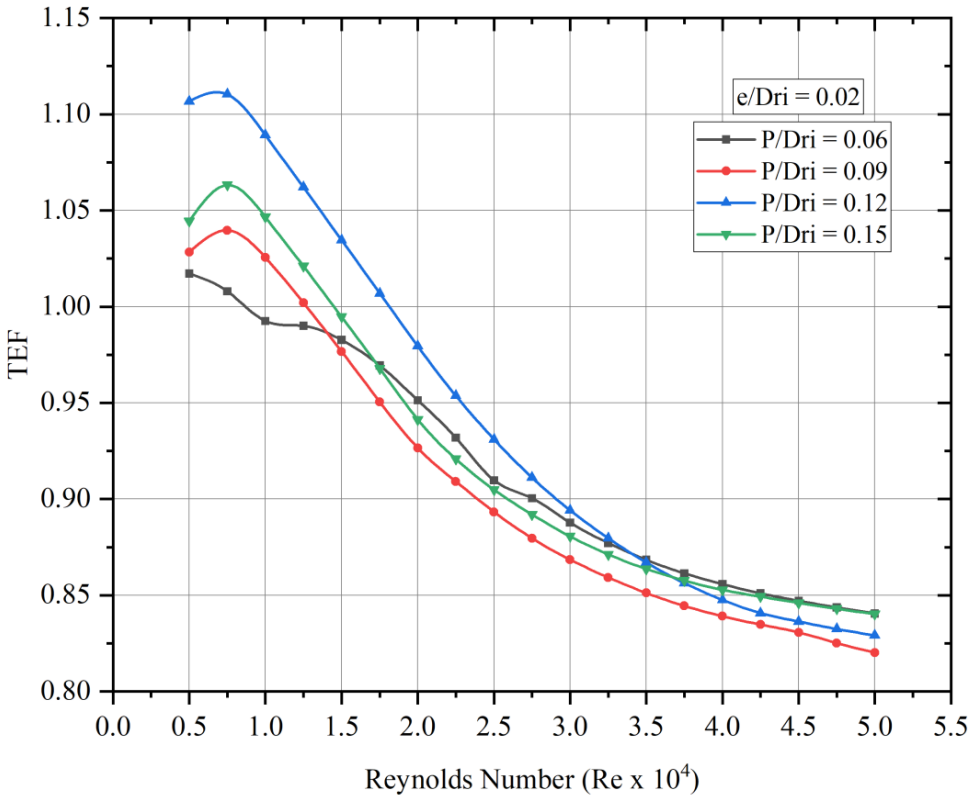

Fig. 4.17: Effect of Corrugation Pitches on TEF for 1.5 mm height

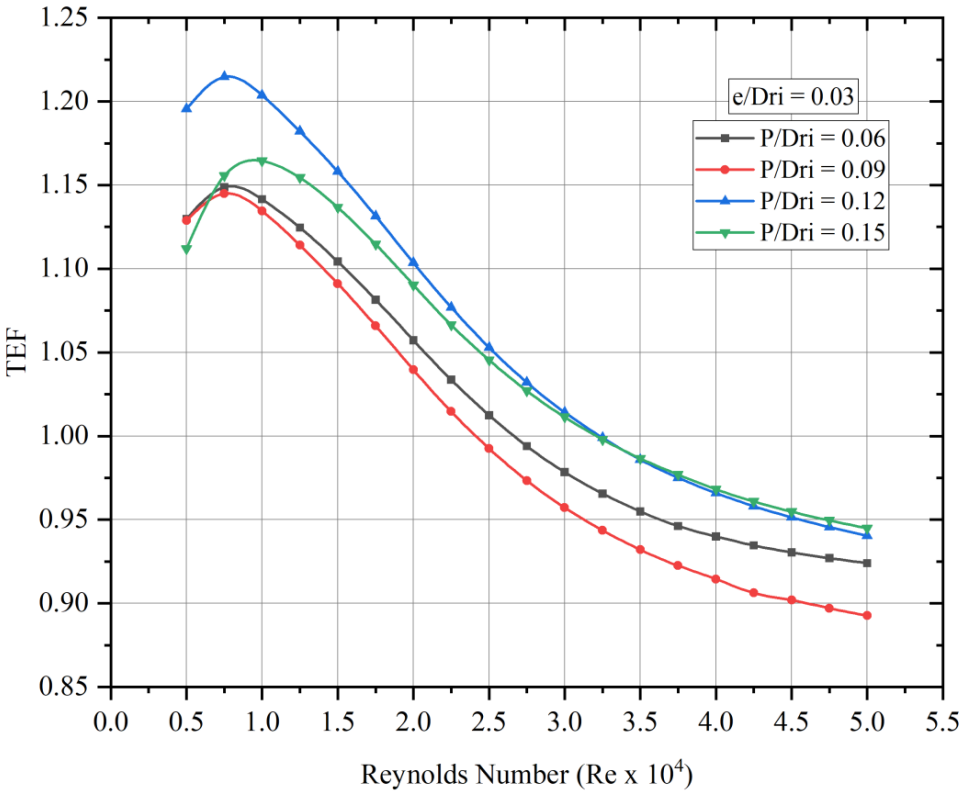

Fig. 4.18: Effect of Corrugation Pitches on TEF for 2 mm height

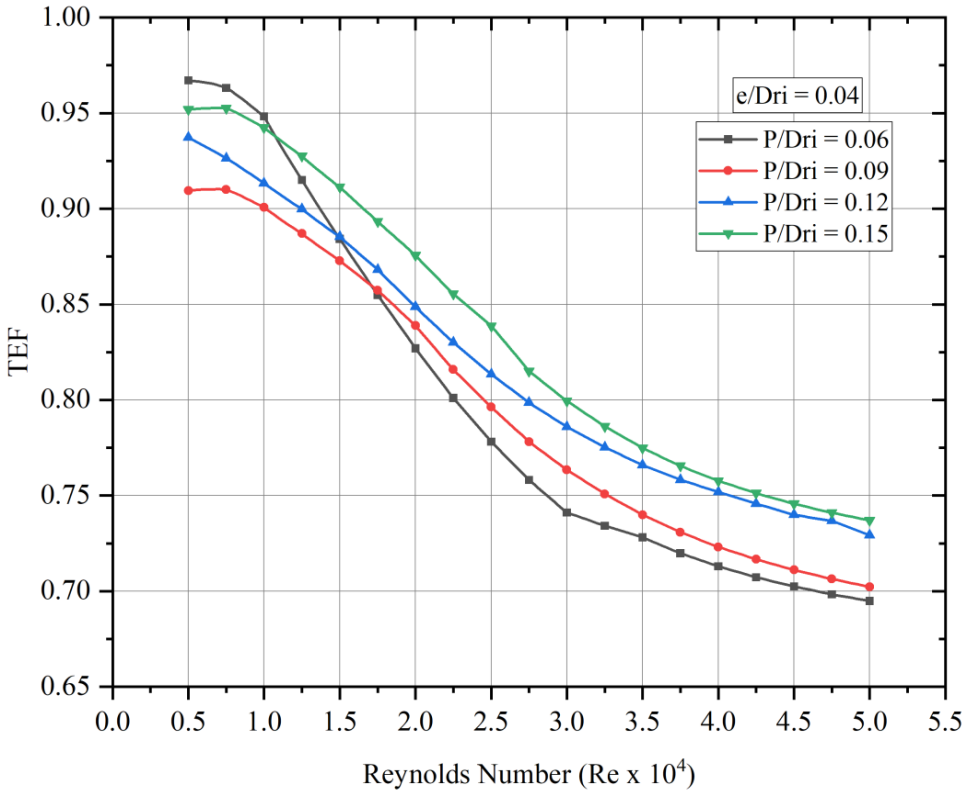

Fig. 4.19: Effect of Corrugation Pitches on TEF for 2.5 mm height

From Fig. 4.17, it can seen that for a height ratio of e/D_{ri} = 0.02 (e = 1.5 mm) and pitch ratio of P/D_{ri} = 0.12 (p = 8 mm), the highest *TEF* achieved is 1.11 for a *Re* equals to 7500. The impact of altering the height ratios with varied pitch ratios can be seen in Figs. 4.18-4.19. According to Fig. 4.18, the *TEF* value is 1.21, which is achieved when the receiver pipe has corrugations with a height ratio of 0.03 (e = 2 mm) and a pitch ratio of 0.12 (P = 8 mm). In contrast to aforesaid discussion, it is pertinent to mention that as the corrugations height further increases; the *TEF* decreases (see Fig. 4.19). Specifically, for height ratio of 0.04 (corresponding to a height of 2.5 mm), data points are consistently below unity, regardless of the pitches examined. It is explained by the fact that, in this instance, the pressure penalty increases more significantly than *Nu* increase.

Based on a comprehensive analysis discussed above, it can be concluded that examined pipe with corrugations measuring 8 mm pitch and 2 mm height is more energy efficient. Furthermore, it can be determined from these plots that the effect of said corrugations on heat transmission is more noticeable at lower range of *Re*. The observed result is associated with the thermal boundary layer thickness, as this thickness is more predominant at lower *Re*. Consequently, the turbulence is more significant at this region.

4.9 Summary of the Chapter

An analysis has been conducted to investigate the performance of modified receiver pipe (here in called as double corrugated) under non-uniform heat flux conditions. The fluctuations in pressure, velocity, and *TKE* are depicted to demonstrate the differences among examined cases. Presented below is a concise overview of the noteworthy outcomes;

- The turbulence, flow mixing, and boundary layer dispersion intensifies when the corrugation arrangement is altered, leading to a notable influence on the thermal-hydraulic performance. The findings indicate that using double corrugation design for receiver pipe enhances the performance.
- The velocity patterns observed in different types of corrugated pipes demonstrate the growth of vortex formation and axial spinning as the flow

advances through them. Consequently, the occurrence of axial whirling and the production of vortexes led to an improvement in heat transfer. Furthermore, the pipe with a 2 mm corrugation height and 8 mm corrugation pitch exhibits larger recirculation size and better mixing flow areas compared to other cases.

- In the vicinity of the wall, turbulent kinetic energy is high because of flow dissociation and reattachment as well as vortex interactions. The increased fluid mixing and circulation flow consequently disturb the thermal boundary layer close to the corrugations. Therefore, the existence of examined corrugations increases turbulence, thereby improving heat transfer. Furthermore, it is seen that as the pitch increases from 4 mm to 8 mm and height of corrugations from 1.5 mm to 2 mm, the turbulent kinetic energy likewise increases. Increasing both parameters further decreases the turbulent kinetic energy as a result of decreased swirl intensity.
- A total of twelve pipe configurations, each with varying corrugation pitches and heights, are examined. The greatest increase in *Nu* is achieved with a 2 mm height and 8 mm pitch. It is recorded in the range of 23.16%-34.98% higher than conventional (smooth) pipe within investigated range of *Re*.
- Due to the presence of proposed designs, average *Nu* gets increased by 6.77% to 28.51% compared to conventional (smooth) pipe. Moreover, the results of the *Nu/Nus* ratio values are consistently above one for all of the examined configurations.
- The presence of axial whirling in corrugated pipes leads to the formation of flow mixing zones, resulting in an increase in pressure drop. This rise is quantified as average friction factor which increases as 1.08 - 4.46 times compared to conventional (smooth) pipes.

CHAPTER 5

OPTIMIZING THERMAL-HYDRAULIC PERFORMANCE OF DOUBLE CORRUGATED RECEIVER PIPE

5.1 Introduction

As mentioned earlier, with fossil fuels becoming scarcer, leading economic instability throughout the globe, leads to a period of uncertainty with regard to the availability of energy. Hence, in light of current circumstances, it is more imperative to explore alternative methods of power production, namely sustainable energy sources, to meet the ongoing energy demands. Consequently, several researchers are now engaged in the exploration of diverse technologies that revolve on harnessing the solar energy and enhancing the performance of solar systems [108,109]. One of the most promising technologies for either fluid heating or electricity generation is concentrated solar power (CSP). For various temperature applications, PTSC are one of the finest CSP solutions [110]. To improve the heat transmission to the fluid in the PTSC, many techniques have been addressed in the literature [1,7]. Previous investigations has analysed heat transfer and resulting friction in many contexts. It is important to investigate under what circumstances the intended value (thermal performance) exceeds the undesirable output (pressure loss). When determining the optimal set of design parameters, design engineers need a straightforward, methodical, and applicable approach to evaluate many performance-defining aspects and their interrelationships. The study conducted by Jafar and Sivaraman [111] investigates the behaviour of receiver pipe of PTSC provided with twisted tape inserts to determine optimal process parameters using statistical tools like design of experiments. The experimental design and analysis of variance carried out confirmed; finally, that twist ratio is the primary characteristic which affects the performance of receiver pipe in PTSC. In another study, conducted for solar air heater by Qader et al. [108], CFD simulation and response surface methodology (RSM) techniques were

used to analyse the air heater thermal performance provided with inclined fins. The optimization outcomes reveal that at Reynolds number (*Re*) 18,243.5 with fin pitch of 19.04 mm, slant angle of 49°, and length of 1.52 mm, optimal solution is obtained. In order to assess, verify, and optimise the experimental output data, Vijayan et al. [112] conducted a numerical analysis on a PTSC system consisting of aluminium oxide based nanofluid. The assessment (finding the parameters that matter and how much they matter) and optimisation are carried out with the help of RSM. Haran and Venkataramaiah [113] also utilizes the ANOVA method to find out the optimised combination of receiver tubes and different fluid those were used in their study. Recently, Sharma et al. [114] proposes a numerical model after carrying out the RSM optimisation for jet impinged SAH (solar air heater) provided with V-shaped (multiple) ribs on its absorber. The research has been done with a number of different design elements such as angle of attack, jet diameter ratio, stream-wise/span-wise jet pitches, and the relative roughness pitch/height. It is clear from the above literature that whatever geometric modification is done in the principal elements of solar collectors, their purpose is to increase heat transmission. From above, it has been stated that it is crucial to recognize the wider importance of comprehending the thermal-hydraulic characteristics of solar collector systems. Above this, it can also be said that very few studies have been focussed on PTSC receiver pipe where RSM optimization has been done. Whereas, for other solar collector systems such as solar air heaters (SAH's), the aforesaid method of design optimization have been extensively utilized. Therefore, this work attempts to fill this gap by carrying out the CFD analysis in conjunction with RSM to examine the impact of PTSC receiver pipe provided with symmetrical convex-concave corrugations (double corrugations) on heat transmission and pressure drop. The primary goal of this investigation is to examine the impact of proposed receiver pipe's geometric parameters such as corrugation pitch, and corrugation height under varying flow rates on *Nu*, pressure drop (friction penalty), and *TEF*. The conducted study compared numerical outcomes of CFD investigation to the RSM model. RSM employs statistical design to provide a better operational parameter for attaining optimal design in defined trials [114]. Prediction models are evolved by optimising inputs which impact output or cause a response based on past system observations. The response evaluates performance

using test trials that adjust input parameters to output for the development of analytical framework which connects parameters empirically [115]. This chapter presents the optimized parameters of the design considerations that are necessary to achieve improved performance.

5.2 RSM (Response Surface Methodology)

This method is employed as a tool for the generation of optimum parameters. It fine-tunes the CFD's operations to provide for the best possible performance. Modelling, forecasting, and optimising the variables all take place inside RSM's standard 3-step process. The relationship between the observed results and the relevant input variables is likewise modelled by RSM. Fig. 5.1 shows the detailed procedure that is being used to optimise the output parameters in a sequential order. RSM plots the intertwined or direct connections between design elements in 2/3-dimensions to represent their interplay. Considering that it is possible to quantify all factors, the response surface may be described by the following equation;

$$y = f(x_1, x_2, x_3, \dots\dots\dots\dots\dots\dots x_n) \quad (5.1)$$

Here, y indicates the response, x_n is the factors.

The Reynolds number (*Re*), corrugation pitch (*P*) and corrugation height (*e*) represents input factors, while Nusselt number (*Nu*), pressure decrease (Δp), friction factor (*f*) and *TEF* are used as outputs to determine the best possible model solution. Data from the real design matrix has been utilised in the modelling of system output [114]. Response plots are created by regression equations derived from the design matrix; for which optimised outputs are taken from simulations. Table 5.1 presents the selected range of parameters on which RSM has been applied.

Table 5.1: Selected Factors and CFD Responses

Factors	Code	Units	Range
Pitch (*P*)	A	mm	4 to 10
Height (*e*)	B	mm	1.5 to 2.5
Reynolds Number (*Re*)	C	---	5×10^3 to 17.5×10^3
Nusselt Number (*Nu*)	Nu	---	39.42 to 138.34
Pressure Drop (ΔP)	DELTA P	Pa	15.15 to 389.33
Friction factor (*f*)	f	---	0.040 to 0.082
Thermal Enhancement Factor (*TEF*)	TEF	---	0.876 to 1.215

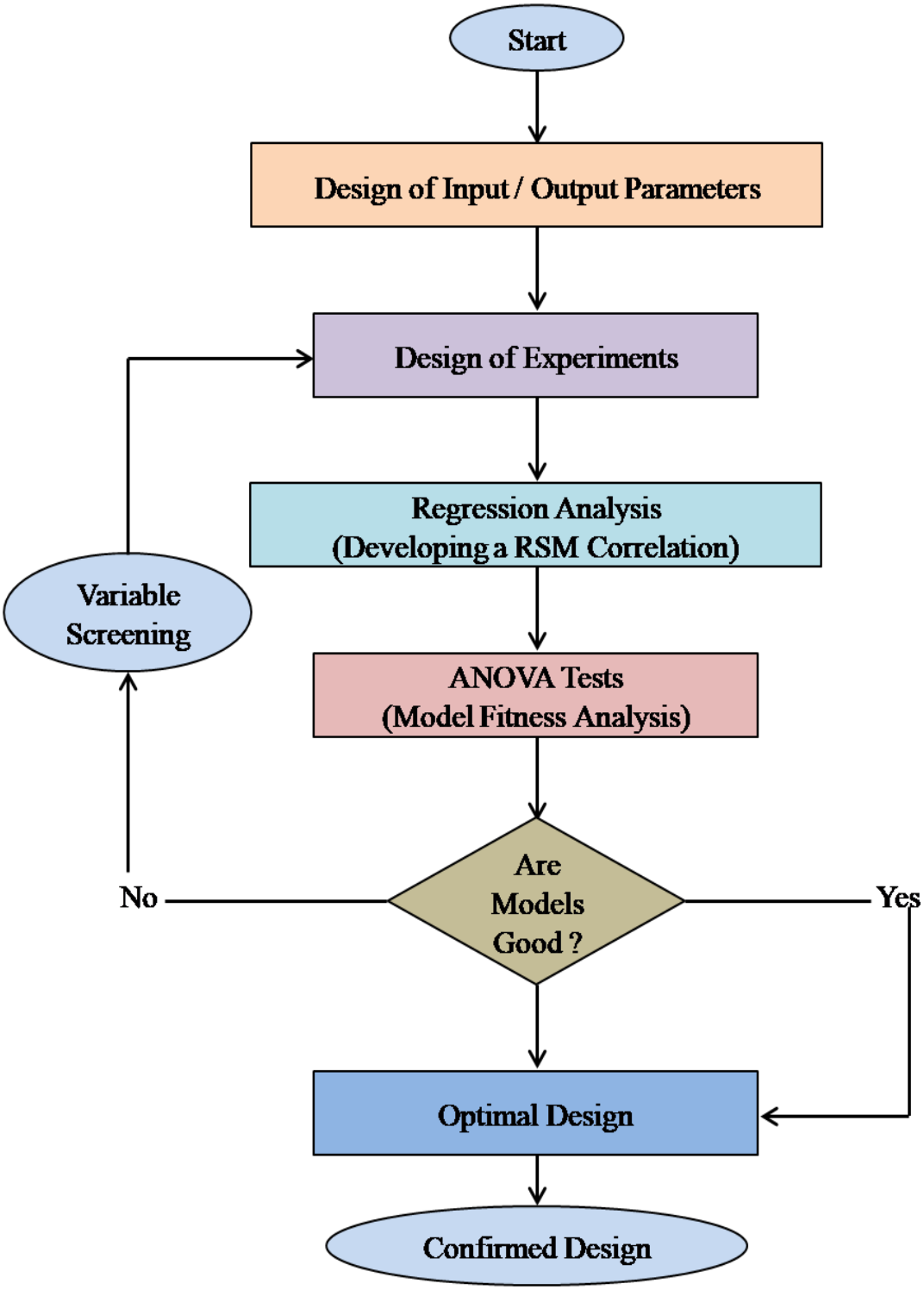

Fig. 5.1: RSM Implementation Procedure

5.3 Analysis of Variance (ANOVA) Analysis

Response factors are analyzed for their input-dependence using the analysis of variance (ANOVA) statistical technique. In the present work, cubic model is adopted

to perform the model analysis. An F-test (analysis of variance) has been carried out to ensure the model validity. Data of Table 5.2 indicates that the observed value of "Prob. > F" has a value less than 0.05, which is associated with 95% confidence level. It means that the implemented cubic model is statistically sound, which is desirable as it confirms the direct influence of the design elements on the Nusselt number. The significance of model terms is assessed using the p-value as a criterion; terms are considered significant if they are valued below 0.0500; terms exceeding 0.1000 are deemed insignificant. Here, the assigned codes A, B, C, AC, BC, A^2, B^2, C^2, A^2C, B^2C, BC^2, A^3, and C^3 are significant model terms. Finally, the data fits well if the R^2 (data variance indicator) value is near to one. As can be visible in Table 5.2, the "predicted R^2" is 0.9999, significantly much closer to "adjusted R^2" of 1.0000, with a difference less than 0.2 indicating that the model is highly precise and accurate. Moreover, in the "Adeq Precision" section, it can be seen that the SNR (signal-noise ratio) is 1027.664, which is much greater than the minimum requirement of 4. Similarly, the effect of controlled inputs has been shown on pressure drop too.

Table 5.2: ANOVA Table-Nu

Source	Sum of Squares	df	Mean Square	F-value	p-value	
Model	42682.67	14	3048.76	1.164E+05	< 0.0001	**significant**
A-*P*	6.51	1	6.51	248.62	< 0.0001	
B-*e*	52.59	1	52.59	2007.52	< 0.0001	
C-*Re*	4328.33	1	4328.33	1.652E+05	< 0.0001	
AC	9.11	1	9.11	347.87	< 0.0001	
BC	0.7388	1	0.7388	28.20	< 0.0001	
A^2	103.24	1	103.24	3941.29	< 0.0001	
B^2	83.07	1	83.07	3171.30	< 0.0001	
C^2	28.98	1	28.98	1106.34	< 0.0001	
A^2C	4.83	1	4.83	184.38	< 0.0001	
AC^2	0.0205	1	0.0205	0.7845	0.3836	
B^2C	7.09	1	7.09	270.70	< 0.0001	
BC^2	1.38	1	1.38	52.55	< 0.0001	
A^3	0.9453	1	0.9453	36.09	< 0.0001	
C^3	0.4026	1	0.4026	15.37	0.0005	

Residual	0.7073	27	0.0262	
Lack of Fit	0.7073	21	0.0337	
Pure Error	0.0000	6	0.0000	
Cor Total	42683.38	41		
Std. Dev.	0.1618		R^2	1.0000
Mean	89.54		Adjusted R^2	1.0000
C.V. %	0.1807		Predicted R^2	0.9999
			Adeq Precision	1027.664

Table 5.3 represents the F-test for pressure drop. Assigned codes A, B, C, BC, A^2, B^2, C^2, A^2C, B^2C, and A^3 represent significant terms. Values of the significant indicators are shown in Table 5.3. The "predicted R^2 = 0.9812 is quite close to the adjusted R^2 = 0.9952, indicating a very high degree of agreement between the two measures. Again, in the "Adeq Precision" section, it can be seen that the signal-to-noise ratio is 102.3767, which is much greater than the minimum requirement of 4.

Table 5.3: ANOVA Table-Δp

Source	**Sum of Squares**	**df**	**Mean Square**	**F-value**	**p-value**	
Model	3.085E+05	14	22037.78	606.71	< 0.0001	**significant**
A-*P*	831.62	1	831.62	22.89	< 0.0001	
B-*e*	2011.72	1	2011.72	55.38	< 0.0001	
C-*Re*	18983.81	1	18983.81	522.63	< 0.0001	
AC	26.07	1	26.07	0.7178	0.4043	
BC	3693.53	1	3693.53	101.68	< 0.0001	
A^2	775.04	1	775.04	21.34	< 0.0001	
B^2	21165.59	1	21165.59	582.70	< 0.0001	
C^2	7453.21	1	7453.21	205.19	< 0.0001	
A^2C	287.10	1	287.10	7.90	0.0091	
AC^2	17.33	1	17.33	0.4770	0.4957	
B^2C	11260.96	1	11260.96	310.02	< 0.0001	
BC^2	138.05	1	138.05	3.80	0.0617	
A^3	829.50	1	829.50	22.84	< 0.0001	
C^3	1.90	1	1.90	0.0524	0.8206	
Residual	980.74	27	36.32			

Lack of Fit	980.74	21	46.70	
Pure Error	0.0000	6	0.0000	
Cor Total	3.095E+05	41		
Std. Dev.	6.03		R^2	0.9968
Mean	111.46		Adjusted R^2	0.9952
C.V. %	5.41		Predicted R^2	0.9812
			Adeq Precision	102.3767

Table 5.4 represents the F-test for friction factor. Assigned codes A, B, C, AC, BC, A^2, B^2, A^2C, B^2C, BC^2 and A^3 represent significant terms. Values of the significant indicators are shown in Table 5.4. The "predicted R^2 = 0.9916 is quite close to the adjusted R^2 = 0.9983, indicating a very high degree of agreement between the two measures. Again, in the "Adeq Precision" section, it can be seen that the signal-to-noise ratio is 146.9777, which is much greater than the minimum requirement of 4.

Table 5.4: ANOVA Table-f

Source	**Sum of Squares**	**df**	**Mean Square**	**F-value**	**p-value**	
Model	0.0056	14	0.0004	1713.39	< 0.0001	**significant**
A-*P*	0.0001	1	0.0001	537.94	< 0.0001	
B-*e*	0.0004	1	0.0004	1843.39	< 0.0001	
C-*Re*	0.0000	1	0.0000	48.20	< 0.0001	
AC	1.140E-06	1	1.140E-06	4.92	0.0352	
BC	0.0000	1	0.0000	98.74	< 0.0001	
A^2	0.0001	1	0.0001	557.37	< 0.0001	
B^2	0.0031	1	0.0031	13229.51	< 0.0001	
C^2	7.515E-08	1	7.515E-08	0.3243	0.5738	
A^2C	3.156E-06	1	3.156E-06	13.62	0.0010	
AC^2	1.338E-08	1	1.338E-08	0.0577	0.8119	
B^2C	0.0001	1	0.0001	282.92	< 0.0001	
BC^2	1.691E-06	1	1.691E-06	7.30	0.0118	
A^3	0.0001	1	0.0001	613.78	< 0.0001	
C^3	3.961E-07	1	3.961E-07	1.71	0.2021	
Residual	6.257E-06	27	2.318E-07			
Lack of Fit	6.257E-06	21	2.980E-07			

Pure Error	0.0000	6	0.0000	
Cor Total	0.0056	41		
Std. Dev.	0.0005		R^2	0.9989
Mean	0.0501		Adjusted R^2	0.9983
C.V. %	0.9612		Predicted R^2	0.9916
			Adeq Precision	146.9777

Further, the F-test carried out on thermal enhancement (TEF) is delineated in Table 5.5. The significant codes factors are A, B, C, AC, BC, A^2, B^2, C^2, A^2C, B^2C, A^3, and C^3. Here, also the predicted R^2 = 0.9769 and adjusted R^2 = 0.9948 difference is less than 0.2, indicating the higher degree of agreement. Also, the SNR ratio equals to 85.9903 presented in "Adeq Precision" represents the high measure than the benchmark value of 4.

Table 5.5: ANOVA Table-TEF

Source	**Sum of Squares**	**df**	**Mean Square**	**F-value**	**p-value**	
Model	0.3428	14	0.0245	564.21	< 0.0001	**significant**
A-*P*	0.0165	1	0.0165	379.11	< 0.0001	
B-*e*	0.0345	1	0.0345	794.40	< 0.0001	
C-*Re*	0.0061	1	0.0061	139.97	< 0.0001	
AC	0.0007	1	0.0007	15.83	0.0005	
BC	0.0006	1	0.0006	14.81	0.0007	
A^2	0.0018	1	0.0018	42.48	< 0.0001	
B^2	0.2198	1	0.2198	5064.65	< 0.0001	
C^2	0.0046	1	0.0046	106.79	< 0.0001	
A^2C	0.0015	1	0.0015	35.29	< 0.0001	
AC^2	0.0001	1	0.0001	1.16	0.2914	
B^2C	0.0003	1	0.0003	6.43	0.0173	
BC^2	0.0001	1	0.0001	2.76	0.1085	
A^3	0.0133	1	0.0133	305.94	< 0.0001	
C^3	0.0007	1	0.0007	15.71	0.0005	
Residual	0.0012	27	0.0000			
Lack of Fit	0.0012	21	0.0001			
Pure Error	0.0000	6	0.0000			

Cor Total	0.3439	41		
Std. Dev.	0.0066		R^2	0.9966
Mean	1.10		Adjusted R^2	0.9948
C.V. %	0.5977		Predicted R^2	0.9769
			Adeq Precision	85.9903

The following are the cubic equations for the Nusselt number (*Nu*), pressure drop (ΔP), friction factor and thermal enhancement factor (*TEF*) in terms of assigned codes:

$$Nu = (92.89276 + 2.29344 \times \mathrm{A} - 3.22079 \times \mathrm{B} + 46.85805 \times \mathrm{C} + 1.19047 \times \mathrm{AC} - 0.36321 \times \mathrm{BC} - 4.36524 \times \mathrm{A^2} - 3.72092 \times \mathrm{B^2} - 2.14202 \times \mathrm{C^2} - 1.35314 \times \mathrm{A^2C} - 0.09440 \times \mathrm{AC^2} - 1.47134 \times \mathrm{B^2C} + 0.84862 \times \mathrm{BC^2} - 0.87901 \times \mathrm{A^3} + 0.46551 \times \mathrm{C^3}) \quad (5.2)$$

$$\Delta P = (85.93161 - 25.91655 \times \mathrm{A} + 19.92090 \times \mathrm{B} + 98.13314 \times \mathrm{C} - 2.01380 \times \mathrm{AC} + 25.68187 \times \mathrm{BC} - 11.96035 \times \mathrm{A^2} + 59.39358 \times \mathrm{B^2} + 34.35148 \times \mathrm{C^2} - 10.43262 \times \mathrm{A^2C} + 2.74114 \times \mathrm{AC^2} + 58.63417 \times \mathrm{B^2C} + 8.49825 \times \mathrm{BC^2} + 26.03883 \times \mathrm{A^3} + 1.01225 \times \mathrm{C^3}) \quad (5.3)$$

$$f = (0.0466 - 0.0100 \times \mathrm{A} + 0.0092 \times \mathrm{B} + 0.0024 \times \mathrm{C} - 0.0004 \times \mathrm{AC} + 0.0020 \times \mathrm{BC} - 0.0049 \times \mathrm{A^2} + 0.0226 \times \mathrm{B^2} + 0.0001 \times \mathrm{C^2} - 0.0011 \times \mathrm{A^2C} - 0.0001 \times \mathrm{AC^2} + 0.0045 \times \mathrm{B^2C} - 0.0009 \times \mathrm{BC^2} + 0.0108 \times \mathrm{A^3} - 0.0005 \times \mathrm{C^3}) \quad (5.4)$$

$$TEF = (1.16176 + 0.11526 \times \mathrm{A} - 0.08246 \times \mathrm{B} - 0.05550 \times \mathrm{C} + 0.01033 \times \mathrm{AC} + 0.01071 \times \mathrm{BC} - 0.01844 \times \mathrm{A^2} - 0.19138 \times \mathrm{B^2} - 0.02708 \times \mathrm{C^2} + 0.02409 \times \mathrm{A^2C} - 0.00466 \times \mathrm{AC^2} - 0.00923 \times \mathrm{B^2C} + 0.00790 \times \mathrm{BC^2} - 0.10417 \times \mathrm{A^3} + 0.01915 \times \mathrm{C^3}) \quad (5.5)$$

The *Nu*, pressure drop/friction factor, and *TEF* for modified receiver may be calculated with reasonable precision using the aforementioned formulae for a specified range of design variables.

Fig. 5.2 shows the comparison among calculated and predicted values of Nusselt number, pressure drop, friction factor and thermal enhancement factor. It can be seen from the pictures that fine agreement between predicted and calculated values is

observed which is necessary for verification of the model. Hence, it can be inferred that the model developed via the use of RSM approach effectively predicts the *Nu*, ΔP, *f*, and *TEF*, within the specified range of parameters with a notable level of precision. It may be stated also on the basis of graphical representations shown in Fig. 5.3, as it is evident from these plots that the residuals exhibit a reasonably linear pattern.

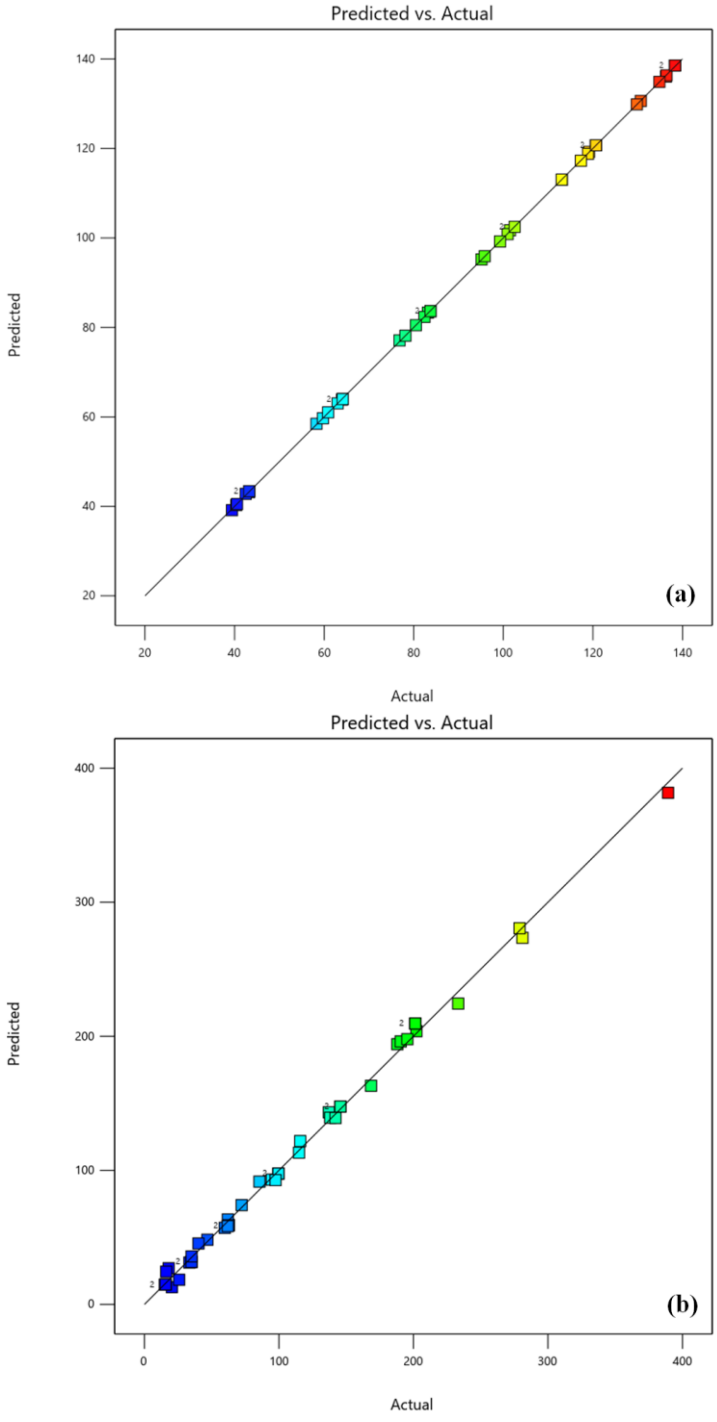

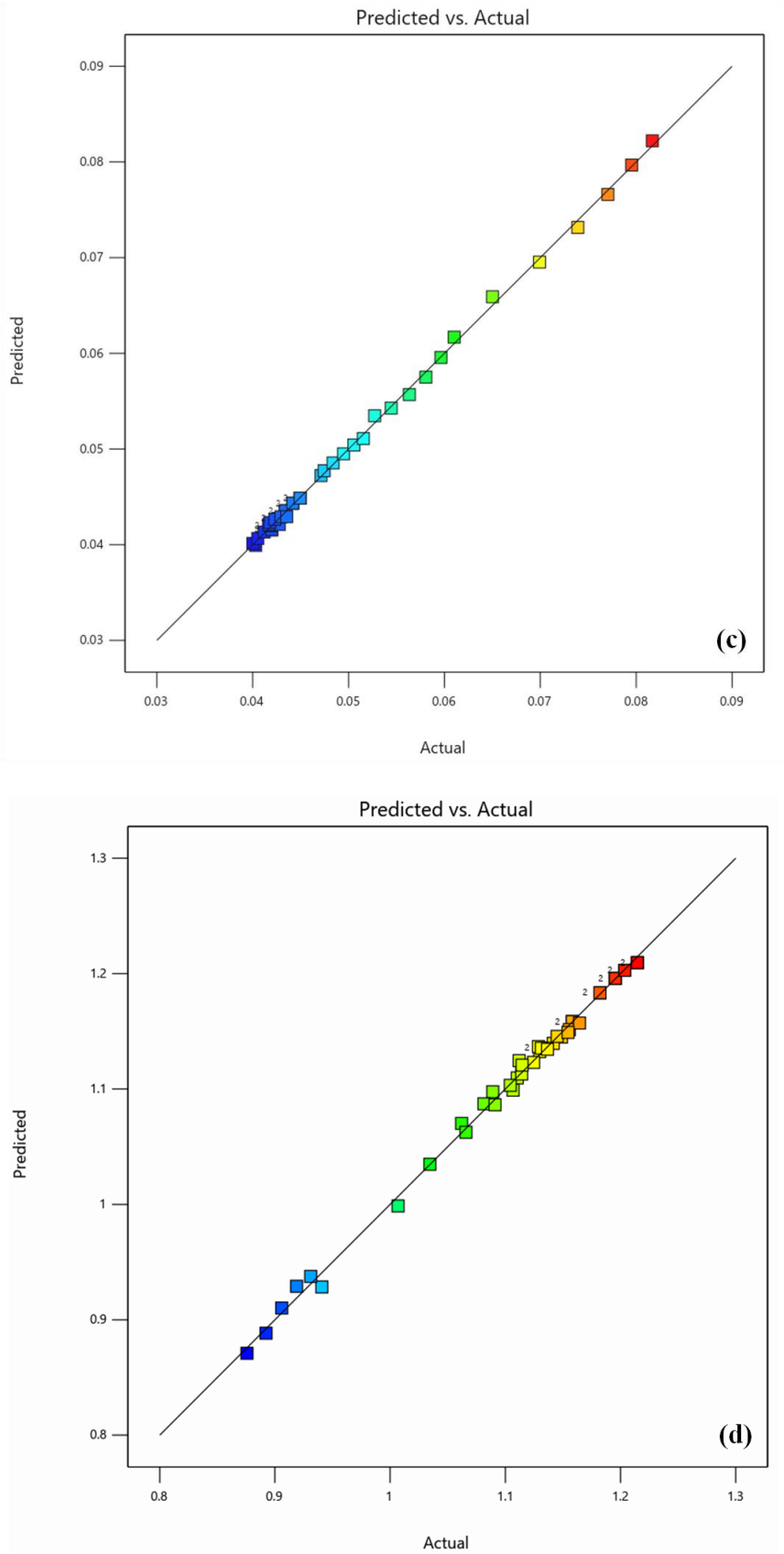

Fig. 5.2: Computed and Predicted Values: (a) Nu, (b) ΔP, (c) f, and (d) TEF

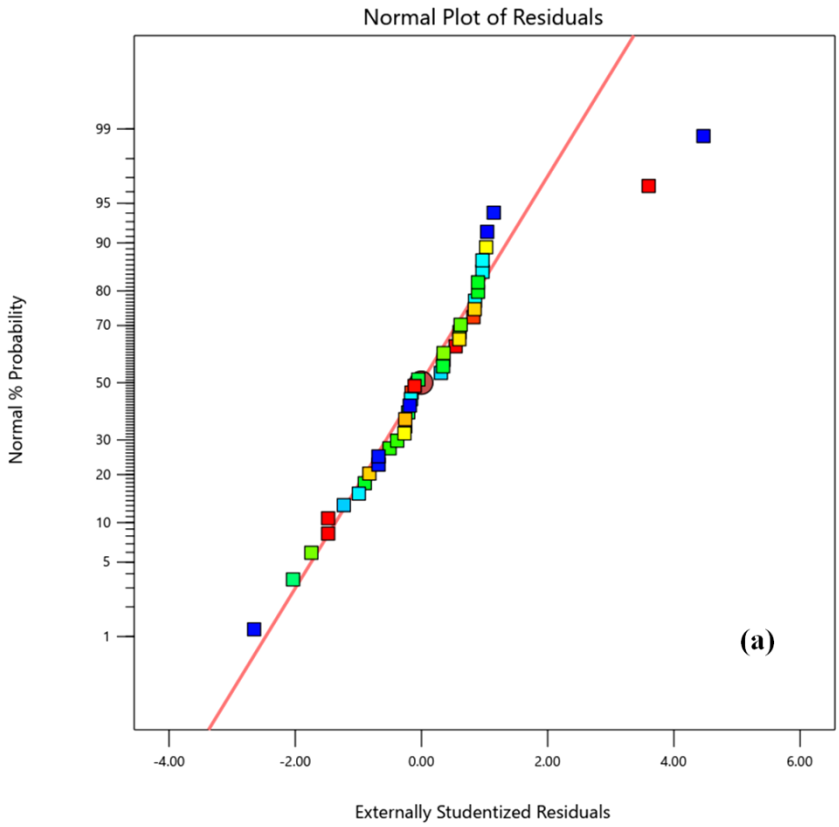
Normal Plot of Residuals
Normal % Probability
99
95
90
80
70
50
30
20
10
5
1
-4.00
-2.00
0.00
2.00
4.00
6.00
Externally Studentized Residuals
(a)

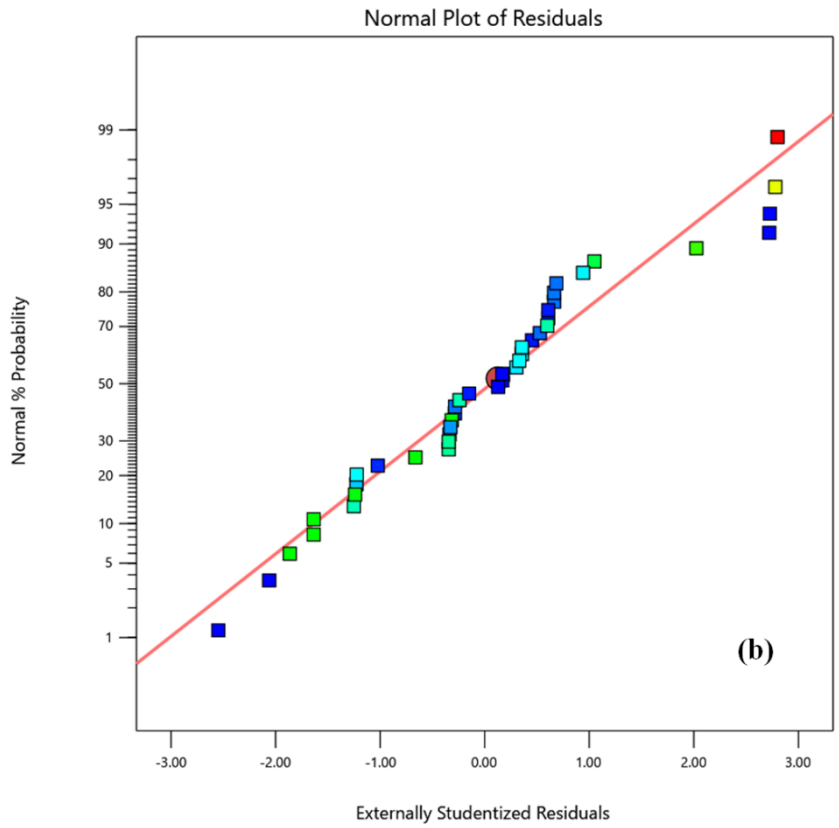
Normal Plot of Residuals
Normal % Probability
99
95
90
80
70
50
30
20
10
5
1
-3.00
-2.00
-1.00
0.00
1.00
2.00
3.00
Externally Studentized Residuals
(b)

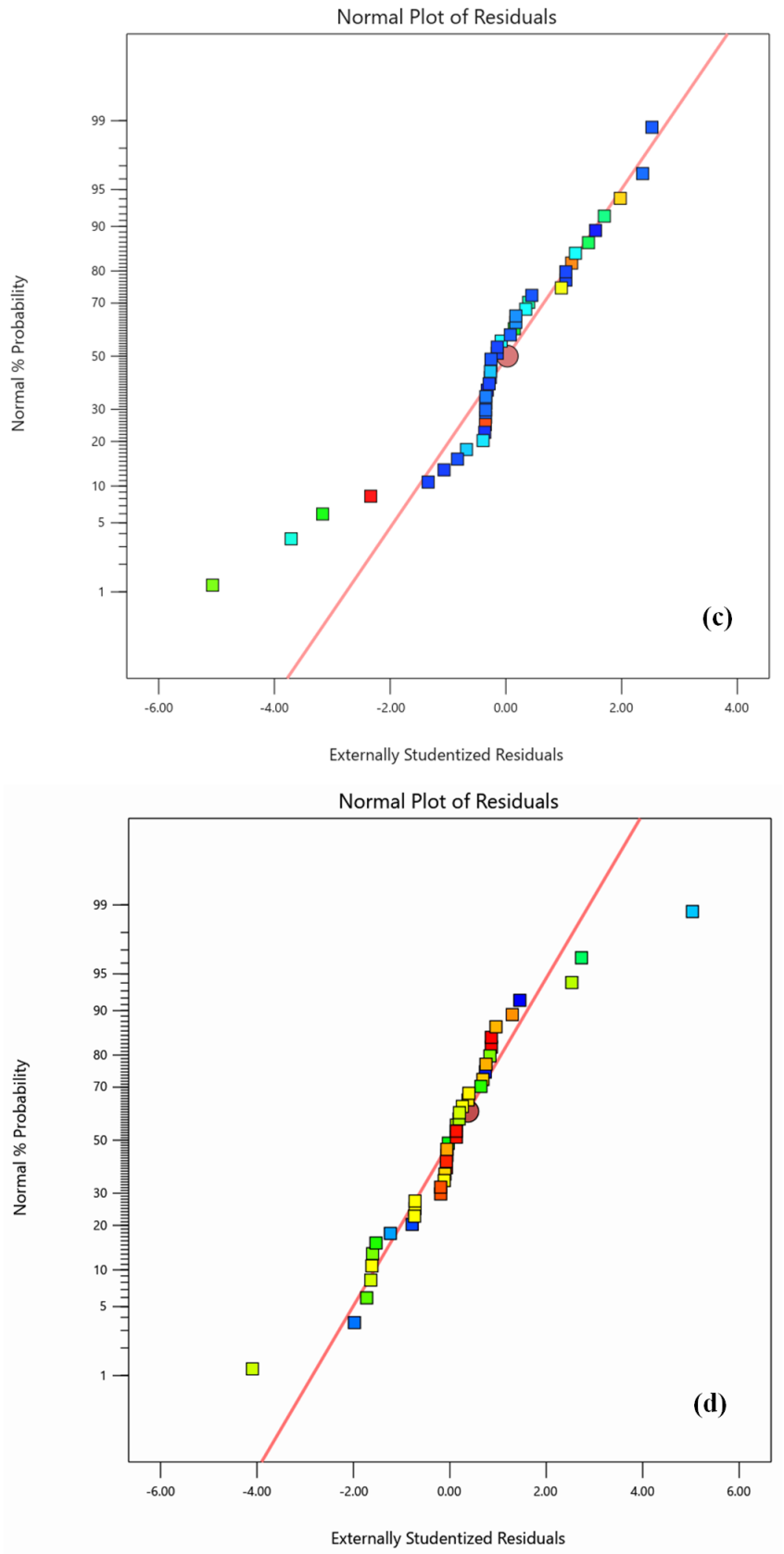

Fig. 5.3: Residuals Plots: (a) Nu, (b) ΔP, (c) f, and (d) TEF

5.4 Heat Transfer Characteristics

The double (symmetrical convex-concave) corrugations are introduced to induce turbulence inside the sub-layer of laminar region, hence augmenting the heat transmission. This facilitates the efficient dissipation of heat from the heated surfaces of the pipe walls. The turbulence and its amplitude are contingent upon the geometric dimensions corrugations. Hence, this study aims to optimize the key elements, such as the pitch, and height of the corrugation. Specifically, the focus is on examining the resulting variations in heat transmission and the pressure drop. The subsequent sections are discussing the effect of said changes.

5.4.1 Effect of Corrugation Pitch (*P*)

The corrugation pitch refers to the distance between successive peaks or troughs in a corrugated surface. It specifically describes the distance between these repetitive geometric features along the length of the receiver pipe of parabolic trough solar collectors. It plays a significant role in determining the thermal performance of corrugated receiver pipes in parabolic trough solar collectors. So, this experiment included observing the impact of corrugation pitch on heat transfer, while maintaining constant height. The effect has been shown in Figs. 5.4 and 5.5, where the Nusselt number and Reynolds numbers are plotted against the different corrugation pitches. The corrugation height has been set at 2 mm, for this experiment. These plots demonstrate a positive correlation between the Nusselt number and the Reynolds number. Additionally, it has been pointed out that the increase in Nusselt number has been observed when pitch size changes from 4 mm to 8 mm. Thereafter, it gets reduces for all values of *Re*. Hence, it is cleared from these plots that maximum Nusselt number has been recorded for 8 mm pitch case. The Nusselt number at this particular pitch is larger, indicating a greater magnitude of turbulence caused by the presence of corrugations. This increased turbulence results in enhanced heat transfer. To distinguish receiver flow behaviour, Fig. 5.6 depicts velocity magnitude field surface streamlines for different settings. In all cases, local velocity rises towards the centre of pipe and declines towards the surface of wall. Liquid flow changes direction and creates vortices because of corrugations. The velocity patterns observed in different types of corrugated pipes demonstrate the axial whirling and the production of vortexes led to an improvement in heat transfer. Furthermore, the pipe with 8 mm

corrugation pitch exhibits larger recirculation size and better mixing flow areas compared to other cases, an indication of better heat transmission.

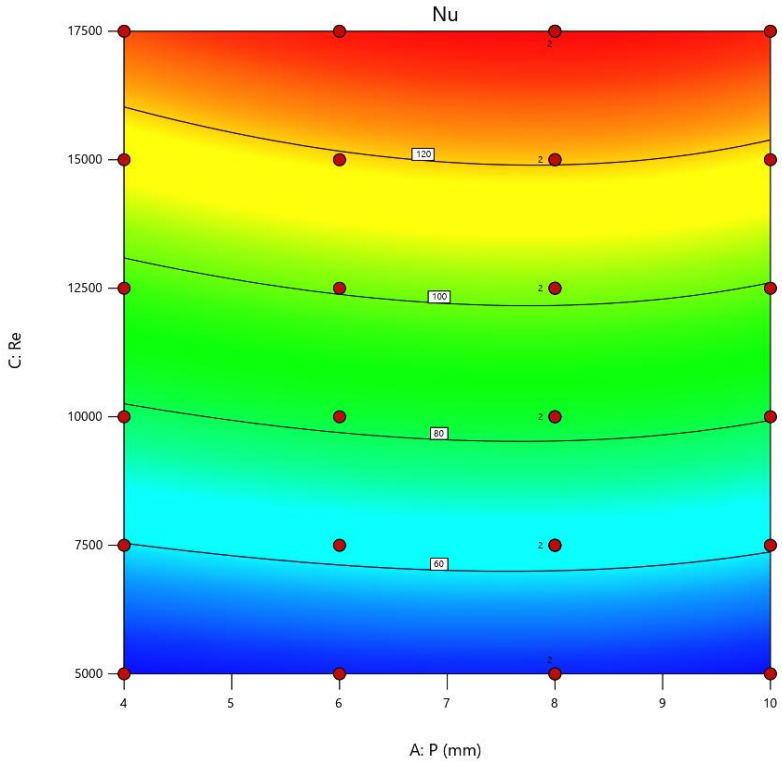

Fig. 5.4: Corrugation Pitch (P) and Reynolds Number (Re) Effect on Nu: Contour Plot

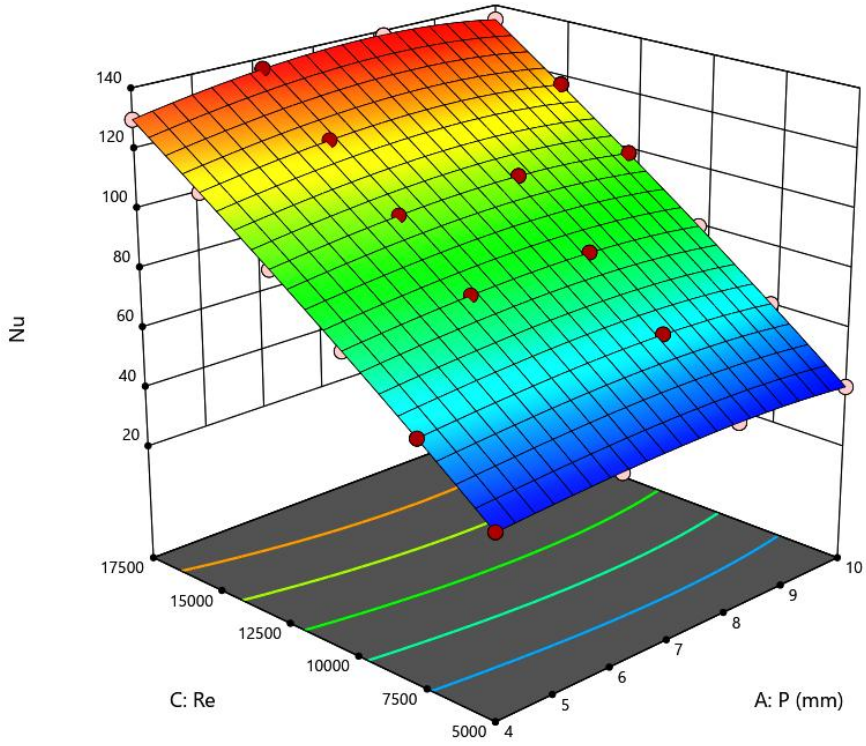

Fig. 5.5: Corrugation Pitch (P) and Reynolds Number (Re) Effect on Nu: 3D Surface

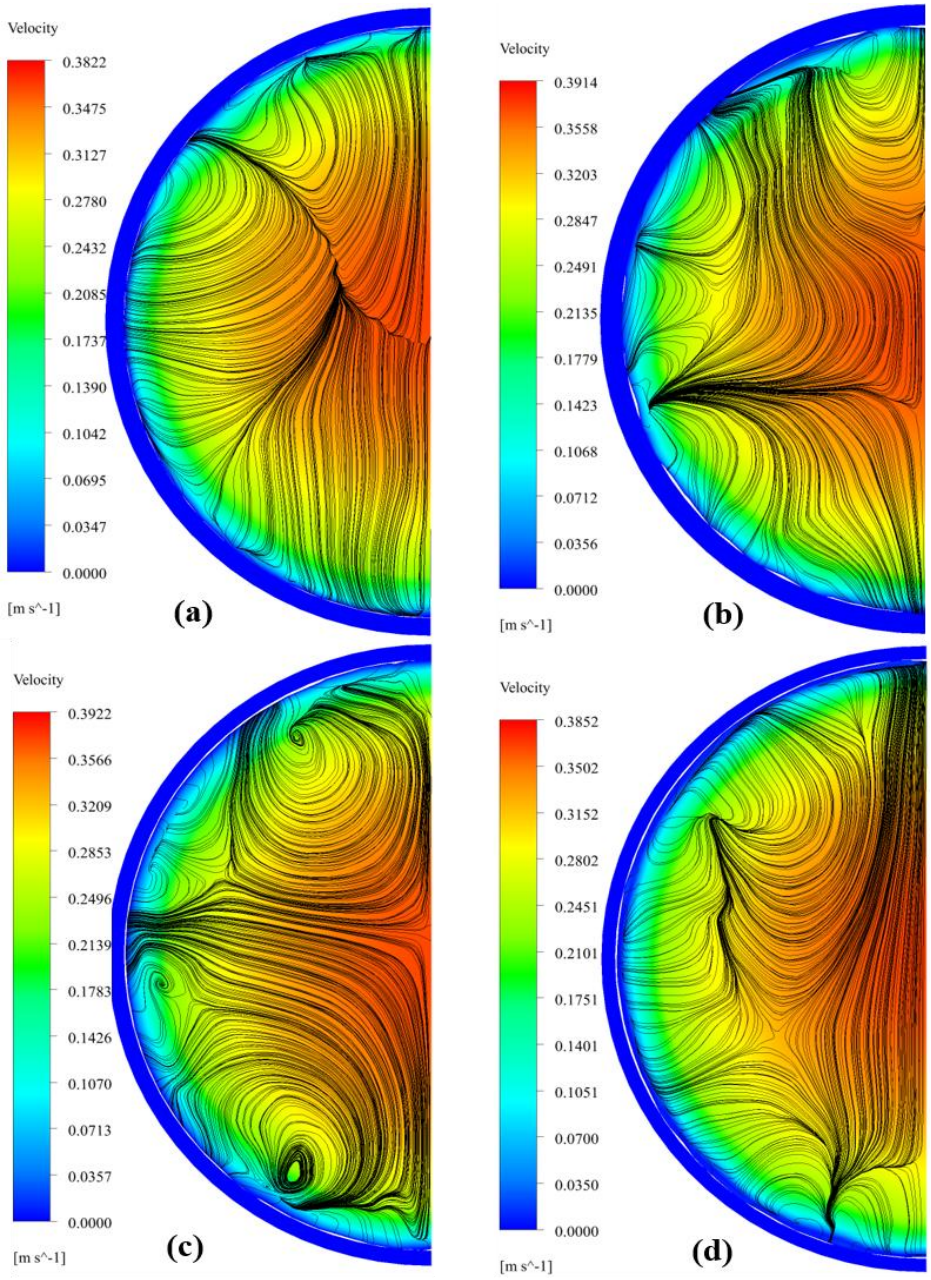

Fig. 5.6: Effect of Corrugation Pitch [(a) 4 mm, (b) 6 mm, (c) 8 mm, and (d) 10 mm]: Velocity Surface Streamlines for *Re* = 17500 and Corrugation Height = 2 mm

5.4.2 Effect of Corrugation Height (*e*)

Corrugation height refers to the vertical distance between the peak and the trough of a corrugated surface. In other words, it is the amplitude or the depth of the corrugations. The corrugation height, along with other parameters like the pitch, plays a critical role in determining the thermal performance of the receiver pipe. Figs. 5.7 and 5.8 show the effect of corrugation height on Nusselt number for different values of Reynolds

number, maintaining fixed value (8 mm) of corrugation pitch. When the height of the corrugations is increased from 1.5 mm to 2 mm, the Nusselt number continues to climb over a variety of flow rate situations, as can be seen from these plots. In addition, the influence that was found on the Nusselt number decreases as the corrugation height further increases, namely from 2 mm to 2.5 mm. The axial whirling and vortex formations inside the pipe significantly affect the turbulence and hence thermal performance. The aforementioned effect can be seen in Fig. 5.9, where it is plainly visible that the swirling tendency of the heat transfer fluid flowing through the receiver pipe increases when the height of corrugation changes from 1.5 mm to 2 mm, and then decreases on further increment in corrugations height from 2 mm to 2.5 mm. This is a clear indication of the effect (recirculation size and mixing flow areas) that was mentioned earlier. As a result, the receiver that is equipped with a corrugations height of 2 mm is the one that achieves the most improvement in heat transmission.

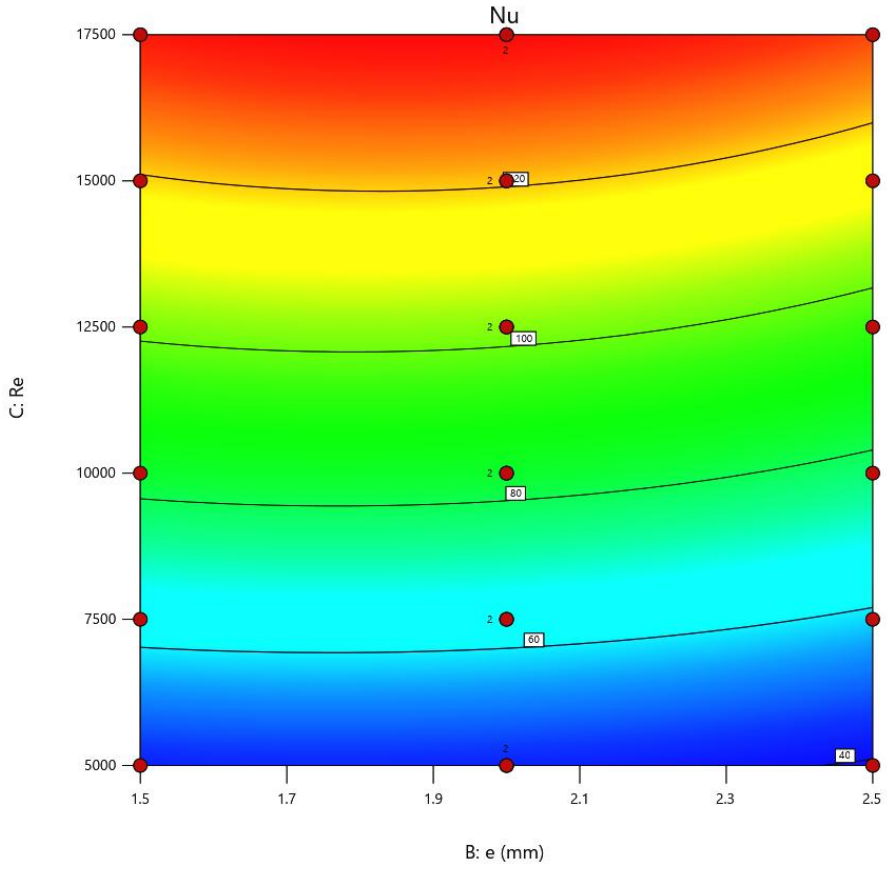

Fig. 5.7: Corrugation Height (e) and Reynolds Number (Re) Effect on Nu: Contour Plot

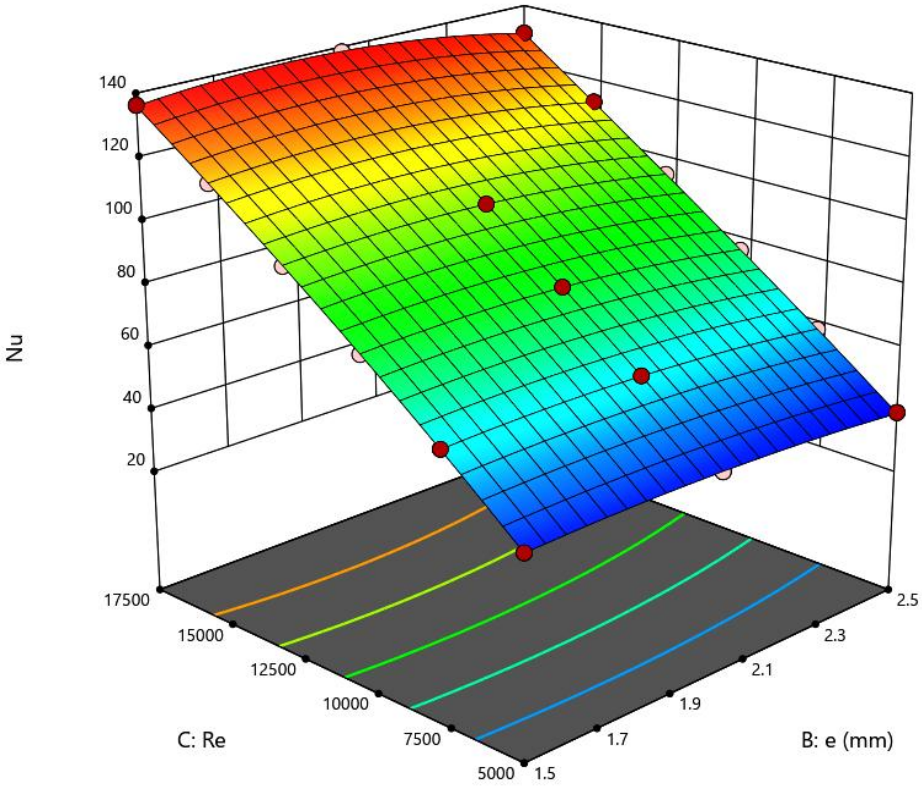

Fig. 5.8: Corrugation Height (e) and Reynolds Number (Re) Effect on Nu: 3D Surface

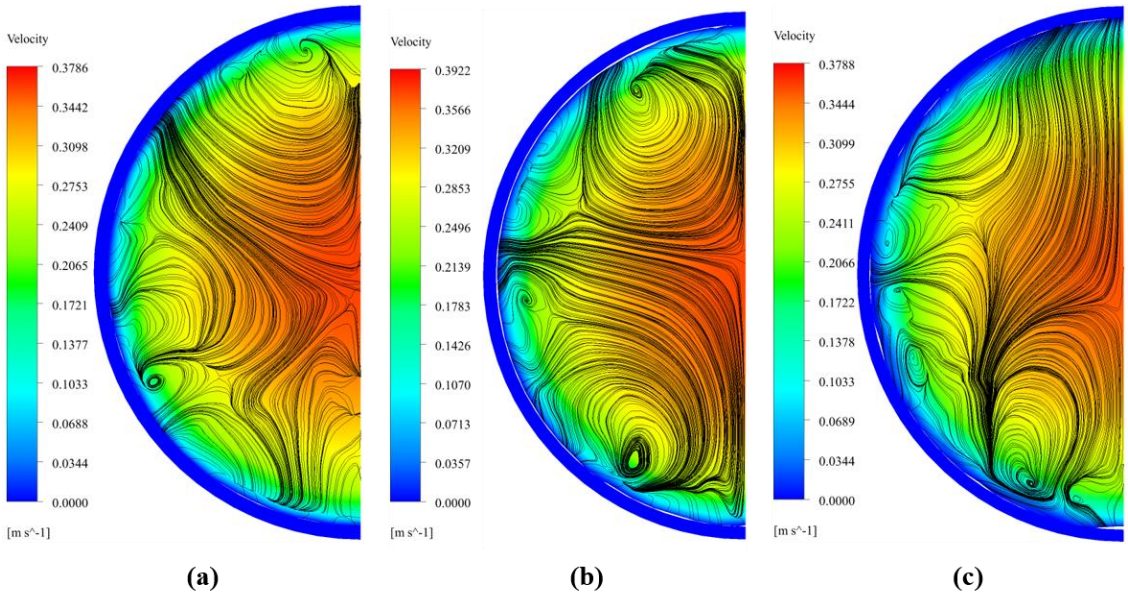

Fig. 5.9: Effect of Corrugation Height [(a) 1.5 mm, (b) 2 mm, and (c) 2.5 mm]: Velocity Surface Streamlines for *Re* = 17500 and Corrugation Pitch = 8 mm

5.5 Hydraulic Characteristics

It has been established that the use of double corrugations contributes to the promotion of heat transmission due to the propensity of swirl and flow mixing. One other effect of the design in question is that it causes an increase in the pressure drop. A demonstration of how such corrugations influence the pressure drop is provided in this section.

5.5.1 Effect of Corrugation Pitch (*P*)

For the purpose of representing the influence on the pressure drop, variations in the corrugation pitch and Reynolds number are used. During the generation of these plots, the height of the corrugation is maintained at a fixed level, but the pitch of the corrugation is susceptible to vary. The plots generated are shown in Figs. 5.10 and 5.11.

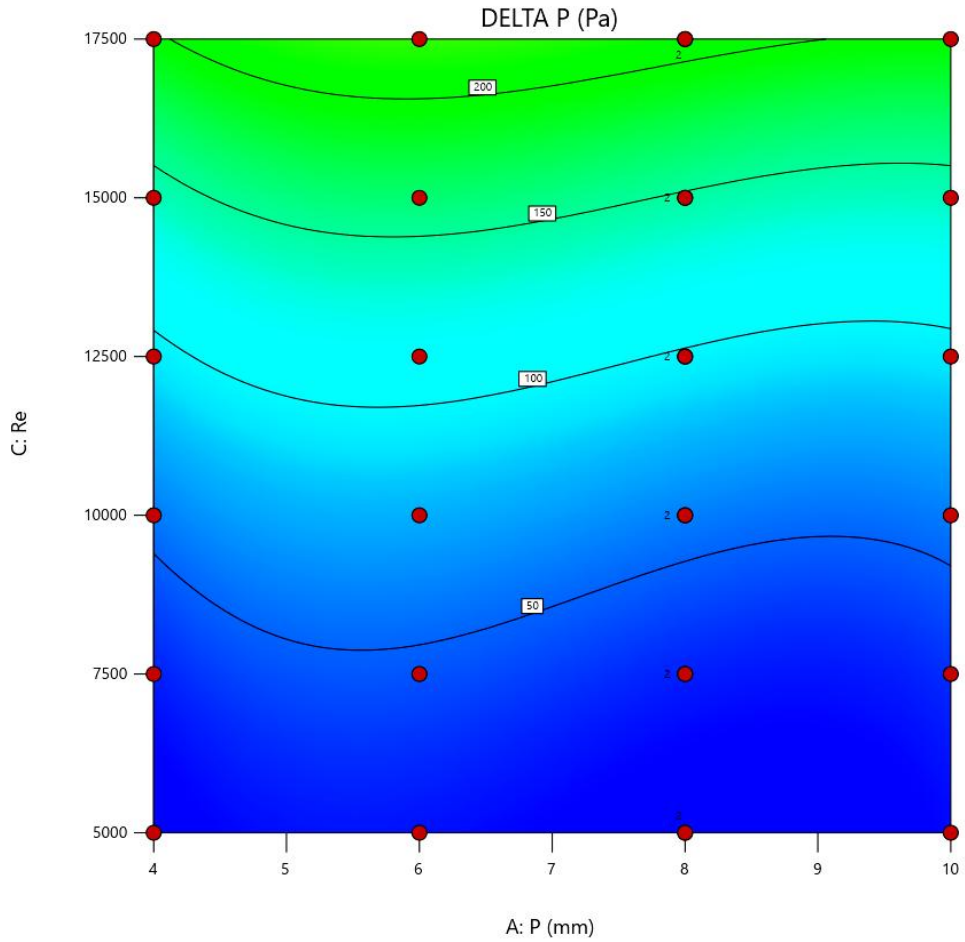

Fig. 5.10: Corrugation Pitch (P) and Reynolds Number (Re) Effect on Pressure Drop (ΔP): Contour Plot

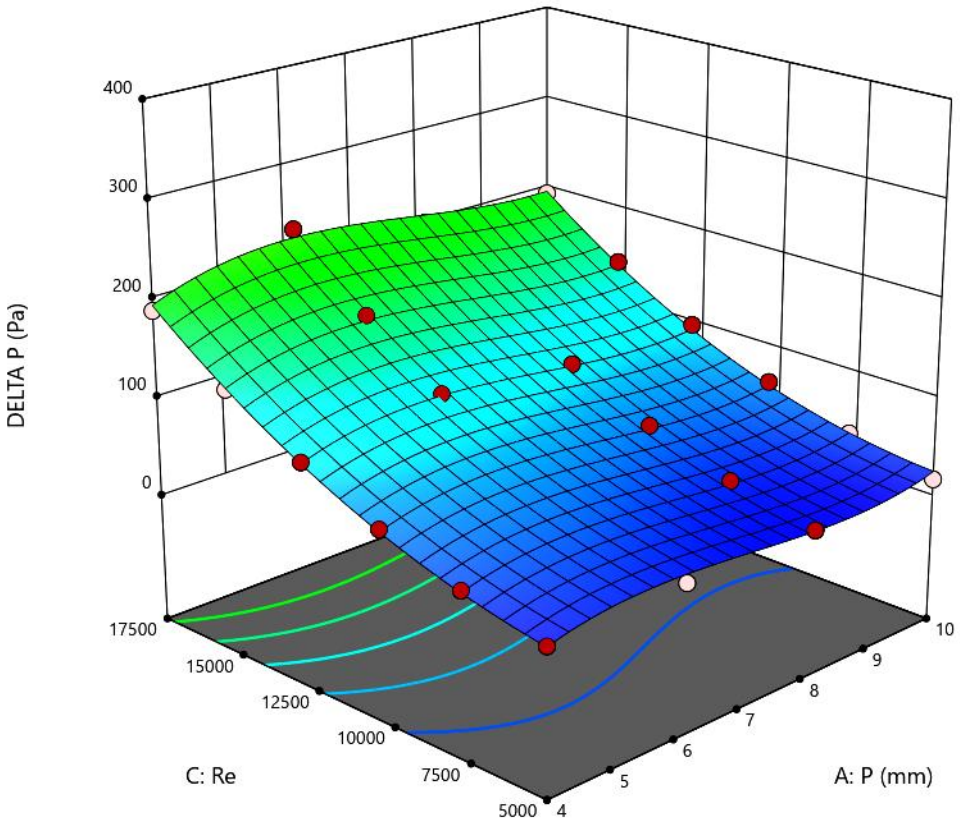

Fig. 5.11: Corrugation Pitch (P) and Reynolds Number (Re) Effect on Pressure Drop (ΔP): 3D Surface

These indicate that the pressure drop increases in proportion to the increase in the Reynolds number. As previously established, presence of corrugations equates to enhanced turbulence. This turbulence, which is the consequence of the corrugations, causes the creation of a vortex inside and around the corrugations, increased flow separation, as well as causes the fluid to encounter more friction. It is unsurprising that all of these factors together lead to an escalation in the pressure drop. Additionally, it can be seen from these plots that the pressure drop increases when the pitch value transitions from 4 mm to 6 mm, and then decreases upto 10 mm pitch case. Maximum pressure drops have been reported for receivers with corrugations that have a pitch size of 6 mm. It may be attributed to the fact that the fluid experiences more frictional resistance as it navigates the tighter and more frequent undulations, leading to a greater loss in pressure. Conversely, a larger corrugating pitch results in more widely spaced corrugations, which create less frequent disturbances in the fluid flow. This reduces the frictional losses, leading to a lower pressure drop.

5.5.2 Effect of Corrugation Height (*e*)

The vertical distance between the peak and trough of a corrugated surface, plays a significant role in determining the pressure drop of fluid flowing through a corrugated pipe. This parameter influences the flow dynamics within the tube, which directly affects the energy required to pump the fluid through the system. Here, Figs. 5.12 and 5.13 are presented to show the behaviour of corrugation height on pressure penalty. It is clearly visible from these plots that Reynolds number increase resulting in rising of pressure drop. This effect occurs due to the flow obstructions and viscosity losses found near the wall surface of pipe. As the height of corrugations start increasing from 1.5 mm to 2 mm, the pressure drop reduces. Thereafter, the further increment in height value to 2.5 mm, it (pressure drop) gets increases. This indicates that a greater amount of resistance has been occurred as the corrugation height gets increased. The peaks and troughs cause the fluid to accelerate and decelerate repeatedly, which increases the energy dissipation in the form of frictional losses. The presence of more frequent vortices inside the pipe, resulting in greater pressure drop.

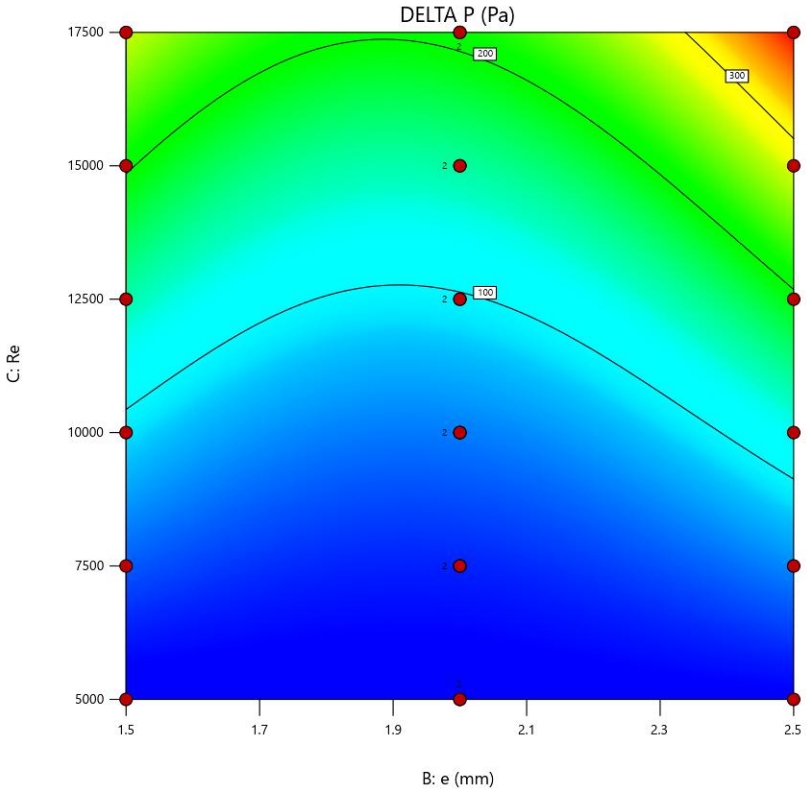

Fig. 5.12: Corrugation Height (e) and Reynolds Number (Re) Effect on Pressure Drop (ΔP): Contour Plot

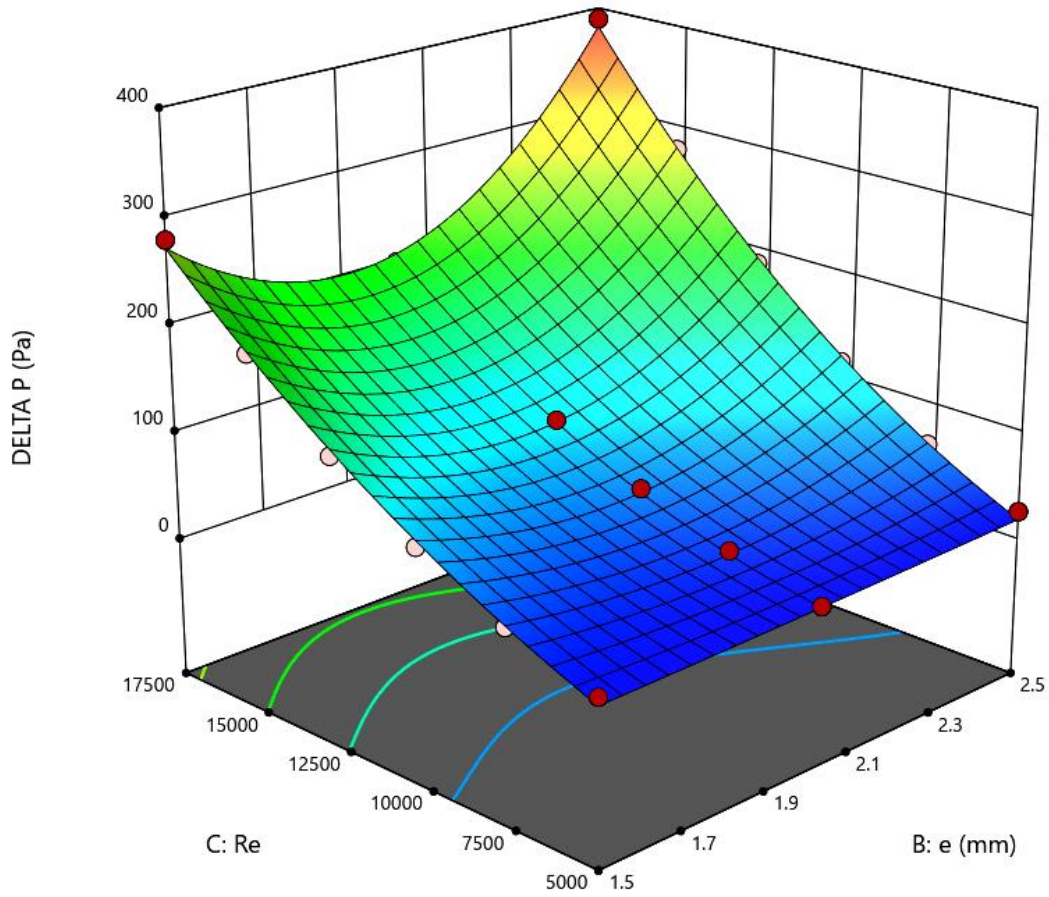

Fig. 5.13: Corrugation Height (e) and Reynolds Number (Re) Effect on Pressure Drop (ΔP): 3D Surface

5.6 Thermal Enhancement Factor (*TEF*)

When using a design that incorporates symmetrical convex-concave corrugations, there is the generation of turbulence near wall region, which disrupts the sub-layer of laminar region. This happens as a consequence of flow mixing/axial whirling and vortex generation around the corrugated faces. Hence, the thermal resistance decreases, and heat transmission increases. The usage of double corrugated receiver pipe, on the other hand, results in an increase in pressure drop, which in turn results in an increase in the amount of power that is needed by the system. In order to accurately characterize the significant aspects of modified receiver pipe, it is necessary to take into account both the thermal and the hydraulic parameters. As a result, it is helpful to estimate the thermal enhancement factor (*TEF*), in order to carry out a comprehensive analysis of the improvement in heat transmission. Finding the

best combinations of corrugation pitch and height for maximum heat transmission with least friction penalty has been estimated with the use of the thermal enhancement factor *TEF*. Figs. 5.14-5.17 show the variation in *TEF* of modified receiver pipe as a function of Reynolds number, corrugation pitch, and corrugation height. It can be seen from these plots that *TEF* increases with rise in Reynolds number, attains maxima and subsequently dropped with further rise. This behaviour of TEF may be characterized by an elevation in the power required for pumping, beyond the thermal benefits, for a certain value of velocity flow rate relative to the geometrical parameters. The CFD trials have determined that the maximum value of *TEF* for double corrugated receiver pipe occurred for pitch size of 8 mm, height of 2 mm, and Reynolds number value of 7500.

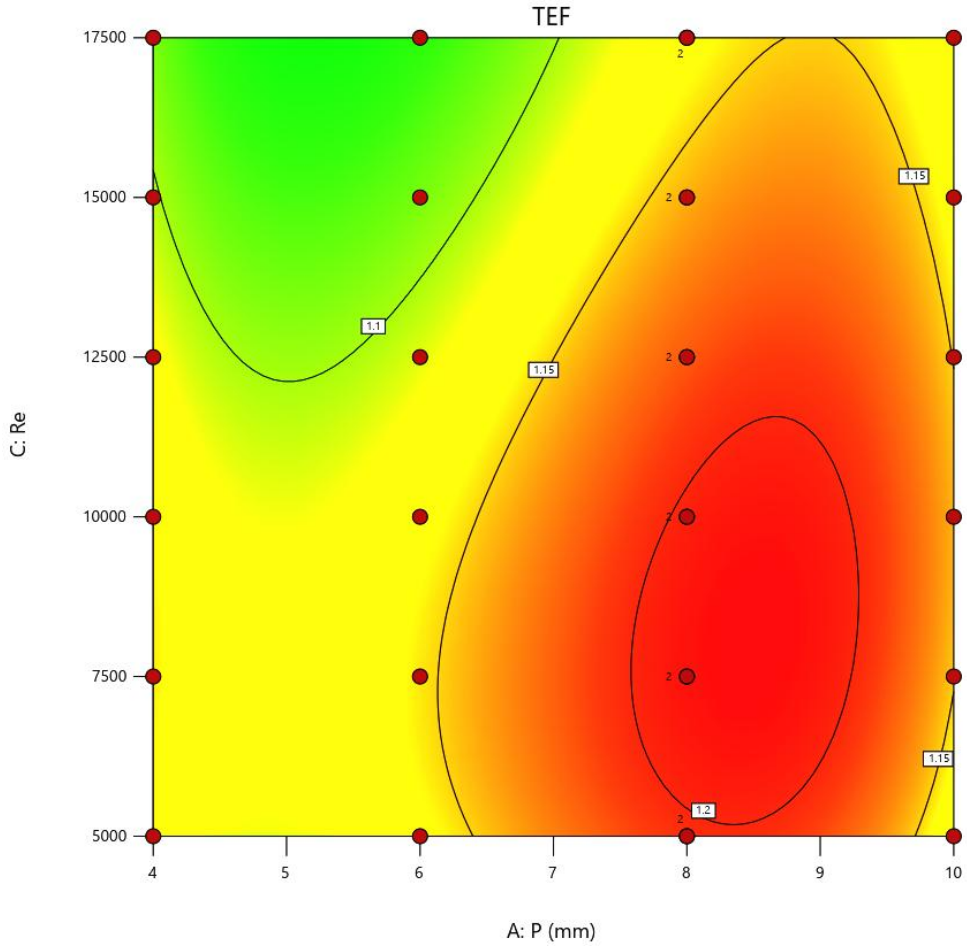

Fig. 5.14: Corrugation Pitch (P) and Reynolds Number (Re) Effect on TEF: Contour Plot

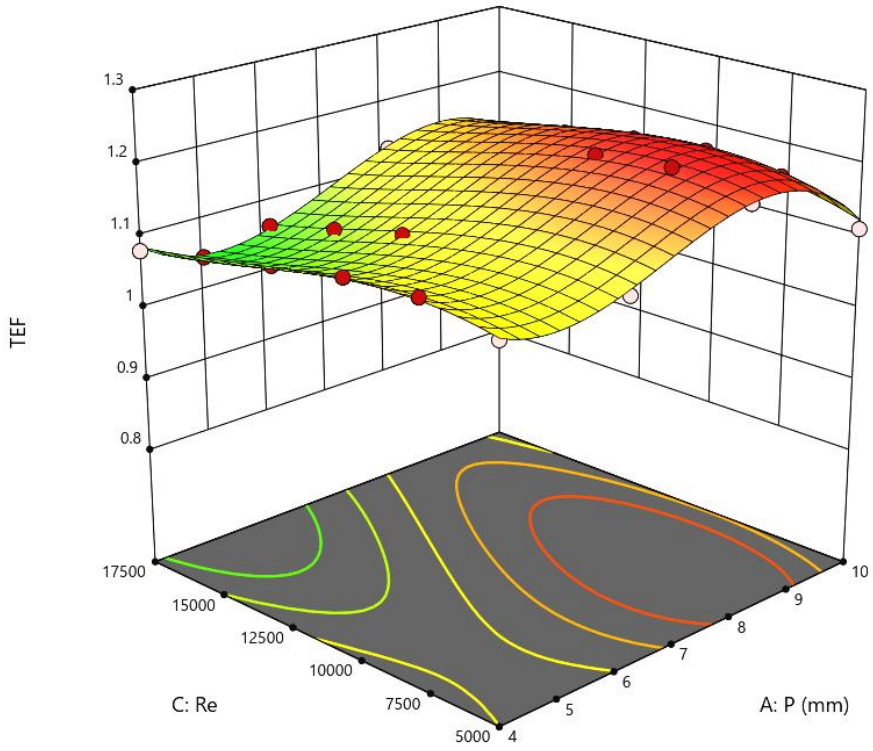

Fig. 5.15: Corrugation Pitch (P) and Reynolds Number (Re) Effect on TEF: 3D Surface

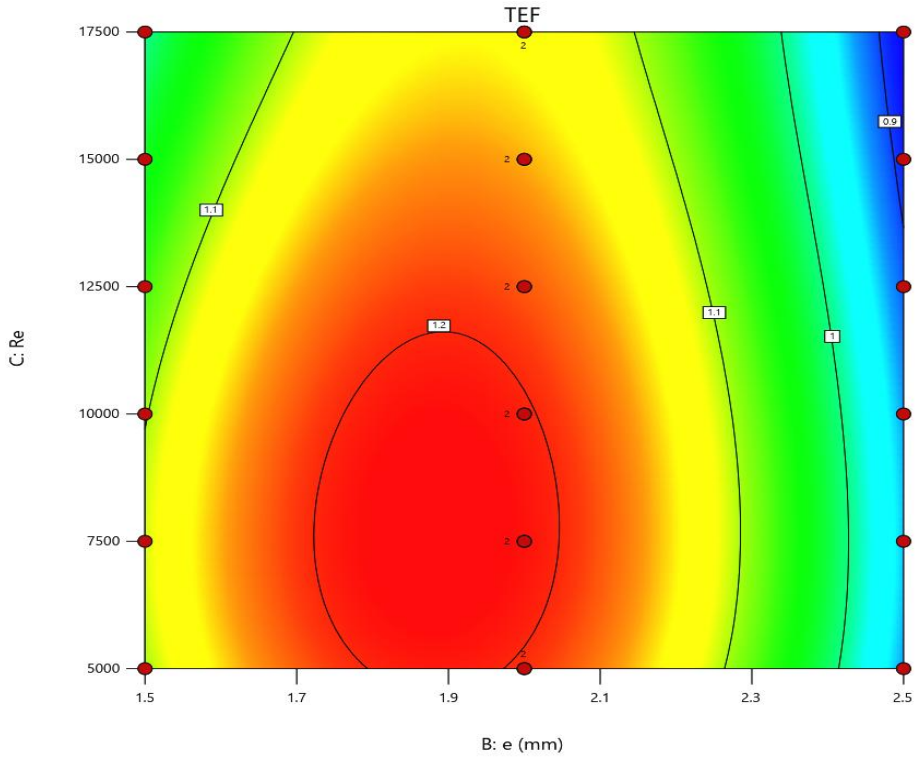

Fig. 5.16: Corrugation Height (e) and Reynolds Number (Re) Effect on TEF: Contour Plot

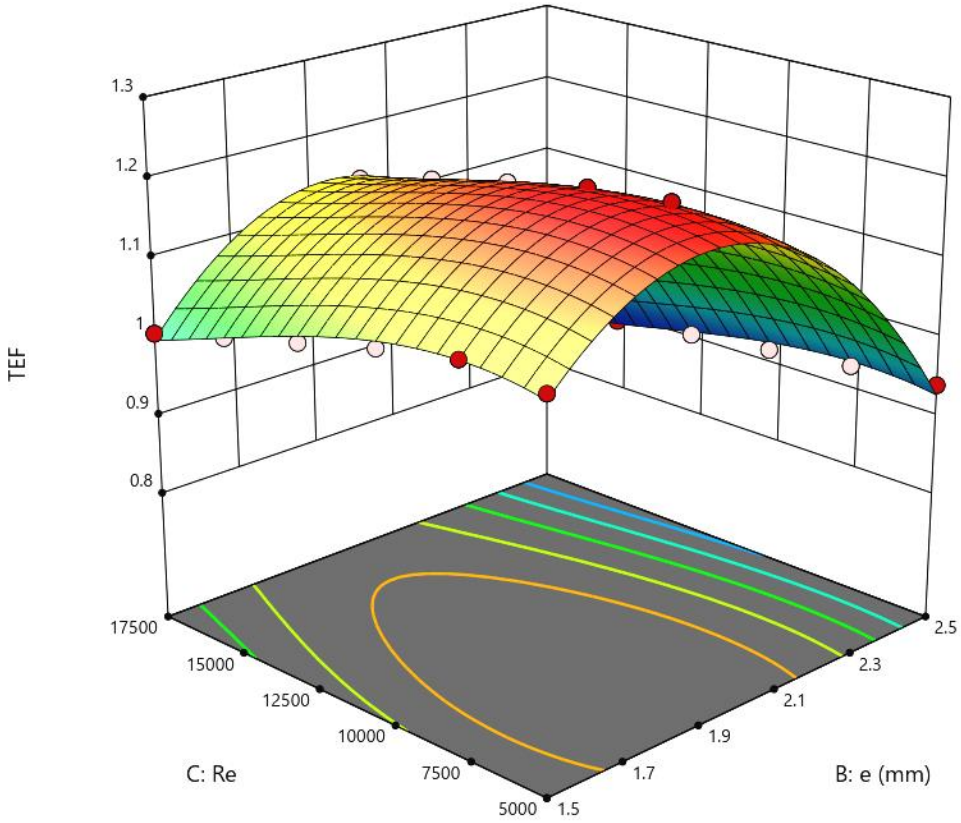

Fig. 5.17: Corrugation Height (e) and Reynolds Number (Re) Effect on TEF: 3D Surface

5.7 Optimization of Design Parameters

The objective of identifying the optimum thermal enhancement factor is to ascertain the associated design variables and their respective values that would result in the most efficient functioning of the PTSC system. Table 5.6 displays the associated design parameters as well as the corresponding response of the model. Figs. 5.18-5.21 reveal the following optimum values of associated design parameters:

- Corrugation Pitch (P) = 8.145 mm, Corrugation Height (e) = 1.918 mm, Re = 7477.55

Table 5.6: Input Parameters Range and Associated Responses

Parameter	Range	RSM Code	Goal
Corrugation Pitch (P)	4 mm - 10 mm	A	In Range
Corrugation Height (e)	1.5 mm - 2.5 mm	B	In Range
Reynolds Number (Re)	5000 - 17500	C	In Range
TEF	0.876 - 1.215	TEF	Maximum

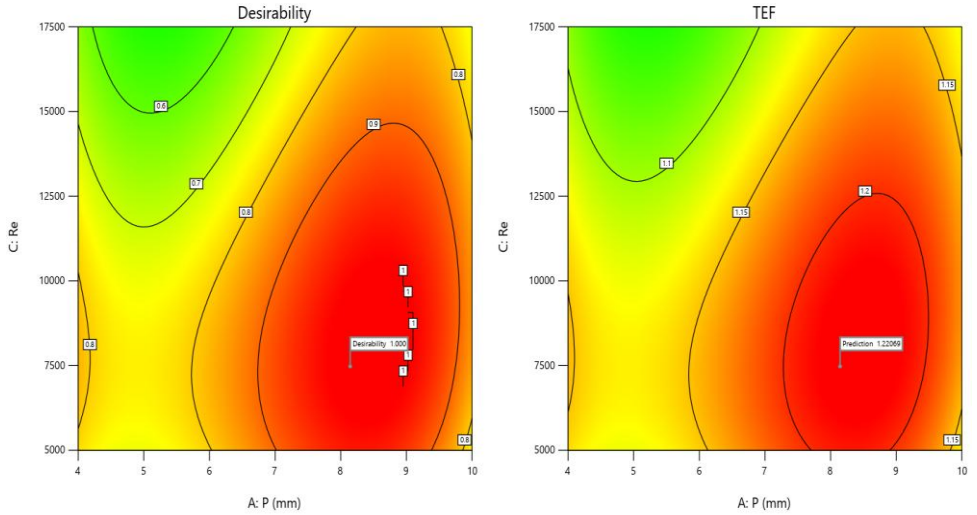

(a)

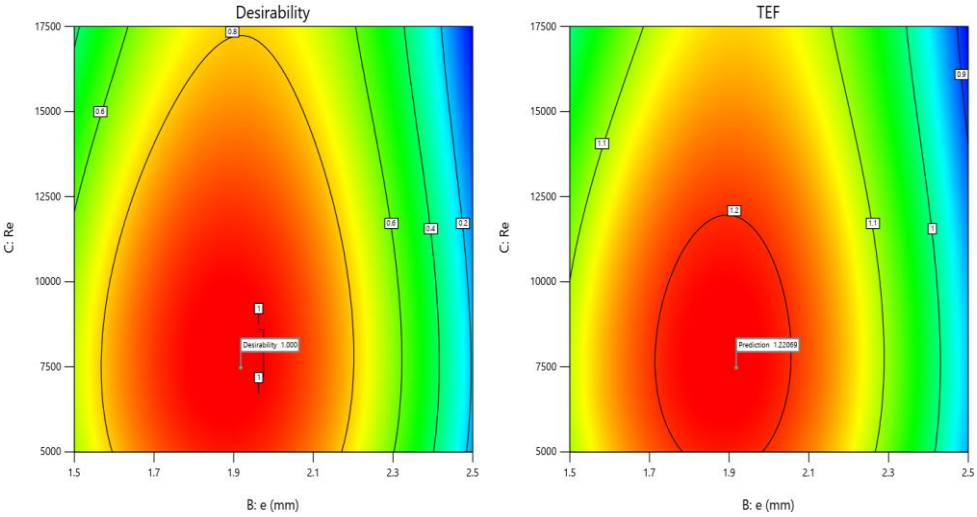

(b)

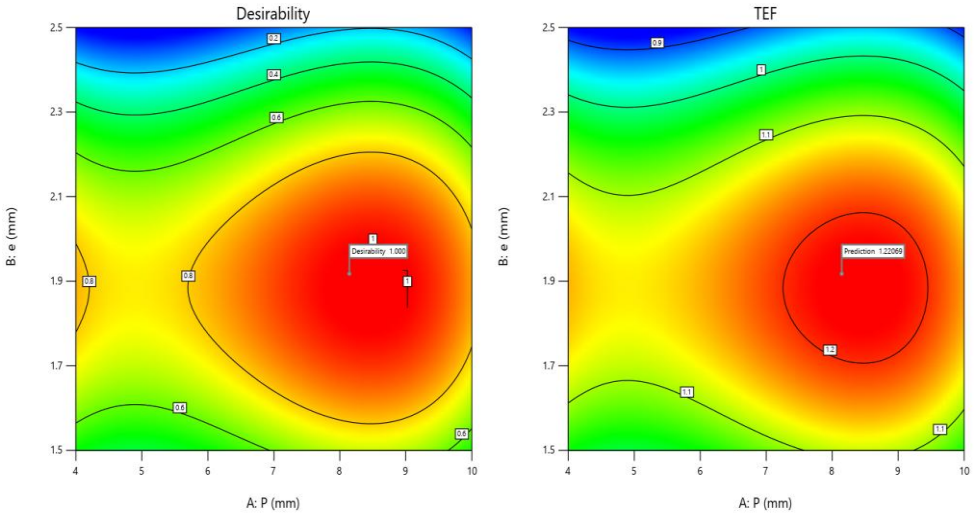

(c)

Fig. 5.18: Contour Plots for Optimized Design Parameters and TEF

Figs. 5.19-5.21 demonstrate that the results developed by RSM model are quite near to the model's maximum expectation. The bar graph presented as Fig. 5.21 demonstrates how close the output is to the ideal outcome, which is represented as a variable ranging from 0 to 1. A desirability of about 1 is considered to be rather satisfactory, and the bar graph depicts how each design aspect has been best tuned to meet the objectives.

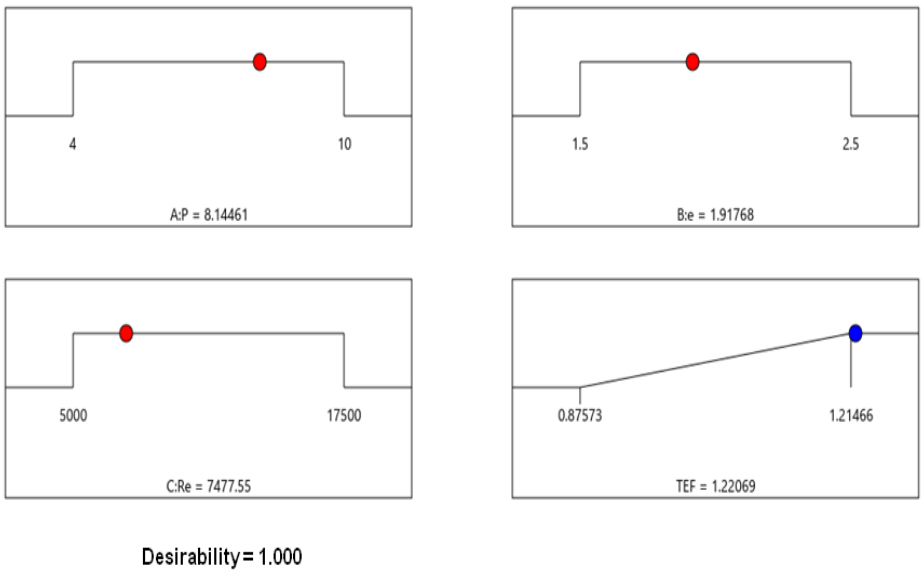

Fig. 5.19: Ramp Graphs for Optimized Design Parameters and TEF

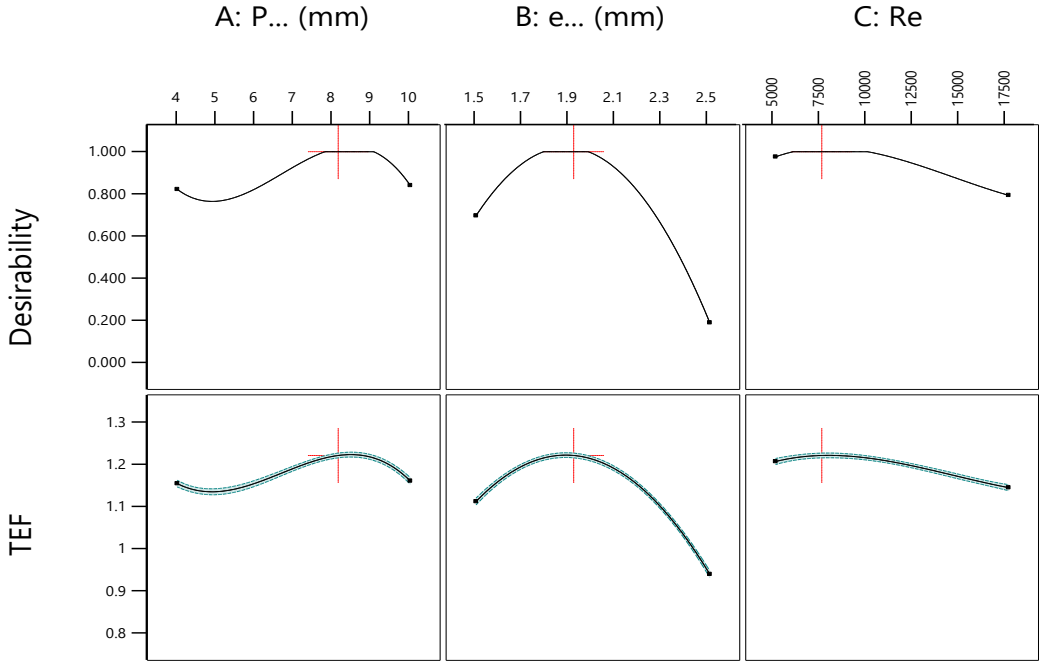

Fig. 5.20: Desirability and Response Plots

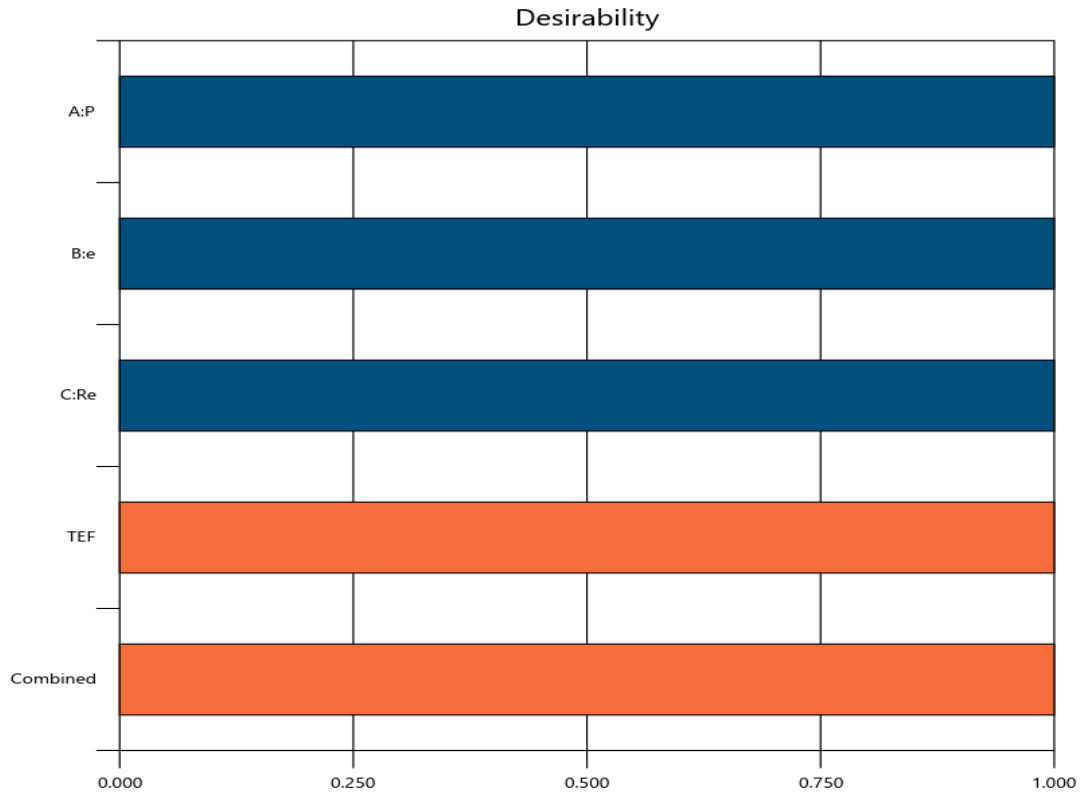

Fig. 5.21: Bar Graph of Desirability for TEF

Moreover, to ascertain the optimal design, a comparison is made between the outcomes of the presented RSM model and the numerical results obtained from CFD investigation, as shown in Table 5.7. Based on these results, it has been determined that the error is minimal, amounting to just 1.29 % when comparing the actual and anticipated values. This indicates a strong concurrence between the implemented response surface methodology (RSM) models and the numerical/CFD model.

Table 5.7: TEF Comparison among CFD and RSM Results for Optimal Parameters

Optimum Parameters	**TEF Outcome**		
	RSM	**CFD**	**Error**
P = 8.145 mm, e = 1.918 mm, Re = 7477.55	1.221	1.237	1.29 %

5.8 Summary of the Chapter

The parameters of the design have been optimized using response surface method (RSM) technique. The following is a concise overview of the notable outcomes derived from this investigation;

- The thermal-hydraulic performance is significantly influenced by the arrangement of corrugations, as it affects the boundary layer dispersion, degree of turbulence, and flow mixing/separation. The outcomes show that thermal performance is greatly influenced by using DCRP.
- The *Nu* shows an upward trend as the corrugation pitch is increased from 4 mm to 8 mm while gets reduced on further rise of pitch value from 8 mm to 10 mm. The Nusselt number exhibits an upward trend as the height of corrugation changes from 1.5 mm to 2 mm, and reduces with the further rise in height.
- In all situations examined a rise in *Re* leads to increase in pressure drop. In a similar vein, it can be seen that pressure penalty tends to escalate as the pitch size changes from 4 mm onwards, attains maxima for 6 mm case and thereafter, gets reduces for remaining pitch sizes. And, in case of constant pitch, it (pressure penalty) is maximum for 2.5 mm corrugation height and minimum for 2 mm height.
- The cubic model implemented while using RSM for the calculation of the Nusselt number, pressure penalty/friction factor, and *TEF* is determined to accurately represent the operational performance of the PTSC receiver pipe with a high level of precision. A comprehensive statistical study has been conducted to verify and validate the model correctness.
- The results revealed the optimal design parameters for modified receiver pipe, resulting in a *TEF* of 1.221: pitch of corrugation (P) = 8.145 mm, height of corrugation (e) = 1.918 mm, and Reynolds number (Re) = 7477.55. The optimised values achieved an approximate match to the desirability of 1, indicating a highly desirable response. Consequently, it can be stated that the heat transfer enhancement system, as devised in this undertaking, is efficacious and has been validated through the application of appropriate analytical methods.
- The RSM results and CFD simulation results are in good agreement with each other. The validation test reveals that the discrepancy between the predicted and actual values is only 1.29%, indicating that RSM model and the numerical model are in excellent agreement. Verification of the validation serves as the ultimate aim of the present investigation.

CHAPTER 6

CONCLUSIONS

This chapter outlines the significant findings of the current study, which aimed to examine the performance of a modified receiver pipe for a parabolic trough. A comprehensive series of computational experiments have been conducted to assess the thermal and fluid flow behaviour of fluid as it moves through the receiver pipe. As a function of geometrical and flow parameters, Nusselt number variation and friction factor/pressure drop are shown. This is done to demonstrate the impact on improvement of heat transfer, which occurs when symmetrical convex-concave corrugations (double corrugations) are incorporated. An investigation has been carried out to determine the performance compared to that of a conventional (smooth) receiver pipe. An analytical model has also been developed to optimize the geometric parameters of a modified receiver of a parabolic trough. This model uses thermal-hydraulic factor criteria and is designed for specific operating circumstances. The findings will assist the designers in this field to anticipate the optimal receiver pipe settings within the intended range of operating circumstances.

From the current investigation following findings can be summarized:

1. The level of turbulence, flow mixing/separation, and dispersion of the boundary layer intensifies with changes in the arrangement of corrugations, hence exerting a substantial influence on the thermal-hydraulic performance of receiver pipe in PTSC.
2. The velocity patterns of several corrugated pipe designs demonstrate the development of vortex formations and axial spinning as the flow advances through the receiver. Consequently, significant improvement in heat transmission has been observed. Furthermore, the pipe with a 2 mm corrugation height and 8 mm corrugation pitch exhibits greater mixing flow regions and recirculation size compared to other examined cases.
3. The vortex interactions lead to a significant increase in turbulent kinetic

energy in close proximity to the wall. As a result, the flow of fluid and heat exchange between the corrugated surfaces and the core sections disrupts the thermal boundary layer in close proximity to the corrugations. Therefore, the existence of convex-concave corrugations amplifies turbulence in comparison to a flat/smooth surface, therefore improving heat transfer. Furthermore, it is apparent that when the pitch length grows from 4 mm to 8 mm and corrugation height from 1.5 mm to 2 mm, there is also an increase in turbulent kinetic energy. Increasing both values further decreases the turbulent kinetic energy as a result of decreased swirl intensity.

4. A total of twelve receiver pipe variants are being examined, each with distinct corrugation pitch lengths and heights. The greatest increase in *Nu* is achieved with an 8 mm pitch and a height of 2 mm. Within the examined Reynolds number range, the increase in Nusselt number has been observed to be between 23.16% and 34.98% compared to a smooth pipe.
5. In contrast to smooth receiver, the average Nusselt number increases by 6.77% - 28.51%.
6. It is evident that the pressure penalty increases as the corrugation pitch increases from 4 mm and reaches its maximum for the 6 mm instance. After that, it decreases for the remaining pitch sizes. The pressure penalty is at its highest at a corrugation height of 2.5 mm and at its lowest for a height of 2 mm, at any constant pitch.
7. The pressure drop increases as a result of the axial spinning, and flow mixing in the corrugated receiver. In various corrugated pipe layouts, the average friction factor value increases from 1.08 - 4.46 times as compared to smooth pipe.
8. The use of response surface methodology (RSM) allowed for the execution of regression analysis on the numerical results, resulting in the determination of correlations between the Nusselt number (*Nu*), pressure drop (ΔP), friction factor, and *TEF* (thermal enhancement factor), with respect to geometrical and flow parameters.

9. The RSM model analysis identified the most effective design parameters for corrugated receiver pipe, having a *TEF* (thermal enhancement factor) of 1.221. The optimized design parameters found from the aforesaid analysis are: corrugation pitch equals to 8.145 mm, corrugation height equals to 1.918 mm. The optimum values closely approximated a desirability of 1, indicating a highly desirable output response. Therefore, it can be concluded that the heat transfer enhancement system, as developed in this work, is effective and has been verified using suitable analytical techniques.
10. RSM model and numerical simulation results are compared to confirm the optimum design. The validation depicts that disparity between the anticipated and observed values is 1.29%, signifying a remarkable concurrence between the RSM model and the CFD model.

To summarise, the double corrugated receiver pipe for the parabolic trough solar collector significantly improves the thermal-hydraulic performance in comparison to smooth (conventional) receiver pipe. The optimization study conducted to maximise the thermal enhancement factor (*TEF*) assists designers in predicting the optimal values of geometric parameters.

Contribution of the Present Thesis

The study has provided correlations for heat transmission in the form of Nusselt number, pressure drop (friction penalty), and thermal enhancement factor. These correlations are valuable for designers to analyse the performance of PTSC within the researched parameter range. The study conducted in this thesis indicates that the double corrugated receiver pipe outperforms the traditional receiver pipe of PTSC in terms of performance, with a large margin. Therefore, it may be used effectively for capturing solar energy. The system is designed to appeal to designers, engineers, students using the model for tutorials, and researchers interested in forecasting the performance of PTSC receiver.

Scope for Future Work

The research conducted in this thesis has laid a foundation for understanding and

optimizing the energy efficient design of receiver pipe of parabolic solar trough collector. However, several areas remain unexplored or could benefit from further investigation. The following outlines the scope for future work:

1. Future research could expand on the investigation of advanced hybrid and composite materials for receiver pipes. While the current work has focused on specific material, the exploration of additional combinations and the development of new composites with superior thermal and mechanical properties could lead to further improvements in receiver pipe performance.
2. The interaction between proposed receiver pipe and advanced heat transfer fluids, such as molten salts, nanofluids, or ionic liquids, could be further explored. Future studies could focus on optimizing the receiver pipe design specifically for these fluids, considering their unique thermal properties and flow characteristics.
3. While the current work primarily riled on numerical simulations, future work could involve extensive field testing of the modified receiver pipe design. Long term performance monitoring would provide valuable data on the durability, efficiency and maintenance requirements of the pipes under various environmental and operational conditions.
4. As solar thermal technology evolves, future studies could explore the integration of the developed receiver pipe designs with emerging technologies, such as high temperature PTSC systems or hybrid systems combining solar thermal with other renewable energy sources.
5. Alternative corrugation profiles, such as rectangular, square, trapezoidal, or triangular can be explored in the future. The effect of number of corrugations, their ring angle, or intermittency can also be explored.

REFERENCES

[1] Salgado Conrado L, Rodriguez-Pulido A, Calderón G. Thermal performance of parabolic trough solar collectors. Renew Sustain Energy Rev 2017;67:1345–59. https://doi.org/10.1016/j.rser.2016.09.071.

[2] Jebasingh VK, Herbert GMJ. A review of solar parabolic trough collector. Renew Sustain Energy Rev 2016;54:1085–91. https://doi.org/10.1016/j.rser.2015.10.043.

[3] Bellos E, Tzivanidis C. Assessment of the thermal enhancement methods in parabolic trough collectors. Int J Energy Environ Eng 2018;9:59–70. https://doi.org/10.1007/s40095-017-0255-3.

[4] Salvi SS, Bhalla V, Taylor RA, Khullar V, Otanicar TP, Phelan PE, et al. Technological Advances to Maximize Solar Collector Energy Output: A Review. J Electron Packag 2018;140. https://doi.org/10.1115/1.4041219.

[5] Ministry of New and Renewable Energy G. Annual Report 2022-23. 2023.

[6] Duffie, John A.; Beckman WA. [John_A._Duffie,_William_A._Beckman]_Solar_Enginee(BookZZ.org).pdf 2005:468.

[7] Akbarzadeh S, Valipour MS. Heat transfer enhancement in parabolic trough collectors: A comprehensive review. Renew Sustain Energy Rev 2018;92:198–218. https://doi.org/10.1016/j.rser.2018.04.093.

[8] Rai GD. Non-Conventional Energy Sources. 4th ed. Khanna Publishers; n.d.

[9] Hafez AZ, Attia AM, Eltwab HS, ElKousy AO, Afifi AA, AbdElhamid AG, et al. Design analysis of solar parabolic trough thermal collectors. Renew Sustain Energy Rev 2018;82:1215–60. https://doi.org/10.1016/j.rser.2017.09.010.

[10] Bellos E, Tzivanidis C. A review of concentrating solar thermal collectors with and without nanofluids. J Therm Anal Calorim 2019;135:763–86. https://doi.org/10.1007/s10973-018-7183-1.

[11] Kumaresan G, Sudhakar P, Santosh R, Velraj R. Experimental and numerical studies of thermal performance enhancement in the receiver part of solar parabolic trough collectors. Renew Sustain Energy Rev 2017;77:1363–74. https://doi.org/10.1016/j.rser.2017.01.171.

[12] Sharma A, Thakur S, Dhiman P. Jet impingement in a V-rib roughened solar air heater: an experimental approach. Energy Sources, Part A Recover Util Environ Eff 2022;44:6970–84. https://doi.org/10.1080/15567036.2022.2105988.

[13] Manikandan GK, Iniyan S, Goic R. Enhancing the optical and thermal efficiency of a parabolic trough collector – A review. Appl Energy 2019;235:1524–40. https://doi.org/10.1016/j.apenergy.2018.11.048.

[14] Sarma D, Barua PB, Rabha DK, Verma N, Purkayastha S, Das S. Flat Plate Solar Thermal Collectors—A Review, 2021, p. 197–209. https://doi.org/10.1007/978-981-16-1550-4_21.

[15] Alshukri MJ, Kadhim Hussein A, Eidan AA, Alsabery AI. A review on applications and techniques of improving the performance of heat pipe-solar collector systems. Sol Energy 2022;236:417–33. https://doi.org/10.1016/j.solener.2022.03.022.

[16] Singh VP, Jain S, Karn A, Kumar A, Dwivedi G, Meena CS, et al. Recent Developments and Advancements in Solar Air Heaters: A Detailed Review. Sustainability 2022;14:12149. https://doi.org/10.3390/su141912149.

[17] Abdulhamed AJ, Adam NM, Ab-Kadir MZA, Hairuddin AA. Review of solar parabolic-trough collector geometrical and thermal analyses, performance, and applications. Renew Sustain Energy Rev 2018;91:822–31. https://doi.org/10.1016/j.rser.2018.04.085.

[18] Abed N, Afgan I. An extensive review of various technologies for enhancing the thermal and optical performances of parabolic trough collectors. Int J Energy Res 2020;44:5117–64. https://doi.org/10.1002/er.5271.

[19] Yılmaz İH, Mwesigye A. Modeling, simulation and performance analysis of parabolic trough solar collectors: A comprehensive review. Appl Energy 2018;225:135–74. https://doi.org/10.1016/j.apenergy.2018.05.014.

[20] Sharma M, Jilte R. A review on passive methods for thermal performance enhancement in parabolic trough solar collectors. Int J Energy Res 2021;45:4932–66. https://doi.org/10.1002/er.6212.

[21] Rungasamy AE, Craig KJ, Meyer JP. A review of linear Fresnel primary optical design methodologies. Sol Energy 2021;224:833–54. https://doi.org/10.1016/j.solener.2021.06.021.

[22] Sun J, Zhang Z, Wang L, Zhang Z, Wei J. Comprehensive Review of Line-Focus Concentrating Solar Thermal Technologies: Parabolic Trough Collector (PTC) vs Linear Fresnel Reflector (LFR). J Therm Sci 2020;29:1097–124. https://doi.org/10.1007/s11630-020-1365-4.

[23] Allouhi H, Allouhi A, Buker MS, Zafar S, Jamil A. Recent advances, challenges, and prospects in solar dish collectors: Designs, applications, and optimization frameworks. Sol Energy Mater Sol Cells 2022;241:111743. https://doi.org/10.1016/j.solmat.2022.111743.

[24] Fernández-García A, Zarza E, Valenzuela L, Pérez M. Parabolic-trough solar collectors and their applications. Renew Sustain Energy Rev 2010;14:1695–721. https://doi.org/10.1016/j.rser.2010.03.012.

[25] Khandelwal DK, Ravi Kumar K, Kaushik SC. Heat transfer analysis of receiver for large aperture parabolic trough solar collector. Int J Energy Res 2019;43:4295–311. https://doi.org/10.1002/er.4554.

[26] Dabiri S, Rahimi MF. Introduction of Solar Collectors and Energy and Exergy

Analysis of a Heliostat Plant. 3rd Int Conf Exhib Sol Energy 2016:1–7.

[27] Bellos E, Tzivanidis C. Alternative designs of parabolic trough solar collectors. Prog Energy Combust Sci 2019;71:81–117. https://doi.org/10.1016/j.pecs.2018.11.001.

[28] Afgan I. Enhancement Techniques of Parabolic Trough Collectors: A Review of Past and Recent Technologies. Adv Civ Eng Technol 2019;3:313–8. https://doi.org/10.31031/acet.2019.03.000563.

[29] No Title n.d. https://www.sbp.de/en/solar-energy [(C) sbp sonne GmbH,%0AStuttgart].

[30] No Title n.d. https.//www.solar-payback.com/technology.

[31] Ghasemi SE, Ranjbar AA. Thermal performance analysis of solar parabolic trough collector using nanofluid as working fluid: A CFD modelling study. J Mol Liq 2016;222:159–66. https://doi.org/10.1016/j.molliq.2016.06.091.

[32] Reddy KS, Kumar KR, Satyanarayana G V. Numerical Investigation of Energy-Efficient Receiver for Solar Parabolic Trough Concentrator. Heat Transf Eng 2008;29:961–72. https://doi.org/10.1080/01457630802125757.

[33] Mohamad A, Orfi J, Alansary H. Heat losses from parabolic trough solar collectors. Int J Energy Res 2014;38:20–8. https://doi.org/10.1002/er.3010.

[34] Ray S, Tripathy AK, Sahoo SS, Bindra H. Performance analysis of receiver of parabolic trough solar collector: Effect of selective coating, vacuum and semitransparent glass cover. Int J Energy Res 2018;42:4235–49. https://doi.org/10.1002/er.4137.

[35] Wang X, Zhang D, Zhang L, Jiang C. Real-time thermal states monitoring of absorber tube for parabolic trough solar collector with non-uniform solar flux. Int J Energy Res 2018;42:707–19. https://doi.org/10.1002/er.3856.

[36] Bellos E, Tzivanidis C, Tsimpoukis D. Optimum number of internal fins in

parabolic trough collectors. Appl Therm Eng 2018;137:669–77. https://doi.org/10.1016/j.applthermaleng.2018.04.037.

[37] Varun, Garg MO, Nautiyal H, Khurana S, Shukla MK. Heat transfer augmentation using twisted tape inserts: A review. Renew Sustain Energy Rev 2016;63:193–225. https://doi.org/10.1016/j.rser.2016.04.051.

[38] Ebrahim Ghasemi S, Akbar Ranjbar A. Numerical thermal study on effect of porous rings on performance of solar parabolic trough collector. Appl Therm Eng 2017;118:807–16. https://doi.org/10.1016/j.applthermaleng.2017.03.021.

[39] Reddy KS, Satyanarayana G V. Numerical Study of Porous Finned Receiver for Solar Parabolic Trough Concentrator. Eng Appl Comput Fluid Mech 2008;2:172–84. https://doi.org/10.1080/19942060.2008.11015219.

[40] Arshad Ahmed K, Natarajan E. Thermal performance enhancement in a parabolic trough receiver tube with internal toroidal rings: A numerical investigation. Appl Therm Eng 2019;162:114224. https://doi.org/10.1016/j.applthermaleng.2019.114224.

[41] V G. New equations for heat and mass transfer in turbulent pipe and channel flow. Int Chem Eng 1976;16:359–68.

[42] Reddy KS, Ravi Kumar K, Ajay CS. Experimental investigation of porous disc enhanced receiver for solar parabolic trough collector. Renew Energy 2015;77:308–19. https://doi.org/10.1016/j.renene.2014.12.016.

[43] Zheng ZJ, Xu Y, He YL. Thermal analysis of a solar parabolic trough receiver tube with porous insert optimized by coupling genetic algorithm and CFD. Sci China Technol Sci 2016;59:1475–85. https://doi.org/10.1007/s11431-016-0373-x.

[44] Sieder EN, Tate GE. Heat Transfer and Pressure Drop of Liquids in Tubes. Ind Eng Chem 1936;28:1429–35. https://doi.org/10.1021/ie50324a027.

[45] Huang ZF, Nakayama A, Yang K, Yang C, Liu W. Enhancing heat transfer in

the core flow by using porous medium insert in a tube. Int J Heat Mass Transf 2010;53:1164–74. https://doi.org/10.1016/j.ijheatmasstransfer.2009.10.038.

[46] Wang P, Liu DY, Xu C. Numerical study of heat transfer enhancement in the receiver tube of direct steam generation with parabolic trough by inserting metal foams. Appl Energy 2013;102:449–60. https://doi.org/10.1016/j.apenergy.2012.07.026.

[47] Kumar BN, Reddy KS. Numerical investigations on metal foam inserted solar parabolic trough DSG absorber tube for mitigating thermal gradients and enhancing heat transfer. Appl Therm Eng 2020;178:115511. https://doi.org/10.1016/j.applthermaleng.2020.115511.

[48] Jamal-Abad MT, Saedodin S, Aminy M. Experimental investigation on a solar parabolic trough collector for absorber tube filled with porous media. Renew Energy 2017;107:156–63. https://doi.org/10.1016/j.renene.2017.02.004.

[49] Method of testing to determine the thermal performance of solar collectors. Stand ASHRAE, United States n.d.

[50] Valizade M, Heyhat MM, Maerefat M. Experimental study of the thermal behavior of direct absorption parabolic trough collector by applying copper metal foam as volumetric solar absorption. Renew Energy 2020;145:261–9. https://doi.org/10.1016/j.renene.2019.05.112.

[51] Ravi Kumar K, Reddy KS. Thermal analysis of solar parabolic trough with porous disc receiver. Appl Energy 2009;86:1804–12. https://doi.org/10.1016/j.apenergy.2008.11.007.

[52] F. P. Incropera, D. P. DeWitt, T. L. Bergman and ASL. Fundamentals of Heat and Mass Transfer. 7th ed. John Wiley & Sons; 2011.

[53] Nasiruddin, Siddiqui MHK. Heat transfer augmentation in a heat exchanger tube using a baffle. Int J Heat Fluid Flow 2007;28:318–28. https://doi.org/10.1016/j.ijheatfluidflow.2006.03.020.

[54] Mahmoudi A, Fazli M, Morad MR, Gholamalizadeh E. Thermo-hydraulic performance enhancement of nanofluid-based linear solar receiver tubes with forward perforated ring steps and triangular cross section; a numerical investigation. Appl Therm Eng 2020;169:114909. https://doi.org/10.1016/j.applthermaleng.2020.114909.

[55] Bozorg MV, Hossein Doranehgard M, Hong K, Xiong Q. CFD study of heat transfer and fluid flow in a parabolic trough solar receiver with internal annular porous structure and synthetic oil–Al2O3 nanofluid. Renew Energy 2020;145:2598–614. https://doi.org/10.1016/j.renene.2019.08.042.

[56] Hatami M, Geng J, Jing D. Enhanced efficiency in Concentrated Parabolic Solar Collector (CPSC) with a porous absorber tube filled with metal nanoparticle suspension. Green Energy Environ 2018;3:129–37. https://doi.org/10.1016/j.gee.2017.12.002.

[57] Ahmed KA, Natarajan E. Numerical investigation on the effect of toroidal rings in a parabolic trough receiver with the operation of gases: An energy and exergy analysis. Energy 2020;203:117880. https://doi.org/10.1016/j.energy.2020.117880.

[58] Kurşun B. Thermal performance assessment of internal longitudinal fins with sinusoidal lateral surfaces in parabolic trough receiver tubes. Renew Energy 2019;140:816–27. https://doi.org/10.1016/j.renene.2019.03.106.

[59] ANSYS. ANSYS Fluent Theory Guide. 2019.

[60] Bellos E, Tzivanidis C, Tsimpoukis D. Multi-criteria evaluation of parabolic trough collector with internally finned absorbers. Appl Energy 2017;205:540–61. https://doi.org/10.1016/j.apenergy.2017.07.141.

[61] Gong X, Wang F, Wang H, Tan J, Lai Q, Han H. Heat transfer enhancement analysis of tube receiver for parabolic trough solar collector with pin fin arrays inserting. Sol Energy 2017;144:185–202. https://doi.org/10.1016/j.solener.2017.01.020.

[62] Petukhov BS. Heat Transfer and Friction in Turbulent Pipe Flow with Variable Physical Properties. Adv Heat Transf 1970;6:503–64. https://doi.org/10.1016/S0065-2717(08)70153-9.

[63] Jensen MK, Vlakancic A. Technical Note Experimental investigation of turbulent heat transfer and fluid flow in internally finned tubes. Int J Heat Mass Transf 1999;42:1343–51. https://doi.org/10.1016/S0017-9310(98)00243-9.

[64] Bellos E, Tzivanidis C, Antonopoulos KA, Gkinis G. Thermal enhancement of solar parabolic trough collectors by using nanofluids and converging-diverging absorber tube. Renew Energy 2016;94:213–22. https://doi.org/10.1016/j.renene.2016.03.062.

[65] Dudley E, Kolb J, Mahoney A, Mancini T, M S, Kearney D. Test results: SEGS LS-2 solar collector. Sandia National Laboratory. Report: SAND94-1884 1994:140.

[66] Zhao Z, Bai F, Zhang X, Wang Z. Experimental study of pin finned receiver tubes for a parabolic trough solar air collector. Sol Energy 2020;207:91–102. https://doi.org/10.1016/j.solener.2020.06.070.

[67] Roldán MI, Valenzuela L, Zarza E. Thermal analysis of solar receiver pipes with superheated steam. Appl Energy 2013;103:73–84. https://doi.org/10.1016/j.apenergy.2012.10.021.

[68] Hachicha AA, Rodríguez I, Capdevila R, Oliva A. Heat transfer analysis and numerical simulation of a parabolic trough solar collector. Appl Energy 2013;111:581–92. https://doi.org/10.1016/j.apenergy.2013.04.067.

[69] Amina B, Miloud A, Samir L, Abdelylah B, Solano JP. Heat transfer enhancement in a parabolic trough solar receiver using longitudinal fins and nanofluids. J Therm Sci 2016;25:410–7. https://doi.org/10.1007/s11630-016-0878-3.

[70] Benabderrahmane A, Benazza A, Samir L. Heat Transfer Behaviors in a

Parabolic Trough Solar Collector Heat Transfer Behaviors in a Parabolic Trough Solar 2016.

[71] Bellos E, Tzivanidis C, Daniil I, Antonopoulos KA. The impact of internal longitudinal fins in parabolic trough collectors operating with gases. Energy Convers Manag 2017;135:35–54. https://doi.org/10.1016/j.enconman.2016.12.057.

[72] Kasperski J, Nemś M. Investigation of thermo-hydraulic performance of concentrated solar air-heater with internal multiple-fin array. Appl Therm Eng 2013;58:411–9. https://doi.org/10.1016/j.applthermaleng.2013.04.018.

[73] Jafar KS, Sivaraman B. Performance characteristics of parabolic solar collector water heater system fitted with nail twisted tapes absorber. J Eng Sci Technol 2017;12:608–21.

[74] Jaramillo OA, Borunda M, Velazquez-Lucho KM, Robles M. Parabolic trough solar collector for low enthalpy processes: An analysis of the efficiency enhancement by using twisted tape inserts. Renew Energy 2016;93:125–41. https://doi.org/10.1016/j.renene.2016.02.046.

[75] Borunda M, Garduno-Ramirez R, Jaramillo OA. Optimal operation of a parabolic solar collector with twisted-tape insert by multi-objective genetic algorithms. Renew Energy 2019;143:540–50. https://doi.org/10.1016/j.renene.2019.05.030.

[76] Mwesigye A, Bello-Ochende T, Meyer JP. Heat transfer and entropy generation in a parabolic trough receiver with wall-detached twisted tape inserts. Int J Therm Sci 2016;99:238–57. https://doi.org/10.1016/j.ijthermalsci.2015.08.015.

[77] Chang C, Xu C, Wu ZY, Li X, Zhang QQ, Wang ZF. Heat Transfer Enhancement and Performance of Solar Thermal Absorber Tubes with Circumferentially Non-uniform Heat Flux. Energy Procedia 2015;69:320–7. https://doi.org/10.1016/j.egypro.2015.03.036.

[78] Bhakta AK, Panday NK, Singh SN. Performance study of a cylindrical parabolic concentrating solar water heater with nail type twisted tape inserts in the copper absorber tube. Energies 2018;11. https://doi.org/10.3390/en11010204.

[79] Ghadirijafarbeigloo S, Zamzamian AH, Yaghoubi M. 3-D numerical simulation of heat transfer and turbulent flow in a receiver tube of solar parabolic trough concentrator with louvered twisted-tape inserts. Energy Procedia 2014;49:373–80. https://doi.org/10.1016/j.egypro.2014.03.040.

[80] Song X, Dong G, Gao F, Diao X, Zheng L, Zhou F. A numerical study of parabolic trough receiver with nonuniform heat flux and helical screw-tape inserts. Energy 2014;77:771–82. https://doi.org/10.1016/j.energy.2014.09.049.

[81] Eiamsa-ard S, Thianpong C, Eiamsa-ard P. Turbulent heat transfer enhancement by counter/co-swirling flow in a tube fitted with twin twisted tapes. Exp Therm Fluid Sci 2010;34:53–62. https://doi.org/10.1016/j.expthermflusci.2009.09.002.

[82] Eiamsa-ard S, Promvonge P. Heat transfer characteristics in a tube fitted with helical screw-tape with/without core-rod inserts. Int Commun Heat Mass Transf 2007;34:176–85. https://doi.org/10.1016/j.icheatmasstransfer.2006.10.006.

[83] Rostami S, Rostami S, Shahsavar A, Shahsavar A, Kefayati G, Goldanlou AS, et al. Energy and exergy analysis of using turbulator in a parabolic trough solar collector filled with mesoporous silica modified with copper nanoparticles hybrid nanofluid. Energies 2020;13. https://doi.org/10.3390/en13112946.

[84] Bilal FR, Arunachala UC, Sandeep HM. Experimental validation of energy parameters in parabolic trough collector with plain absorber and analysis of heat transfer enhancement techniques. J Phys Conf Ser 2018;953. https://doi.org/10.1088/1742-6596/953/1/012030.

[85] Waghole DR, Warkhedkar RM, Kulkarni VS, Shrivastva RK. Experimental

investigations on heat transfer and friction factor of silver nanofliud in absorber/receiver of parabolic trough collector with twisted tape inserts. Energy Procedia 2014;45:558–67. https://doi.org/10.1016/j.egypro.2014.01.060.

[86] Liu P, Zheng N, Liu Z, Liu W. Thermal-hydraulic performance and entropy generation analysis of a parabolic trough receiver with conical strip inserts. Energy Convers Manag 2019;179:30–45. https://doi.org/10.1016/j.enconman.2018.10.057.

[87] Zhu X, Zhu L, Zhao J. Wavy-tape insert designed for managing highly concentrated solar energy on absorber tube of parabolic trough receiver. Energy 2017;141:1146–55. https://doi.org/10.1016/j.energy.2017.10.010.

[88] Mwesigye A, Bello-Ochende T, Meyer JP. Heat transfer and thermodynamic performance of a parabolic trough receiver with centrally placed perforated plate inserts. Appl Energy 2014;136:989–1003. https://doi.org/10.1016/j.apenergy.2014.03.037.

[89] Deshmukh PW, Vedula RP. Heat transfer and friction factor characteristics of turbulent flow through a circular tube fitted with vortex generator inserts. Int J Heat Mass Transf 2014;79:551–60. https://doi.org/10.1016/j.ijheatmasstransfer.2014.08.042.

[90] Mwesigye A, Bello-Ochende T, Meyer JP. Multi-objective and thermodynamic optimisation of a parabolic trough receiver with perforated plate inserts. Appl Therm Eng 2015;77:42–56. https://doi.org/10.1016/j.applthermaleng.2014.12.018.

[91] Diwan K, S. Soni M. Heat Transfer Enhancement in Absorber Tube of Parabolic Trough Concentrators Using Wire-Coils Inserts. Univers J Mech Eng 2015;3:107–12. https://doi.org/10.13189/ujme.2015.030305.

[92] Yılmaz İH, Mwesigye A, Göksu TT. Enhancing the overall thermal performance of a large aperture parabolic trough solar collector using wire coil inserts. Sustain Energy Technol Assessments 2020;39.

https://doi.org/10.1016/j.seta.2020.100696.

[93] Gunes S, Ozceyhan V, Buyukalaca O. The experimental investigation of heat transfer and pressure drop in a tube with coiled wire inserts placed separately from the tube wall. Appl Therm Eng 2010;30:1719–25. https://doi.org/10.1016/j.applthermaleng.2010.04.001.

[94] Kalidasan B, Shankar R, Srinivas T. Absorber Tube with Internal Hinged Blades for Solar Parabolic Trough Collector. Energy Procedia 2016;90:463–9. https://doi.org/10.1016/j.egypro.2016.11.213.

[95] Li X, Chang H, Duan C, Zheng Y, Shu S. Thermal performance analysis of a novel linear cavity receiver for parabolic trough solar collectors. Appl Energy 2019;237:431–9. https://doi.org/10.1016/j.apenergy.2019.01.014.

[96] Shiina Y, Fujimura K, Kunugi T, Akino N. Natural convection in a hemispherical enclosure heated from below. Int J Heat Mass Transf 1994;37:1605–17. https://doi.org/10.1016/0017-9310(94)90176-7.

[97] Huang Z, Li ZY, Yu GL, Tao WQ. Numerical investigations on fully-developed mixed turbulent convection in dimpled parabolic trough receiver tubes. Appl Therm Eng 2017;114:1287–99. https://doi.org/10.1016/j.applthermaleng.2016.10.012.

[98] Muñoz J, Abánades A. Analysis of internal helically finned tubes for parabolic trough design by CFD tools. Appl Energy 2011;88:4139–49. https://doi.org/10.1016/j.apenergy.2011.04.026.

[99] Loni R, Ghobadian B, Kasaeian AB, Akhlaghi MM, Bellos E, Najafi G. Sensitivity analysis of parabolic trough concentrator using rectangular cavity receiver. Appl Therm Eng 2020;169. https://doi.org/10.1016/j.applthermaleng.2020.114948.

[100] Kasaeian A, Daviran S, Azarian RD, Rashidi A. Performance evaluation and nanofluid using capability study of a solar parabolic trough collector. Energy

Convers Manag 2015;89:368–75.
https://doi.org/10.1016/j.enconman.2014.09.056.

[101] Akbarzadeh S, Valipour MS. Energy and exergy analysis of a parabolic trough collector using helically corrugated absorber tube. Renew Energy 2020;155:735–47. https://doi.org/10.1016/j.renene.2020.03.127.

[102] Fuqiang W, Zhexiang T, Xiangtao G, Jianyu T, Huaizhi H, Bingxi L. Heat transfer performance enhancement and thermal strain restrain of tube receiver for parabolic trough solar collector by using asymmetric outward convex corrugated tube. Energy 2016;114:275–92.
https://doi.org/10.1016/j.energy.2016.08.013.

[103] Biswakarma S, Roy S, Das B, Kumar Debnath B. Performance analysis of internally helically v-grooved absorber tubes using nanofluid. Therm Sci Eng Prog 2020;18:100538. https://doi.org/10.1016/j.tsep.2020.100538.

[104] Sharma M, Jilte R. Heat transfer and hydraulics for a novel receiver pipe of solar parabolic trough: a computational approach. Environ Sci Pollut Res 2023. https://doi.org/10.1007/s11356-023-28097-5.

[105] SolCast. Historical Data 2021. https://www.toolkit.solcast.com.au/historical.

[106] Hong Y, Du J, Wang S, Huang SM. Heat transfer and flow behaviors of a wavy corrugated tube. Appl Therm Eng 2017;126:151–66.
https://doi.org/10.1016/j.applthermaleng.2017.07.135.

[107] Kline SJ, McClintock FA. Kline_McClintock1953.pdf. Mech Eng 1953:3–8.

[108] Qader BS, Supeni EE, Ariffin MKA, Talib ARA. RSM approach for modeling and optimization of designing parameters for inclined fins of solar air heater. Renew Energy 2019;136:48–68. https://doi.org/10.1016/j.renene.2018.12.099.

[109] Gawande VB, Dhoble AS, Zodpe DB, Chamoli S. Experimental and CFD-based thermal performance prediction of solar air heater provided with right-angle triangular rib as artificial roughness. J Brazilian Soc Mech Sci Eng

2016;38:551–79. https://doi.org/10.1007/s40430-015-0391-8.

[110] Zhang Y, Ma S, Yue W, Tian Z, Yang C, Gao W. Energy, exergy, economic and environmental (4E) evaluation of a solar-integrated energy system at medium–high temperature using CO2 as the parabolic trough collector (PTC) working medium. Energy Convers Manag 2023;296:117683. https://doi.org/10.1016/j.enconman.2023.117683.

[111] Syed Jafar K, Sivaraman B. Optimization of performance characteristics in the absorber with twisted tapes inserts of parabolic trough collector using response surface methodology. ARPN J Eng Appl Sci 2015;10:3457–64.

[112] Gopalsamy V, Senthil R, Varatharajulu M, Karunakaran R. Application of response surface methodology to predict the optimized input quantities of parabolic trough concentrator. Int J Renew Energy Dev 2020;9:393–400. https://doi.org/10.14710/ijred.2020.30092.

[113] Haran VH, Venkataramaiah P. Optimization and simulation of solar parabolic collector with different absorber tubes and working fluids. AIP Conf Proc 2020;2297. https://doi.org/10.1063/5.0030133.

[114] Sharma A, Thakur S, Dhiman P, Kumar R. Effect of jet-impingement and surface roughness on performance of solar air heater: Experimental study and its optimization. Expert Syst Appl 2024;238:122208. https://doi.org/10.1016/j.eswa.2023.122208.

[115] Gorawar MB, Balikai VG, Revankar PP, Khatawate VH. Performance studies of Solar Air Collector through Design of Experiment approach. IOP Conf Ser Mater Sci Eng 2020;955:012072. https://doi.org/10.1088/1757-899X/955/1/012072.

LIST OF PUBLICATIONS

JOURNALS

1. Mridul Sharma and Ravindra Jilte, "A Review on Passive Methods for Thermal Performance Enhancement in Parabolic Trough Solar Collectors," International Journal of Energy Research, 45 (4), 4932-4966, 2021, DOI: 10.1002/er.6212 (SCI Indexed).
2. Mridul Sharma and Ravindra Jilte, "Heat Transfer and Hydraulics for a Novel Receiver Pipe of Solar Parabolic Trough: A Computational Approach", Environmental Science and Pollution Research, 1-22, 2023, DOI: 10.1007/s11356-023-28097-5 (SCI Indexed).
3. Mridul Sharma, Aashish Sharma, Ravindra Jilte, and Satyam Thakur "Optimizing Thermal-Hydraulic Performance of Parabolic Trough Solar Collector Receiver Pipe through Corrugation Design: A Numerical Simulation and Response Surface Methodology Study", (Under Review with Journal: Applied Thermal Engineering).

CONFERENCES

1. Mridul Sharma and Ravindra D. Jilte, "Numerical Investigation on Thermal Performance of Parabolic Trough Collector under Varying Rim Angle and Non-Uniform Solar Flux Condition", 20th ISME Conference on Advances in Mechanical Engineering, held at IIT Ropar, India during 19th-21st May, 2022 (Paper ID-4212).
2. Mridul Sharma and Ravindra D. Jilte, "Effect of Varying Heat Flux Conditions on Performance of Receiver Tube of Parabolic Trough Solar Collector", International Conference on Simulation, Automation & Smart Manufacturing (SASM 2021), (IEEE Conference), held at GLA University, Mathura, India during 20th-21st August, 2021 (Paper ID-121).